Thermal Analysis of a Feedwater Heater Tubesheet through Coupling of a 1D Network solver and CFD

Department of Mechanical and Aeronautical Engineering

Faculty of Engineering, Built Environment and Information Technology

University of Pretoria

Haimi Jordaan

Supervisors: Prof PS Heyns, Dr S. Hoseinzadeh

October 2019

Dissertation submitted in partial fulfilments of the requirements for the degree Master of Engineering in Mechanical Engineering

Abstract

Title:	Thermal Analysis of a Feedwater Heater Tubesheet through Coupling of a 1D Network solver and CFD.
Author:	Haimi Jordaan
Supervisor:	Prof PS Heyns, Dr S. Hoseinzadeh
Keywords:	Feedwater heater; coupled 1D/3D, CFD; tubesheet; temperature distribution; Fluent, Flownex; numerical modelling; thermal analysis

A feedwater heater is a typical component in power plants which increases the cycle efficiency. Over the last decade, renewable energies have significantly developed and been employed in the power grid. However, weather conditions are inconsistent and therefore produce variable power. Fossil fuel power stations are often required to supplement the variable renewable energies, which increased the rate of power cycling to an unforeseeable extent over the past decade. Power cycling results in changes in the flow rate, pressure, and temperature of a feedwater heater's inlet flows. In a tubesheet-type feedwater heater, these transients induce cycling stress in the tubesheet and failures due to thermal fatigue occur. The header-type feedwater is currently employed in high pressure applications as it is more resistant to thermal fatigue compared to the tubesheet-type. However, the tubesheet-type is more cost effective to construct and maintain. It would be advantageous if the cyclic thermal stresses in the tubesheet can be better analysed and alleviated to support the use of the tubesheet-type.

A detailed transient temperature distribution of the tubesheet is required to understand the thermal fatigue. Normally, engineers opt towards a full CFD to obtain such results. However, the size and complexity of a feedwater heater is immense and cannot be simulated practically solely using CFD spatial elements. This study developed a multiscale approach that thermally couples 1D network elements, CFD spatial elements, and macroscopic heat transfer correlations to reduce the computational expense substantially. The combination of the various selected techniques and the specific application of this methodology is unique. This approach is capable of obtaining the detailed transient temperature distribution of the tubesheet in a reasonable time, as well as include the effects of the upstream and downstream components within the network model. The methodology was implemented using Flownex and Ansys Fluent for the 1D network and CFD solvers, respectively. The internal tube flow was modelled using 1D network elements, while the steam was modelled with CFD. Thermal discretisation, mapping, and convergence were considered to create a robust methodology not limited to feedwater heaters only. Additionally, a method was developed to analyse flow maldistribution in tube-bundles using the coupled 1D-3D approach.

The implementation of the methodology consists of two parts, of which one is for development purposes, and the other serves as a demonstration. The development was done on a simple TEMA-FU heat exchanger which is representative of a feedwater heater. The methodology was tested by varying the primary fluid's flow rates, changing the fluid media, and conducting transient simulations. The temperature distributions obtained were compared against a full CFD model and corresponded very well with errors less than 4%. A reduction in computational time of more than 40% was achieved but is highly dependent on the specific problem. Improvements to be made in future studies include the accuracy of the laminar case method and the stability of the flow maldistribution algorithm.

The methodology was demonstrated by applying it to an existing industrial feedwater heater. No plant data was available to use for input conditions and therefore were assumed. The steam in the DSH was modelled using 3D CFD elements and the tube flow with 1D network elements. The condensing zone's heat transfer was approximated using an empirical correlation. A steady state case was simulated and the outlet temperatures corresponded well with the manufacturer's data. The temperature distribution of the tubesheet and surrounding solids were obtained. Finally, assumed sinusoidal transient perturbations to the inlet conditions were imposed. It was evident that the thermal gradients of both sides of the tubesheet were misaligned which highlights the thermal lag and inertia that cause differential temperatures.

The 1D-CFD methodology was developed successfully with results that proved to correspond well, for a wide range of conditions, to full CFD. The methodology was applied and can be, in future work, validated with experimental results or extended by modelling upstream and downstream components in the network solver.

Acknowledgements

I wish to acknowledge Eskom and the management of EPPEI for sponsoring my research and hope that this study would add value to the organisation. I am grateful for the Centre for Asset Integrity Management for the funding that I received.

I would like to firstly acknowledge my academic supervisor, Prof PS Heyns who provided guidance from the beginning of my independent study to the end of this dissertation. I strongly appreciate all the time he dedicated for meetings and trips to MWP. His experience and insights proved invaluable in many scenarios.

Dr S Hoseinzadeh is also acknowledged for his role as co-supervisor and the guidance he given throughout the year. Furthermore, his advice towards the CFD setup and meshing is highly appreciated. I want to thank Mr G de Klerk, my industry mentor, who proposed the specific application for the project. He also provided technical insights throughout the completion of the study and was always willing to assist whenever required.

Special credit is given towards the late Dr M Hindley, who proposed the methodology's concept and provided technical and project guidance throughout. His enthusiasm for the project was contagious, and he will be remembered for his inspiration.

Finally, I am deeply grateful for the support of my friends and family. Exceptional appreciation is given towards my significant other who sacrificed, for my sake, many early night's rests, weekends, and time. She provided the love and support to motivate me to persevere.

Table of Contents

Nomenclature

English Letters

Symbol	Description	Unit
A	Area	m^2
d	Inner pipe diameter	m
D	Outer pipe diameter	m
f	Friction factor	
h	Convection heat transfer coefficient	$W/m^2 K$
k	Thermal conductivity	W/m K
m	Mass	kg
n	Number of nodes/iterations	
Nu	Nusselt number	
p	Fluid pressure	Pa
Pr	Prandtl number	
Re	Reynolds number	
S	Arc length	m
T	Temperature	°C
V	Velocity of fluid	m/s
X	Downstream position	m
x, y, z	Local coordinate	m

Greek Symbols

Symbol	Description	Unit
ρ	Fluid density	kg/m^3
ϕ	Arbitrary flow variable	
θ	Normalized temperature	
μ	Dynamic viscosity	m^2/s

Subscripts

0	initial
∞	free stream properties
c	cold
h	hot
L	length
p	pressure
q	heat transfer rate
t	thermal, Tube

w	wall

Acronyms and Abbreviations:

1D	One-dimensional
3D	Three-dimensional
ACT	Ansys Customisation Toolkit
CFD	Computational Fluid Dynamics
CHT	Conjugate Heat Transfer
DCZ	Drain Cooling Zone
DSH	Desuperheater
DSZ	Desuperheating Zone
DTL	Data Transfer Links
FEM	Finite Element Method
FFT	Fast Fourier Transform
FSI	Fluid-Structure Interaction
FVM	Finite Volume Method
GUI	Graphical User Interface
HTC	Heat transfer Coefficient
HVAC	Heating, Ventilation and Air Conditioning
LMTD	Logarithmic mean temperature difference
PPT	Parallel Pipe Theory
STHX	Shell-and-tube Heat Exchanger
TEMA	Tubular Exchangers Manufacturers Association
TUI	Text User Interface
UDF	User Defined Function

1. Introduction

1.1 Background

In any steam power plant, turbines, pumps, condensers, and many more components function together to supply power to the grid. A power plant is operational when these components are connected to work together to create a basic steam cycle. It is no secret that failures occur frequently, and much time and effort have been devoted by many to understand and avert the negative impacts thereof. A feedwater heater is a common component in most power plants to improve the cycle efficiency. These components are also not immune to failures.

This project was commenced by and is of interest to a local power supplier in South Africa, who considers replacing the header type feedwater heaters with tubesheet type feedwater heaters in future power plants, in high-pressure applications. Header type feedwater heaters are better suited to alleviate thermal strain but are challenging to maintain and expensive to construct. Conversely, the tubesheet-type is subjected to high thermal stresses, especially in the tubesheet, which cause reliability issues. However, the tubesheet types are more straightforward and compact, which leads to a reduction in size, weight and total cost. If the thermal stresses within the tubesheets could be analysed with sufficient detail and accounted for, especially during transient conditions, the tubesheet type FWH would be more advantageous to use over a header type. Feedwater heaters have been designed primarily using engineering standards and codes to ensure a safe design. Frequent observations of failure mechanisms in feedwater heaters include:

- Vibrating damage
- Steam erosion
- Thermal fatigue

This investigation focuses on thermal transients, which are directly responsible for thermal fatigue failure. Temperature gradients drive thermal fatigue within the structure, which results in disproportional thermal expansion and induced stress. In a tubesheet-type feedwater heater, the tubesheet experiences the highest level of thermal gradients as there is hot steam on one side and cool feedwater on the other. There is a necessity to be able to accurately determine the temperature distribution in the tubesheet so that design optimisation could be made accordingly. Acquiring data from operating feedwater heaters would be accurate but is in most cases is impractical for many reasons. Using computational engineering methods such as finite element methods (FEM) and computational fluid dynamics (CFD) have increasingly proven to be valuable for analysing structures, flow, and their interactions (FSI). One major issue with these methods, especially CFD, is that analysing the three-dimensional (3D) flow domain of an entire feedwater heater is presently impractical due to the large computational power required to approximate the Navier-Stokes equations.

A need, therefore, exists to simplify the analysis so that similar thermal results as captured by CFD can be achieved using a fraction of the computational power. The compromise would be an acceptable range of solution accuracy and certainty. Particular zones, such as the steam-side have very complex flow characteristics that are difficult to capture while other zones, such as the internal flow within tubes, are elementary and easily definable. In feedwater heaters, there are typically hundreds of tubes in which the flow could be simplified from 3D CFD to one-dimensional (1D) network elements due to its simplicity. Utilising the 1D elements could potentially lead to a significant reduction in computational resources. Furthermore, the effects of upstream and downstream components from the feedwater heater could be modelled and implemented as continuously updated boundary conditions. This investigation seeks to develop a methodology that can switch between the various scales of solvers in the appropriate regions to obtain a balance between computational expense and accuracy. The methodology developed has the purpose of creating a framework for future work with a wide range of applicability.

1.1.1 Feedwater Heater Operation

The type of feedwater heater that this study focused on is a closed vertical feedwater heater that is used in high-pressure applications. A feedwater heater preheats the water before it passes through the boiler, which decreases the steam generation irreversibilities. Increasing the number of feedwater heaters in a plant results in higher efficiency, but there is a balance between capital cost and the efficiency gained. Most designers find that seven stages of cascaded feedwater heaters provide an optimum balance (Terranova and Gibbard, 2006). For reference, the flow of a simple tubesheet type feedwater heater is illustrated in Figure 1.1. Bled steam from the turbine enters the shell and transfers heat to the feedwater that flows toward the boiler.

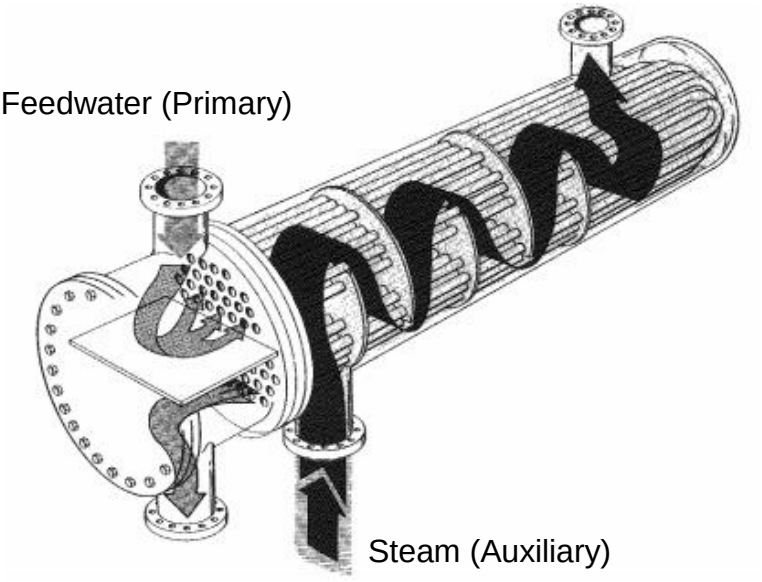

Figure 1.1: Tubesheet type feedwater heater illustration.

A feedwater heater consists of different zones that describe the dominant state of the bled steam. These zones are depicted in Figure 1.2 (Terranova and Gibbard, 2006) in which the desuperheating, condensing and drain cooling zones are shown. These zones are not all present in every feedwater heater design and depend on its location in the cycle and its purpose. When the bled steam from the turbine enters the feedwater heater, the steam is still in a superheated vapour state. The desuperheating zone (DSZ) is located at the feedwater heater's inlet and provides the opportunity for the feedwater to be heated to above the saturation temperature. As heat is transferred from the steam, its temperature lowers along the DSZ. After the steam has transferred all its sensible heat in the superheated state, it becomes saturated and latent heat is transferred to the feedwater in the condensing zone. The majority of the heat transferred in a feedwater heater occurs in the condensing zone. Finally, some heat exchangers have a sub-cooled/drain cooling zone (DCZ) in which the condensate steam continues transferring sensible heat in the liquid state to the feedwater.

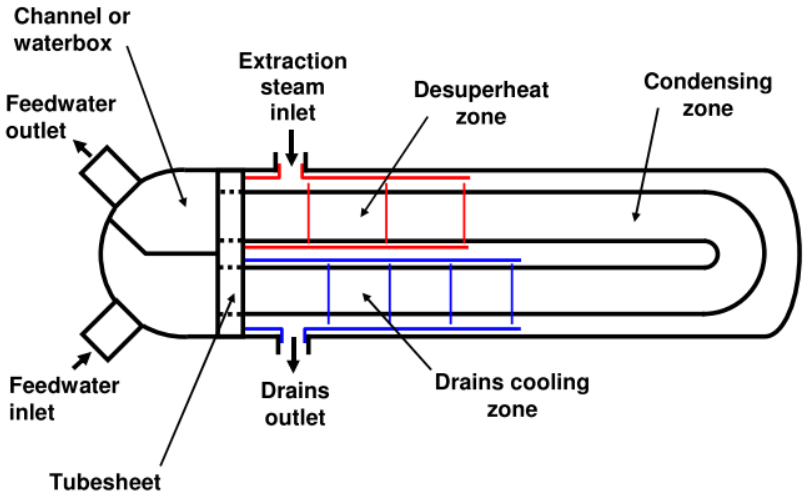

Figure 1.2: Tubesheet feedwater heater zone layout (Terranova and Gibbard, 2006).

Assumed temperatures of the steam and the feedwater along the feedwater heater are shown in Figure 1.3 (El Hefni and Bouskela, 2018), which categorises the mentioned zones. These temperature regions are necessary to know and understand as the domains are discretised accordingly in the proposed methodology, which is presented in Chapter 2. In the DSZ and DCZ, shrouds are used which separate the zones from the condensing surface and optimises the area for sensible heat transfer. Furthermore, baffles or grids are utilised to direct the flow of the steam and increase heat transfer. They also serve as support for the tubes in the bundle.

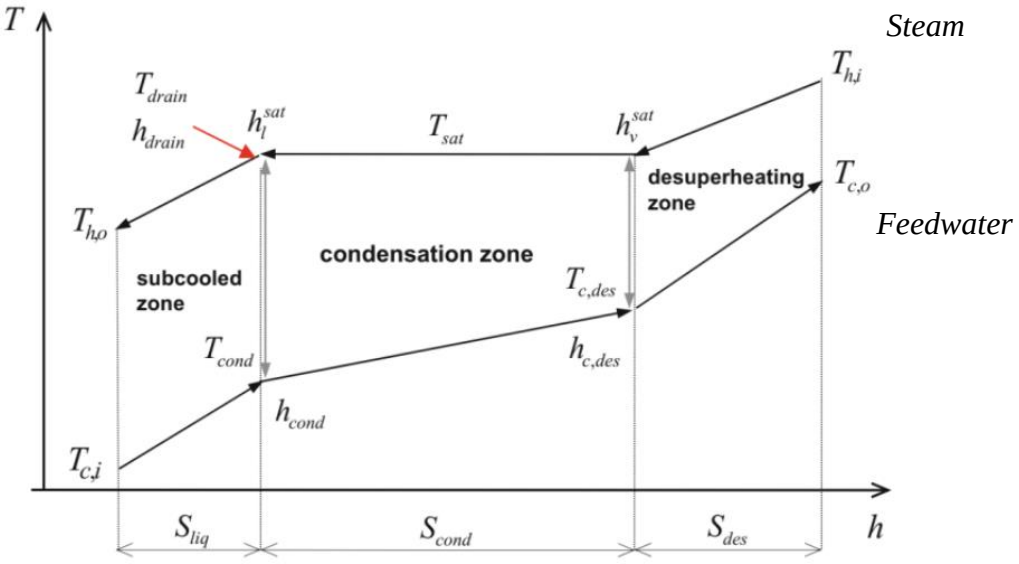

Figure 1.3: Temperature approximation along feedwater heater for steam and feedwater (El Hefni and Bouskela, 2018).

1.1.2 Thermal Solver Classification

Presently, engineers have the ability more than ever to solve complex engineering problems using computational methods such as FEM and CFD due to its proven capability. Much research has been dedicated to extending the capabilities of all these approaches but not very often has the various solution methods been combined for a coherent analysis throughout. This investigation seeks to couple spatial elements such as FEM and CFD, with network elements and components for computational efficiency. These various solvers are briefly introduced in this section with particular attention towards the coupling model types that exist between CFD and network elements.

FEMs have proven to be irreplaceable in the field of structural analysis for decades. Performing a structural analysis due to thermally induced stresses is often used in industry and modelling the thermal loads without the use of fluid cells has the advantage of using significantly fewer elements than a CFD analysis. It requires the user to specify the heat transfer boundary conditions at the fluid-solid interfaces. These can either be in the form of a constant temperature, heat flux, or convection coefficient and free stream temperature. The FEMs then approximate the heat equation for the variational initial boundary value problem to approximate the temperature distribution.

Since the user is required to specify the boundary conditions, a good understanding of the problem and its heat transfer is required, which is often not straightforward. The reason is that the general mode of heat transfer between fluids and solids in heat exchangers is forced convection which requires knowledge of the convection coefficient, h, and free stream temperature, T_∞. Decades of research have provided numerous correlations for convection coefficients of typical cases, but not nearly enough to cover all possible cases. As soon as the context of the problem changes outside the correlation's applicability, it is no longer valid and CFD or experimental tests are usually required to estimate h. This occurs especially in cases with complicated flow and geometries such as industrial heat exchangers.

CFD is a very well-known method to analyse and solve fluid flows that fundamentally approximates the Navier-Stokes equations using numerical methods. It has been proven to be able to calculate the convection coefficient quite accurately in several applications where no correlations exist. This is done by solving the conjugate heat transfer problem, which Section 1.2 describes. Calculating the convection coefficients requires computational resources that inflate as the model increase in complexity and size. Practically, CFD is therefore generally used to model localised components and regions without considering of the system effects that upstream or downstream components might have. Nevertheless, CFD has proven to be an invaluable engineering tool able capable of approximating all phenomena necessary for this investigation.

1D network solvers are used to model the combination of various standard components joined in a network. These solvers approximate the flows with the use of an extensive database of correlations and material properties as well as numerical schemes in 1D to approximate the governing equations for mass, momentum and energy. The computational cost associated with this type of analysis is negligible in comparison with CFD and results have proven to be reliable. It is therefore especially useful to model entire systems to incorporate the effects of upstream and downstream conditions.

FEMs, CFD, and 1D solvers all have their advantages and disadvantages. However, the ideal would be to integrate these methods in the areas in which they are most suitable and couple them to exchange data. This is referred to as a hybrid approach and requires coupling with CFD methods that are capable of simulating custom components. Using a combination of various element types and methods is referred to as a multiscale approach. CFD and FEM elements are referred to as spatial elements as these elements have geometrical attributes in the ‘spatial’ domain. Filimonov (2017) described three different approaches to couple network and spatial elements. These are illustrated in Figure 1.4 and are referred to as:

- Fully separated model
- Hydraulically unified model
- Hydraulically disconnected model

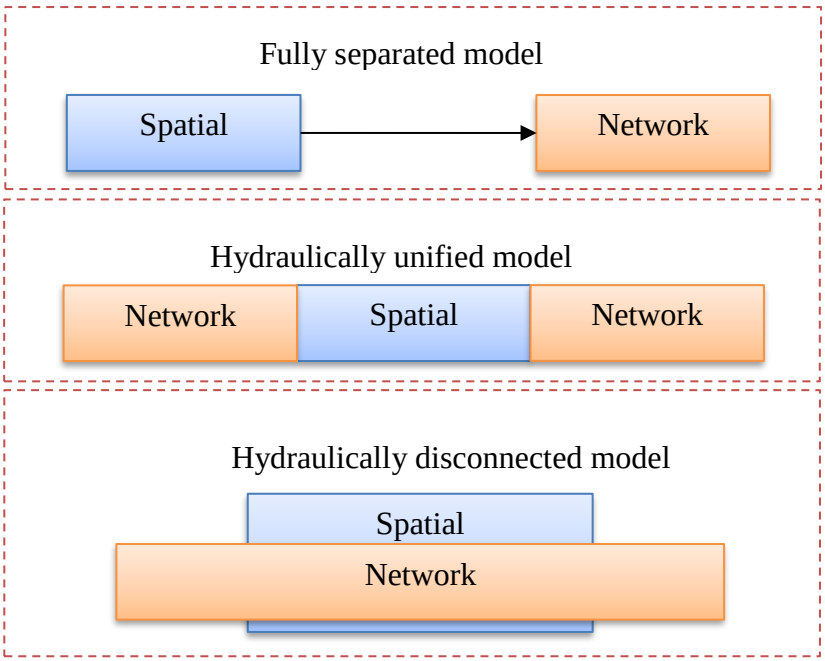

Figure 1.4: 1D Network and CFD coupling types.

Fully Separated Model

A fully separated model refers to the spatial and network parts being calculated completely separately, from which the outputs of the one solver is used as inputs of another. Typically, separate software products that are appropriate for the application are used. This is the most popular approach used in industry due to the lack of a requirement to make any modification between software to transfer data. An excellent example of a fully separated model is determining the hydraulic resistance of a non-standard component using spatial methods as an input in the network model. Restrictions that are associated with this methodology are that a large number of 3D calculations are often required to construct a robust relationship for different flow rates and inlet conditions in the network. Recent techniques to reduce the computational effort include using the response surface method (RSM) (Hanna *et al.*, 2017) or the neural network method (NNM) (Checcucci *et al.*, 2011).

Hydrodynamically unified model

If a relationship cannot be constructed using a fully separated model, due to the large number of flow dependencies, a good alternative would be to use a hydrodynamically unified model. A hydrodynamically unified model exchanges boundary conditions simultaneously between spatial and network elements. This is also commonly referred to as co-simulation, and leading network solvers like Flowmaster and Flownex have integrated CFD packages such as Fluent and CFX within their environments. The network software uses third-party software such as MpCCi or preCICE, which are dedicated coupling interfaces to exchange boundary conditions.

These models have increased in popularity over the years, and an excellent example of where a hydrodynamically unified model could be used is to model an HVAC system for a server room. For this application, the inputs and outputs of the CFD domain (the server room) are dependent on the upstream and downstream 1D network flow inputs as indicated in Figure 1.5. A few other works in which the approach is featured are from Papukchiev *et al.* (2009), Ljubijankic *et al.* (2011) and Arias (2006).

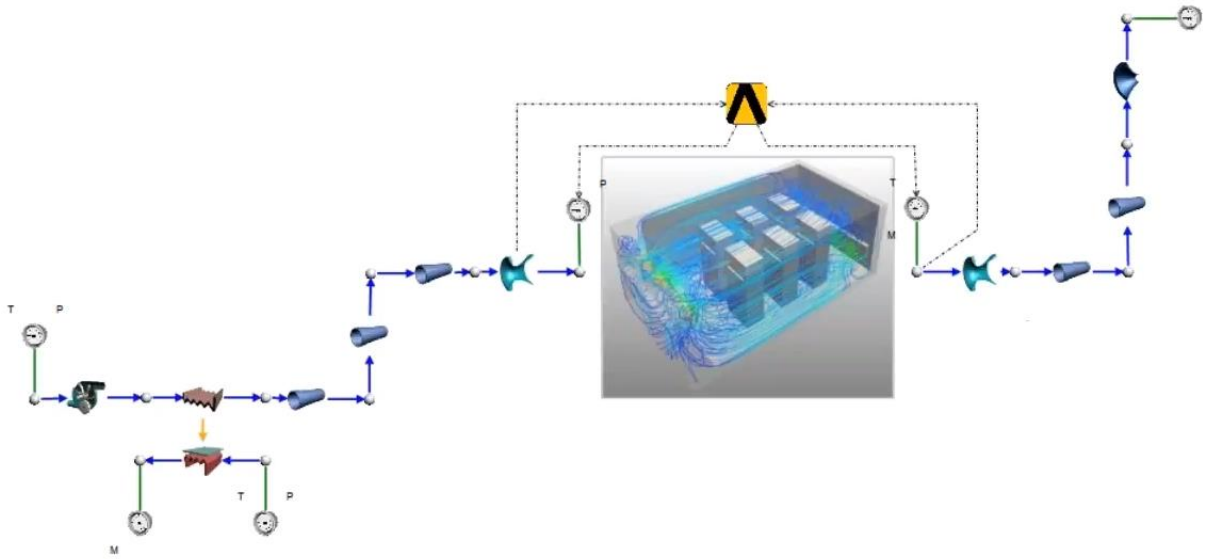

Figure 1.5: 1D-3D co-simulation example of HVAC system.

Hydrodynamically Disconnected Model

In this type of 1D/CFD approach, the network elements penetrate the spatial area. Most applications that use this approach would be of a thermal analysis such as the work done by Koekemoer, du Toit and Kruger (2018) and Filimonov (2017), who both modelled heat exchangers using 1D network elements to represent the tubes. The shell-side flow's spatial elements surround the internal flow 1D network elements and transfer data transversely across the boundaries between solvers. Flow characteristics can also be modelled using a hydrodynamically disconnected model when CFD provides the inputs and outputs of the flow. This method is portrayed and developed in this investigation while accounting for flow maldistribution by using CFD spatial elements to provide inputs to the network elements.

1.2 Heat Transfer Theory

A good understanding of the heat transfer theory with regards to coupling would form the basis from which the proposed methodology would be developed. This section provides the necessary theory involving heat transfer coupling strategies which could offer inspiration towards the development of a 1D network and a CFD coupled approach. It also reviews a few of the numerous heat transfer correlations that are applicable for both internal and external flows in feedwater heaters.

1.2.1.1 Conjugate Heat Transfer

Conjugate heat transfer is used to describe the processes which involve the thermal interaction between solids and fluids. The most general heat transfer in media can be described by the modes of heat transfer which are:

- Conduction: Diffusion of heat due to temperature gradients. A measure of the amount of conduction for a given gradient is the thermal conductivity, *k*, of a material.
- Convection: Heat that is carried away by a moving fluid. The flow can either be induced by external influences, forced convection, or by buoyancy forces (natural convection). Convective heat transfer is tightly coupled to the fluid flow solution.
- Radiation: Transfer of energy by electromagnetic waves between surfaces with different temperatures, separated by a medium that is at least partially transparent to the (infrared) radiation. Radiation is especially important at high temperatures, e.g. during combustion processes, but can also have a measurable effect at room temperatures.

It is useful when dealing with a combination of these heat transfer modes to describe the network in terms of thermal resistances, as shown in Figure 1.6 below for a typical pipe in a heat exchanger. Analogous to current in an electric circuit, the heat transfer in series resistors are equal and divides in parallel arrangements. For this investigation, depending on the case, it would be advantageous if the internal convection and tube conduction could both be approximated using 1D elements.

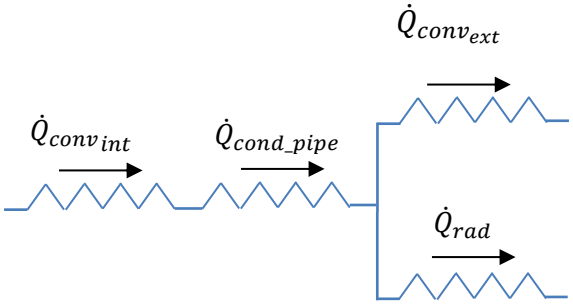

Figure 1.6: Typical pipe thermal resistance.

The dimensionless numbers that are associated with heat transfer have become standard in several of the correlations. The essential dimensionless parameters for this study are the Prandtl (Pr) number, Reynolds (Re) number and the Nusselt (Nu) number. The Prandtl number describes the ratio between momentum diffusivity and thermal diffusivity. In simpler terms, it relates the velocity and the thermal boundary layers (Cengel and Ghajar, 2015). The very well-known Reynolds number describes the ratio of the inertial and viscous forces in a tube and could be represented by Equation 1.1, where a Re < 2300 is generally represents laminar flow and Re > 4600 in pipes turbulent flow (Cengel and Ghajar, 2015):

$$Re = \frac{\rho V_{avg} D}{\mu} = \frac{4\dot{m}}{\mu \pi D} \tag{1.1}$$

The Nusselt number is the ratio of total heat transfer in convection dominated systems to the conductive heat transfer and is used in the majority of heat transfer correlations to obtain the convection coefficient. This is given by Equation 1.2 which also indicates its dependent variables which are the conductivity, k, and the characteristic diameter D (McAdams, 1942):

$$Nu = \frac{hD}{k} = f\left(\frac{Dv\rho}{\mu}, \frac{\mu}{k/c_p}, L/D\right) \tag{1.2}$$

An age-old problem has always been to obtain the heat transfer coefficient specific to flow characteristics. An abundance of experimental work has been done on recurring geometries and flow types. However, not all geometrical features and flow characteristics are within the defined parameters, and then the correlations are no longer valid. One solver that has proved in many studies to be reliable if adequately executed is CFD (Yari *et al.*, 2015), and it would, therefore, be advantageous if a good understanding of the coupling procedures was known to imitate it with a 1D solver. In most CFD solvers, the fluid domain is most commonly calculated using the finite volume method (FVM) to approximate the Navier-Stokes equations and their derivatives. The heat transfer within the solids is governed by the elliptical Laplace or parabolic differential equation, and FEMs are utilized to solve (Dorfman and Renner, 2009). In the most general conjugate problem, the temperature and heat flux distributions along the interface of a fluid are the primary unknowns and exchanged according to the developed algorithm.

There are two methods to solve conjugate heat transfer (CHT) problems or fluid structure interaction (FSI) problems commonly. The first is the monolithic method in which the equations are solved simultaneously in a single solver as is done by Malatip, Wansophark and Dechaumphai, (2006). It consists of a global system of equations that includes fluid and solid subdomains. The second is the partitioned method in which every domain is solved separately, updating the boundary conditions systematically, and coupling is done by exchanging the boundary values. The partitioned approach once again ties into an explicit or implicit solver type between the 1D flow and the CFD. The partitioned approach was a more attractive option for this investigation as processing global matrices implicitly without third-party software was deemed unnecessarily difficult. These are often referred to as explicit and implicit methods, and each method has its advantages which are described in Table 1.1 below:

Table 1.1: Advantages and disadvantages of numerical methods.

	Advantages	Disadvantages
Explicit	-Simple and easily implemented -Fast for simple flow -Accurate	-Time step and space step sizes are limited due to numerical instability. -Slow for highly nonlinear problems:
Implicit	-Unconditionally Stable -Better suited for nonlinear problems	-Complicated to implement -Potentially slow if matrices are large and sparse

At the interface between the fluid and solid region in the conjugate heat transfer model, the convective heat transfer is coupled with the conductive heat transfer by means of either a Neumann, Dirichlet, or Robin condition. These are briefly introduced as it was required that the exchanging variables between spatial and network elements were selected with intent. The Dirichlet boundary condition is a boundary condition that prescribes a temperature to the boundary Γ, and is given by:

$$T_D = T_D \text{ on } \Gamma_D \tag{1.3}$$

A Neumann boundary condition prescribes the heat flux at the boundary

$$k\frac{\partial T}{dn} = q_N \text{ on } \Gamma_N \tag{1.4}$$

Finally, a Robin boundary condition is a weighted combination of a Dirichlet and Neumann boundary condition.

$$aT + b\frac{\partial T}{dn} = g \text{ on } \Gamma_R \tag{1.5}$$

The Robin boundary condition usually is described as a convective boundary condition in most heat transfer problems and is given as:

$$k\frac{\partial T}{dn} + h(T - T_\infty) = 0 \tag{1.6}$$

and in the most common and simple form in which the heat transfer coefficient is h and the reference temperature is T_∞, it must fulfil the imposed conditions.

$$q = h(T - T_\infty) \tag{1.7}$$

These three types of boundary conditions are used at the interfaces between the solid and fluid domain and iterated until convergence with many developed algorithms. These can be used in various combinations in which each has advantages and disadvantages in terms of the accuracy, convergence rate and stability. For this study, inspiration from the Robin boundary conditions was used as the heat transfer coefficient *h,* could be determined from the known internal correlations

and the reference temperature, T_∞, mapped to the corresponding nodes. These quantities could then be exchanged in the developed systematic manner, which is discussed in Chapter 2.

1.2.1.2 Review of Internal Flow Heat Transfer Correlations

There exist numerous heat transfer correlations that have been developed throughout the years. The various applications and limits of each are summarised and evaluated based on the applicability to this study. The thermal correlations considered in this study are only related to convection heat transfer. As was previously described, the Nusselt number is a function of a variety of flow and geometrical parameters, and most convection correlations are of the following form:

$$Nu = \frac{hD}{k} = aRe^{n}\mathrm{Pr}^{\mathrm{m}}\left(\frac{L}{D}\right)^{e}\left(\frac{\mu}{\mu_w}\right)^{j} \tag{1.8}$$

where the w subscript indicates the properties evaluated at the wall. A summary of various correlations in the form of Equation 1.8 is presented below for internal tube forced convection (McAdams, 1942; Cengel and Ghajar, 2015; Allie and Fuls, 2016) .

Table 1.2: Coefficients of Equation 1.8 for internal turbulent tube flow correlations.

Correlation Tag	Year	Constants				
		a	n	m	e	j
McAdams I	1925	0.0178	0.83	0.38	0	0
Dittus-Boelter (Heating)	1930	0.0243	0.8	0.4	0	0
Dittus-Boelter (Cooling	1930	0.0265	0.8	0.3	0	0
Nusselt	1931	0.036	0.5	1/3	0.055	0
Seider-Tate	1936	0.027	0.8	1/3	0	0.014

These correlations are quite simple to implement but have limited applicability with uncertainties as high as 25% (Cengel and Ghajar, 2015). These correlations are acceptable if limited data is available and for the sake of simplicity. However, this study opted to use Gnielinski's (1976) correlation which has uncertainties of approximately 10% and has increased accuracy within the transitional flow region. Gnielinski's correlation is given in Equation 1.9 with its range of applicability. For transitional flow, which generally occurs for Reynolds numbers between 2300 and 4000, Gnielinski's equation is recommended for use with a modification to the friction factor proposed by Abraham, Sparrow and Tong (2009).

$$Nu = \frac{(f/8)(Re-1000)Pr}{1+12.7(f/8)^{0.5}(Pr^{2/3}-1)} \qquad \begin{pmatrix} 0.5 \le Pr \le 2000 \\ 3\times10^{3} < Re < 5\times10^{6} \end{pmatrix} \tag{1.9}$$

In feedwater heaters, various geometrical features can affect the heat transfer in tubes which include the pipe bends as well as the thermally developing entry lengths. These effects are especially significant for laminar flow and diminish as turbulence intensity increases. For laminar flow around a U-bend, the downstream flow has increased heat transfer due to the secondary flow effects. The correlation developed by Abdelmessih (1979) is suitable and is given as:

$$Nu = \left[4.364 + 1.955 \times 10^{-6} Re^{1.6} De^{0.8} e^{-0.0725\left(\frac{X}{d_i}\right)}\right]\left(\frac{\mu_b}{\mu_w}\right)^{0.14} \tag{1.10}$$

where X is the position along the downstream tube and D_e is the Dean number defined by:

$$D_e = Re\sqrt{\frac{D}{2R_c}} \tag{1.11}$$

When flow enters a pipe section, the thermal boundary layer has not yet been fully developed. In laminar flow this entry length is significantly longer than turbulent flow due to the intense mixing caused by induced vortices. Therefore, if flow in a tube is laminar, the thermal entry length L_t can be approximated by (Cengel and Ghajar, 2015):

$$L_t \approx 0.05\, Re\, \mathrm{Pr}\, D \tag{1.12}$$

for which the Nusselt number in the thermal entry length can be determined from:

$$Nu = 3.66 + \frac{0.065\left(\frac{D}{L}\right) Re\, Pr}{1 + 0.04\left[\left(\frac{D}{L}\right) Re\, Pr\right]^{\frac{2}{3}}} \tag{1.13}$$

The applicable internal heat transfer correlations have been reviewed and are used throughout the methodology. The external heat transfer is solved using CFD for which the method is described in detail in Chapter 2. However, the heat transfer in well-defined external flow zones in a FWH were modelled using empirical correlations, which were specific to FWH-5A and are described in Section 4.1.

1.3 Literature Survey

1.3.1 Feedwater Tubesheet analysis

Tubesheet analysis is the basis of this investigation for which a temperature distribution is required as a load input. The mechanical stress in the tubesheet is hoop stress caused by the interaction with surrounding regions. Cyclic stresses occur due to the thermal transients of the perforated area that respond quickly, while the temperature responses of the surrounding regions are delayed. This induces transient stresses that are superimposed in the already existing thermal stress of steady state cases. Cyclic conditions result in cyclic stresses which lead to thermal fatigue. Literature was surveyed to identify how other researchers analyse the thermal stresses of a tubesheet with special consideration to the modelled temperature distribution. There have been many studies in which sophisticated FEMs have been used, while the specified thermal conditions lack such sophistication. It was noted that many researchers impose temperature boundary conditions to the tubesheet. This is sufficient if the specified temperatures are found from on-site measurements (Liu *et al.*, 1999) or if an elementary thermal analysis suffices (Guo and Jianping, 2011). A few studies have specified heat transfer coefficients, but are in some works specified rounded values of for instance 10000

W/m^{2}K, like Jiuyi, Caifu and Huifang (2018) did. Mao *et al.* (2016) estimated the convection coefficient of the internal flow and applied it to the tube interfaces. The majority of thermal FEM studies impose temperatures boundaries on the tubesheet (Li, Qian and Yu, 2011; Patil and Anand, 2017). Nevertheless, there is a very limited amount of work that include a detailed temperature distribution for the use of structural analysis. This problem is partially addressed by this investigation.

1.3.2 1D Thermal Models

As shell-and-tube heat exchangers (STHX) are generally large in size and CFD is not always practical for design, researchers have developed various methods to calculate feedwater heater's heat transfer effectively. The use of network solvers or modular dynamic solvers with an extensive library of general components and phenomena are utilised in which the computational time is relatively insignificant.

One method in which heat exchangers are analysed is by using standard components and heat transfer correlations that approximate the overall values such as the outlet temperature and pressure of the flows. In many studies, many sections of a system are incorporated to estimate upstream and downstream effects within the process. For instance, le Grange (2018) used a 1D network solver to model a feedwater heater, deaerator and turbine using Flownex. The model was capable of capturing transient conditions, to a degree, and the results agreed well with experimental data. Meinke *et al.* (2011) similarly, modelled a fuel burner considering upstream and downstream components in which the results compared very well to plant measurements. These models can determine overall system parameters, but do not contain sufficient detail for a stress analysis.

The work that was performed by Zaversky, Sánchez, and Astrain (2014) focused on object oriented modelling of a shell-and-tube heat exchanger for concentrated solar power. The researchers used Modelica, a physical system modelling language, and its standard library to set up a 1D fluid flow model of the STHX. The governing differential equations were based upon the FVM to solve the general mass and energy balances. Their model was capable of calculating transients accurately. The model was partitioned into window and cross-flow zones. These are illustrated in Figure 1.7 (Zaversky, Sánchez and Astrain, 2014). Their approach was implemented on a case study of a typical heat exchanger and provided consistent results for both steady state and transient simulations. Rousseau and Gwebu (2018) described the application of a 1D thermofluid network approach to model a superheater heat exchanger with complex flow arrangement. CFD was not used and maldistribution was also accounted for as fluid properties change with temperature using the parallel pipe theory method that is described in Section 2.2. These approaches indicate the effectiveness of 1D thermal networks but can often lack the level of detail provided by CFD.

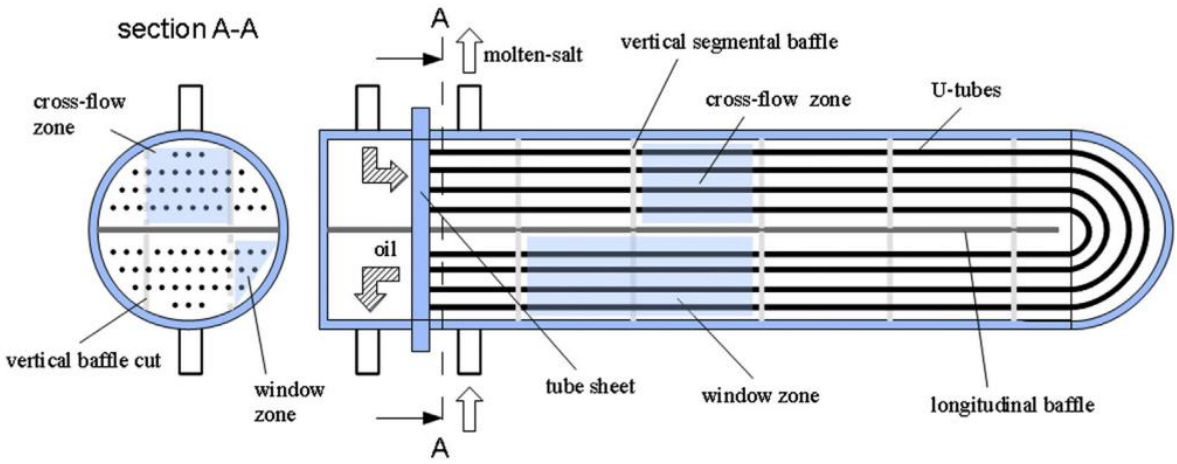

Figure 1.7: TEMA-FU type STHX zone partitions (Zaversky, Sánchez and Astrain, 2014).

Another study that uses a similar approach of combining correlations, but much more fitting to this study, was the reliability, thermal, and uncertainty analysis specific to tubesheet feedwater heater conducted by Allie and Fuls (2016). In their study, a comprehensive library of heat transfer correlations relating to geometric variations of tubesheet feedwater heater and flow models are provided. Industry feedwater heaters were analysed, and agreeable results were obtained for only steady state conditions. The correlations presented are crucial to create a 1D model of a feedwater.

1.3.3 **Software Coupling**

Attention has been addressed in the past by various researchers towards coupling 1D flow to CFD or 3D FEM. Most of the work is still very recent (past 10 years), and it was noted that the rate of work towards development into coupling methods is undoubtedly increasing. Surprisingly enough, the earliest efforts made towards 1D FSI have been made in the bio-medical field where large arterial networks are modelled in 3D space. Examples include work done by Kaser et al. (1998) Sherwin *et al.* (2003), and Johnson *et al.* (2011). A few of these works include heat transfer models to and from arterial networks in the governing equations.

The coupling of solvers is generally performed explicitly or implicitly which is analogous to the CHT monolithic and partitioned coupling methods. Kruger and du Toit (2006) described the same methods in their work back then. Information transfer between network solvers and CFD can be performed in two different ways which are referred to as an ‘internal’ implicit coupling and ‘external’ explicit approach (Kruger and Du Toit, 2006). The implicit method is implemented by assembling the equations into a global matrix and solving simultaneously. On the other hand, the explicit approach keeps the solver equations separate and exchanges data explicitly across boundaries using node-averaged values or direct linking of cell boundaries (Kruger and du Toit, 2006).

Coupling 1D to CFD is mostly done by means of co-simulation where the inlet and outlet boundaries of the CFD domain are coupled to a 1D network (Fang, Spoor and Ghiaasiaan, 2017) (Ljubijankic *et al.*, 2011). These refer back to the hydrodynamically unified models. A methodology that is

similar to this study is the work conducted by Kruger and Du Toit (2006). They described a coupled 1D and CFD model to simulate a boiler. Koekemoer, Du Toit and Kruger (2018) the feasibility of an elementary air-cooled heat exchanger. Both studies obtained very good results for their simulations. The difference in this study is that the transient simulation results are provided as well as the additional aspects are considered such as flow groupings, polynomial mapping and significantly increased problem complexity. Kruger, Le Grange and Greyvenstein (2009) developed a 1D-3D hydrodynamically disconnected model for the flow inside the micro-channel of a heat exchanger and 3D CFD for the heat distribution inside the core. Network and porous spatial elements were connected on a per-cell basis by assembling a global matrix of the connecting thermal resistances and was solved implicitly.

Previous work that pertains to coupling 1D models to either CFD or directly to FEM was reviewed. Botha and Hindley (2015) analysed a boiler using a 1D network solver coupled with spatial FEMs. They incorporated a one-way FSI that transferred temperature data between solvers to capture the thermal loads on a boiler structure. The thermal loads of the tubes induced stress in the surrounding structures and resulted in failures. They successfully implemented a 1D fluid model for a collective boiler tube length of 4787 m and achieved results that corresponded very well to measured temperature data. Their process of modelling the system is illustrated in Figure 1.8 in which the interaction between the 1D flow and 3D FEM is highlighted. However, their 1D flow results were obtained by varying the flue gas temperature and heat transfer coefficient such that the numerical results represented the known experimental results, as illustrated in Figure 1.8 by the 1D internal validation loop. More specifically, throughout the transient simulation, the heat transfer coefficient was kept constant while the flue gas temperature was varied to fit experimental data. This is a valid approach in their case as experimental data of the physical model. However, the approach is inadequate when no experimental data exists, such as during the design phase.

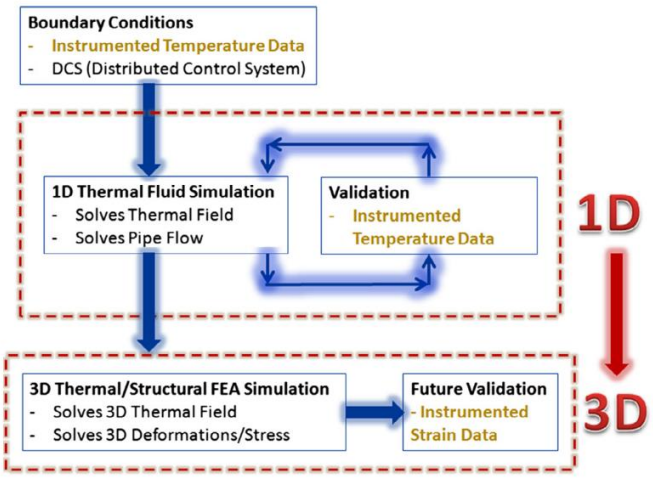

Figure 1.8: Modelling approach used by Botha and Hindley (2015).

1.3.4 Flow maldistribution

In many heat exchangers, especially the smaller ones, the fluid tends to preferentially flow specific tubes of a bundle. The mass flow rates will, therefore, be non-uniform across the bundle and the heat transfer effectiveness (ϵ) can be adversely affected. This phenomenon is referred to as flow maldistribution. The most dominating maldistributed property is the velocity of the flow that enters, which can lead to backflow in the other tubes in some extreme cases (Lalot *et al.*, 1999). An example of flow maldistribution in a square header can be seen in Figure 1.9. Flow maldistribution does not only affect the heat transfer by altering the Reynolds number within tubes but also, indirectly, decreases heat transfer by accelerating the rate of fouling in tubes that have stale flow (Kitto and Robertson, 1989). With time the effects become substantial, and failures are an inevitable result.

It should be noted that in practice, the assumption of uniform flow in heat exchangers is commonly employed (Bejan and Kraus, 2003). This is justified for many designs of heat exchangers, but one should be able to account for it with a coupled approach for a more robust model when the maldistribution is indeed significant. Maldistribution is highly dependent on the geometrical features of a model, and significant attention has been directed towards optimising the geometry to reduce maldistribution. Other methods to reduce maldistribution include perforated grids between inlet and header (Lalot *et al.*, 1999) or using orifices and nozzles at tube inlets, which have been proven effective (Said *et al.*, 2015).

In practice, the gross flow maldistribution is often the parameter of interest and mathematical models have been developed and validated, like the work done by Mohammadi and Malayeri (2013). Such a model would have been useful for this investigation, but their specific model deals only with the maximum deviations and captures the symmetric profile of the gross flow. Nonetheless, this concept and many others approach in which the maldistribution is correlated to the pressure drop across tubes is employed in the development of an approach to deal with maldistribution in this study.

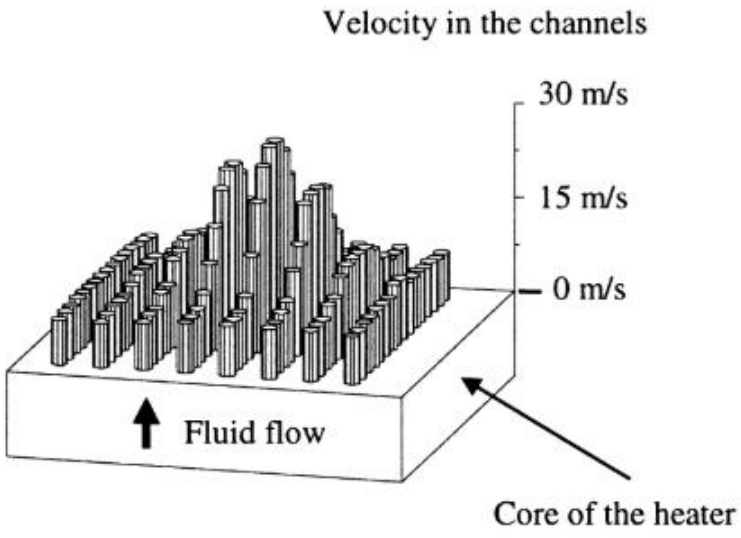

Figure 1.9: Flow maldistribution example of square header (Lalot *et al.*, 1999).

A substantial amount of work has been done to investigate maldistribution using CFD, and good agreement to experimental results for STHX have been obtained, like the work performed by Kim *et al.* (2009). For this investigation, flow maldistribution would have to be taken into account by lumping tubes into groups that are associated with their expected mass flow rates. This investigation does not attempt to alleviate flow maldistribution, but to merely account for it. It should be noted that maldistribution is generally quantified as a percentage based upon the deviation from uniform flow. Flow rates of up to 20% difference are quite standard for flow maldistribution, and these differences can considerably affect the heat transfer results of this investigation.

1.4 Scope of Work

1.4.1 Problem Statement

Large industry heat exchangers such as feedwater heaters and boilers are very intricate with regards to geometry and flow in certain regions. Performing a thermal analysis on these structures is no easy task as typical tube bundles can consist of hundreds of parallel tubes that are long as well. Many previous thermal analyses have used lumped and segmented correlations for a first-order simulation or by using either full CFD and its derivatives such as the heat exchanger and porous media models. Although these methods have proven their worth in industry, they typically have a narrow scope of applicability, and are computationally demanding or inaccurate if conditions and geometries are varied from the standard case. All the methods have their benefits and drawbacks but very seldom are these methods combined and coupled in the regions where each is most suitable. A methodology is required that can be applied to custom flows and geometries while retaining accuracy and reducing the computational resource demand of full CFD.

The methodology would finally have to aid in the determination and visualisation of the temperature gradients within tubesheets of feedwater heaters. The methodology should be able to capture transients so that recurrence of thermal fatigue in tubesheets can be alleviated so that tubesheet-type feedwater heaters become a viable option to replace the header type for high-pressure applications. A need for a model exists that can consider the effects that the upstream and downstream components might have on the feedwater heater. The use of 1D network solver would be useful for this. Finally, the effects of temperature and flow maldistribution are often considered uniform, but realistically seldom are. A need exists to be able to quickly verify this assumption and the effects of maldistribution on the heat transfer if it is indeed present. Finally, the proposed methodology should be able to be applied repeatably, and therefore minimal user intervention and experience should be required.

1.4.2 Aim and Objectives

This study aims to investigate the feasibility of using a multiscale coupled methodology between 1D/3D CFD elements together with FEM and existing empirical heat transfer correlations, with the purpose to obtain the temperature gradients of a feedwater tubesheet. The proposed methodology seeks to model the tube bundles using a 1D network solver while the shell side flow is modelled

using CFD. Methods to extract the data for FEM applications should also be described to ultimately analyse the thermal fatigue. The objectives of this dissertation are given as follows:

- Provide a useful hybrid computational tool for simplifying tube-bundle heat transfer applications
- Validate the proposed methodology using full CFD
- Ensure the methodology is straightforward without the use of third-party software.
- Investigate limits of methodology on a simplified problem representative of a feedwater heater.
- Indicate the method of thermal load transfer for structural analysis.

Achieving these objectives would be the first of many to justify the switch from a header-type to a tubesheet-type feedwater heater in coal fired power plants. The developed methodology seeks to lay a foundation for future endeavours and extensive additional work is required to justify the feedwater heater type switch.

Detailed analysis of a tubesheet-type feedwater heater would encourage the use of it in high-pressure applications, which is currently overshadowed by the more expensive header-type designs which alleviate thermal fatigue more effectively. The current global situation is that the header type is predominantly employed in power plants as it is economically more viable due to the increased equipment life (Youssef, 1993; Band, Benten and Stahlhut, 2007). If the reliability and equipment life of the tubesheet design is extended, it can greatly benefit coal fired power plants from a cost perspective to shift from the header-type to the tubesheet-type. Furthermore, the development of this methodology would contribute to the analysis of several heat transfer applications such as boilers and is not only limited to a feedwater heater.

The proposed methodology combines a variety of uniquely developed and existing techniques to form a wholly coherent thermal analysis. No other literature was found that addresses the coupling of 1D elements specific for the use of obtaining the temperature distribution on tubesheets. Neither has a coupled 1D-CFD method been found that analyses flow maldistribution in heat exchangers, even though the process is quite intuitive and uncomplicated.

In comparison with existing work that comprises of 1D-CFD thermally coupled methods, this study utilizes a unique mapping procedure between solvers. The studies, described in Section 1.3.3, used uniform values as transfer variables in the discretised sections. These result in discontinuities between elements and sections. In many cases this method is adequate, but this study seeks to improve the general method by introducing a polynomial mapping procedure which creates a continuous function along elements and sections. Furthermore, attention towards the procedure and effects of the discretisation of elements at the 1D-CFD interface is provided in this study while this has been neglected by others. An advantage of the Characteristics Discretisation method is that it requires no equations specific to the identified zones to be implemented unlike the 1D thermal models described in Section 1.3.2.

These techniques are not necessarily the most sophisticated that exist, but the combination of several for one analysis is unique. The proposed methodology is required to be capable of modelling steady state and transient conditions as well as to be applied to a wide range of flow inputs such as media selection and geometric irregularities. No other study was found that has applied the coupling of a 1D network solver with CFD and tested it to this extent.

1.4.3 Overview of Problems

This investigation comprises of two main parts. The development of the methodology, and application and demonstration of the methodology. Both parts were modelled using Fluent V19.4 and Flownex as the software.

Development

For the development of the methodology, a shell-and-tube heat exchanger was created that resembles the Tubular Exchanger Manufacturers Association (TEMA) FU type. A TEMA-FU type shell-and-tube heat exchanger is similar to a feedwater heater as both consists of U-Tube bundles, baffles and fixed tubesheets. This problem could be solved by modelling all the shell-side flow with 3D CFD elements and the internal tubes with 1D network elements. In the design of the geometry and problem, various conditions had to be kept in mind so that the problem would firstly represent a feedwater heater and to, secondly, test the full applicability of the methodology. Some of these aspects are:

- Substantial temperature difference between inlet and outlets for both the tube-side (primary) and shell-side (auxiliary) fluid.
- Flow maldistribution.
- Baffles and sophisticated geometrical features typical in heat exchangers such as a tubesheet and channels.
- Transient inputs.

The coupled 1D-CFD approach is validated by comparing it to a full CFD model. This would be the first stage of validation, as no experimental data was available. Using only full CFD for validation purposes is sufficient as the difference in results between the full CFD and 1D-CFD coupled approach is entirely dependent upon the internal tube flow which is straightforward to approximate and ordinarily matches well with experimental data. If numerical discrepancies in the shell side flow existed, these could affect both methods the same and results would still align with each other. This problem assumes that there is no phase change in fluids, as this would have been an unnecessary complication to have during development of the methodology.

The model was designed to be simple, with no unnecessary complications that could diminish the troubleshooting process. Therefore, very few tubes were modelled so that each can be treated on an individual basis in the pre- and postprocessing stages. Also, the selection and management of hundreds of tubes would be extremely time consuming. It was still a requirement that a large tube bundle should be handled but is addressed in the next part of the dissertation. The tube's diameter was exaggerated slightly to compensate for fewer tubes while keeping a balance in volume between

the auxiliary and primary fluid. Doing so ensures that the change in temperature is significant in the primary and the auxiliary fluid.

Methodology Demonstration

After the methodology was developed and tested on an elementary problem, it was endeavoured to demonstrate the methodology on a realistic representation of a feedwater heater. The feedwater heater that was modelled was based on a real operational feedwater heater and is referred to as FWH-5A in this study. It consists of a desuperheating and condensing zone with design parameters available for each. All of the internal flow was modelled with the 1D network elements, which lead to a substantial reduction in computational resources as FWH-5A consists of 560 U-tubes. Due to the large size of FWH-5A, it was opted to model only a portion of the shell-side flow in the desuperheater (DSH) and feedwater outlet with the developed methodology. Consequently, a detailed temperature distribution of the most severe thermal gradient regions of the tubesheet could be obtained. This region was located at the steam inlet and feedwater outlet. The remaining thermal parameters were obtained using appropriate correlations in the respective zones. The model was validated for a steady state case by comparing with the design parameters provided.

1.5 Dissertation Layout

This dissertation commences with an introductory chapter that describes the background, literature, primary problem and strategy that applies to this study. The proposed methodology to the problem is then presented and discussed in detail in Chapter 2. This methodology was used in both the TEMA-FU and FWH-5A problems. The TEMA-FU problem is outlined in Chapter 3, where its specific setup is firstly described, and subsequently, the results. In Chapter 4, the FWH-5A problem is introduced. Similarly to the TEMA-FU chapter, the setup and modelling strategy of FWH-5A are first discussed. The results follow thereafter and include steady and transient case simulations. This dissertation is finally concluded with a summary of the objectives achieved and recommendations for future work.

1.6 Conclusion

An introduction to the investigation of coupling 1D network to 3D CFD elements to evaluate the temperature gradients in a tubesheet was presented. It provided a background to the problem and relevant heat transfer theory. Literature was surveyed in which work done by others with regards to tubesheet stress analysis, multiscale coupling methods, and flow maldistribution was evaluated. The Chapter finally concludes by describing the scope of this study, the novelty, and overview of the dissertation problems and layout.

2. Methodology

This chapter describes the methodology that is used to couple the CFD with the 1D network solver. The strategies for implementing the methodology differ slightly for both of the considered problems, but the core methodology remains the same. The main steps in the methodology are defined as:

1. Model geometry and mesh.
2. Conduct a flow maldistribution analysis.
3. Discretise thermal flow domain
4. Set up CFD
5. Set up 1D solver
6. Co-simulate
7. Transfer solid domain temperatures to a structural analysis
8. Repeat Steps 3-6 if discretisation zones were unsatisfactory

These steps are highlighted throughout this chapter. The methodology presented is the final version and numerous improvements were made during the development process. Some of which are discussed.

2.1 Thermal Coupling Process

The method in which the thermal properties of 1D network elements are coupled to 3D spatial elements is described in this section. Both solvers have to satisfy the energy equation, and many share the same heat transfer variables. As a result, an implicit relationship exists and requires the solvers to exchange data iteratively for convergence. For this methodology, the transfer variables were selected to be the heat transfer rate, $\dot{Q}$, obtained from the spatial elements as well as the convection coefficient, h, and the mean temperature fluid T_∞ calculated by the network solver. This coupling process is depicted in Figure 2.1 below. It may be recalled from the literature that this approach is based on the Robin CHT boundary condition. The exchange of variables at the interface of the solvers is depicted in Figure 2.1. The parameters are transferred from one solver to the other by utilizing an explicit coupling strategy which was described in Section 1.2. This method is simple to implement and sufficient for weakly dependant problems such as the thermal interaction between network and spatial elements. Each respective solver iterates a specified amount locally and afterwards, exchanges data between the two solvers. This is referred to in this study as local and global iterations respectively and are also depicted in Figure 2.1 where ϕ is an arbitrary flow variable with the subscript i and superscript j is the position and timestep index respectively.

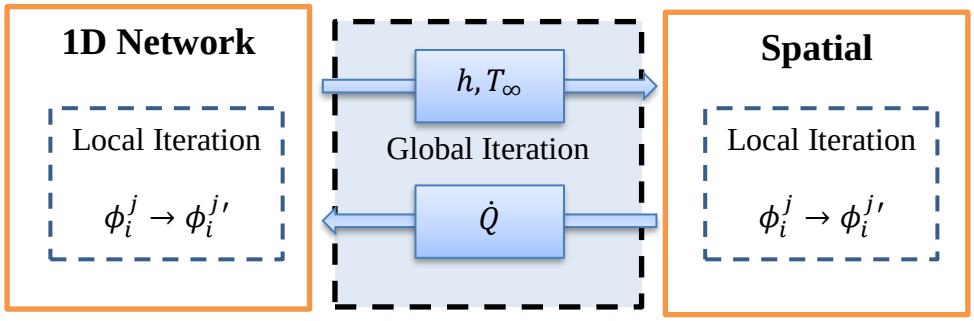

Figure 2.1: Macroscopic thermal coupling procedure.

All the thermal coupling occurs at the boundary walls of each respective tube. These boundaries can be represented in two ways. The first includes the tube walls within the CFD calculation as spatial elements and use FEMs to solve, while the second models the pipe walls as 1D thermal resistances and can be done in either Fluent or Flownex. The second method is computationally more efficient with a small trade-off in accuracy. These approaches are depicted in Figure 2.2 below. The first approach is useful when the tube temperatures are of interest in a detailed stress analysis or when the conduction heat transfer is considerable in the longitudinal direction of the tube. The latter reduces the number of elements required and consequently results in lower computational times.

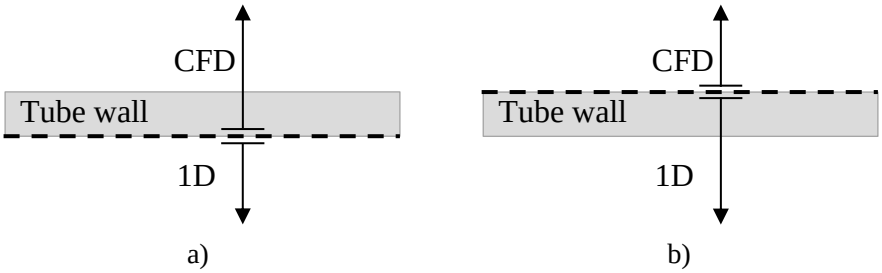

Figure 2.2: Tube wall modelling approach a) Spatial tube wall boundaries, b) Network tube wall boundaries.

The above forms the basis of the thermal coupling procedure that is used in this work. This is the main idea of the coupling strategy, but many other aspects are required for the method to be successful and are described in the following sections.

2.2 Flow Coupling Process

In this study, accounting for flow maldistribution is also considered to ensure a robust solver. Similar to the thermal coupling, a 1D network solver can be used from which two methods are identified. The first method, based on hydraulic parallel pipe theory (PPT), uses the fact that the pressure loss in each parallel pipe is equal (White, 2011). In a U-bend tube bundle, this includes the primary and secondary losses which consist of:

- Pipe friction
- Inlet and outlet of the channel
- Bends

The bend losses of a U-tube differ for each row of tubes as the radius of each is increased. Determining the specific flow rate for each tube requires an iterative approach to solve, as an implicit relation exists due to the flow rate and pressure being strongly dependent on each other. It would be trivial solving for every tube, and therefore the tubes were lumped into specified groups, each with different U-bend radii. This method is straightforward to implement but is capable of only accounting for flow maldistributions of minor magnitudes. Its most significant drawback is that it does not consider biased flow due to a positive flow pressure directed towards particular tube groups, which is why the second method was developed.

The second method models the channel and a small portion of the length of the tubes using spatial CFD elements. The lengths of the tubes should ideally be longer than the turbulence recirculation bubble to ensure minimal backflow at outlet boundaries. Applying this method to a problem requires a systematic approach that consists of several steps which is illustrated in Figure 2.3. The first step is to conduct an initial run with the backflow pressure, P_{b_i}, of the tube outlet boundary conditions set equal to zero. This assists in developing an understanding of the flow tendency towards certain tubes when there is no resistance. Flow groups are categorized and defined after based on the flow tendencies accordingly. The mass flow rate within the tube bundle, m_g, is distributed among all tubes uniformly initially in the 1D solver.

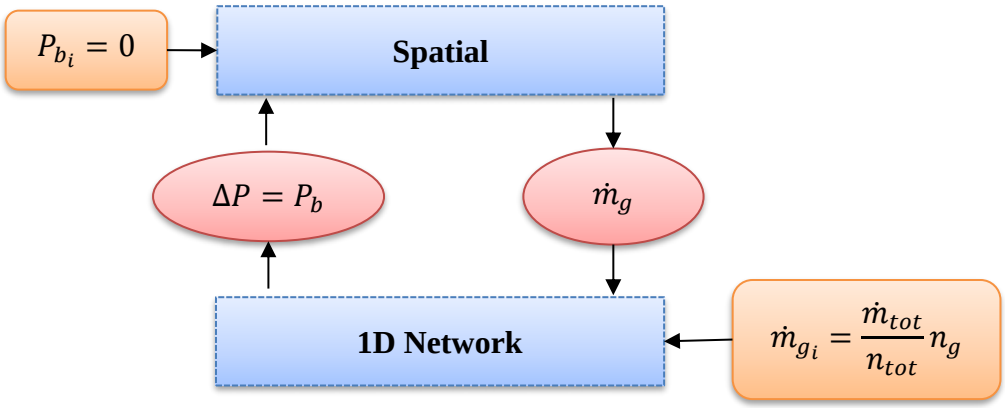

Figure 2.3: Flow coupling process diagram.

Similar to the thermal coupling process, variables are exchanged between the network and spatial elements to achieve flow convergence. Starting with the 1D network solver in Figure 2.3, it calculates the pressure drop within the flow groups and transfers the backflow pressure to the CFD solver as a pressure boundary condition. The biased flow groups have higher pressure drops due to the greater Reynolds number present within the respective tubes. A greater backpressure will reduce the mass flow rate in the biased flow groups which severely affects the maldistribution. The newly calculated outlet mass flow rates are transferred then back to the 1D network solver as depicted to complete the loop.

The coupling procedure was found to converge relatively slowly, compared to the thermal coupling, due to the flow transfer variables being dispersive. Stiff relaxation factors were

therefore implemented and are essential for improved convergence. This is further discussed in Section 2.3.3.

2.3 Convergence Analysis

The proposed methodology is based on an iterative approach, and therefore the solution converged after several local and global iterations. The method in which variables are exchanged affects the convergence rate. Ways in which the convergence rate can be improved are discussed below for a steady state and transient case in this section.

2.3.1 Steady State Simulation

Achieving global convergence required data to be transferred several times from Flownex to Fluent while the solvers iterate locally as well. The timing of when a global iteration was triggered had an effect on the convergence rate. Three different trigger timings were identified. The first trigger timing of a global iteration is whenever both solvers have achieved complete local convergence. This method was usually sufficient when only thermal variables were transferred but was highly ineffective when there were flow dependencies between the solvers. This was due to the significant agitations it caused to the residuals in the CFD flow governing equations. The spatial domain, which uses the majority of computational time, was then required to be essentially re-evaluated after each global iteration.

On the other side of the spectrum, the second method consists of performing a local iteration after each CFD local iteration. This method nullified the implemented relaxation factors, and the solution did not converge. Also, transferring data between solvers consumed peripheral computational time, and its magnitude depended on the number of variables transferred. The time required per iteration was therefore increased substantially if a global iteration was triggered after each local CFD iteration.

The last was the most efficient method in which a fixed number of spatial iterations were specified before a global iteration must occur. The choice of the number of iterations is dependent upon the problem. In this study, the number is chosen based upon the number required for the initial CFD's residuals to reduce by 10 %, which was about 20 iterations in most cases. It should be noted that the amount changes significantly based upon the chosen CFD solution scheme and algorithms. The network solver was allowed to converge fully for each global iteration as the time required to do was insignificant. In Figure 2.4, the process of data transfer and convergence is conveyed.

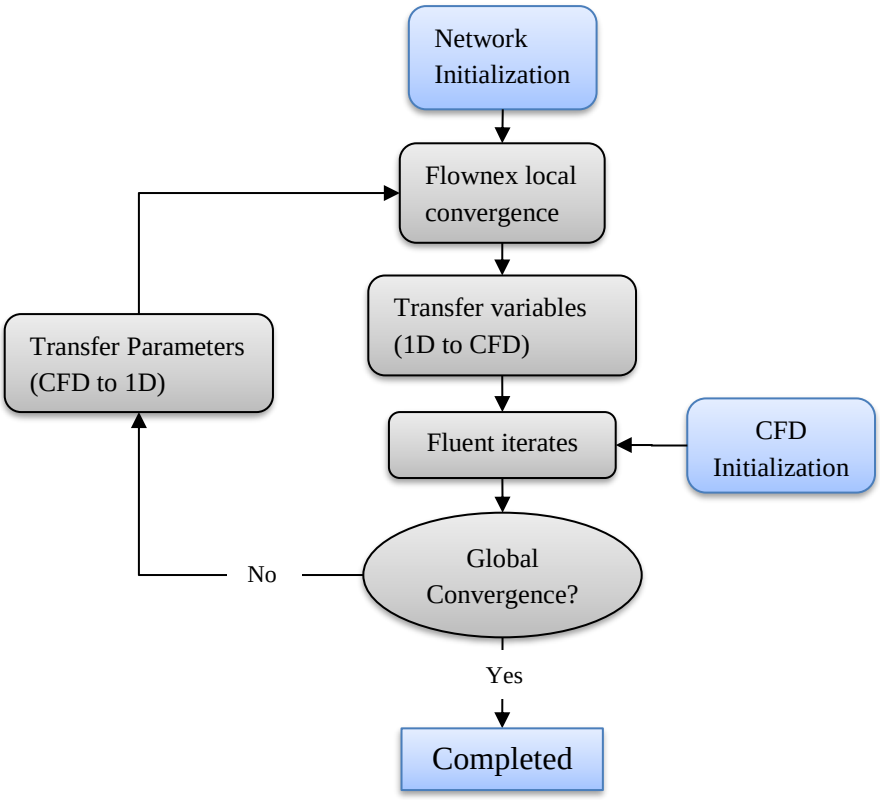

Figure 2.4: Steady State coupling Algorithm between Flownex and Fluent.

Global iterations were executed until global convergence was achieved, but it was necessary to predict when global convergence was achieved to terminate the simulation. For global convergence, the CFD and 1D network solver residuals as well as the change in transfer variables must be sufficiently close to zero. The CFD residual criteria are discussed in Section 2.6.1, but the change in transfer variables per global iteration was set to 0.01%. From the performed simulations, it was found that the CFD solver usually converged last. The solution would end once the residuals and change in variables were satisfactorily close to zero. A global iteration is triggered by Flownex when it sends a user specified command to the text user interface (TUI) of Fluent. For steady state, the standard '*solve iterate n'* command was used where '*n*' indicates the number of local Fluent iterations to be conducted.

2.3.2 **Transient**

Performing a transient simulation is nearly identical to the steady state procedure in terms of data transfer. A Gauss-Seidel numerical scheme was adopted for transient simulations as it was simple to implement and unsusceptible to instability. The time marching procedure is illustrated in Figure 2.5. The network solver transfers its variables at the end of a timestep to the initial timestep of the CFD solver. It should be noted that there may develop a minor offset between software timesteps due to the selection of the numerical scheme. This may lead to considerable errors if the timestep sizes are defined too large.

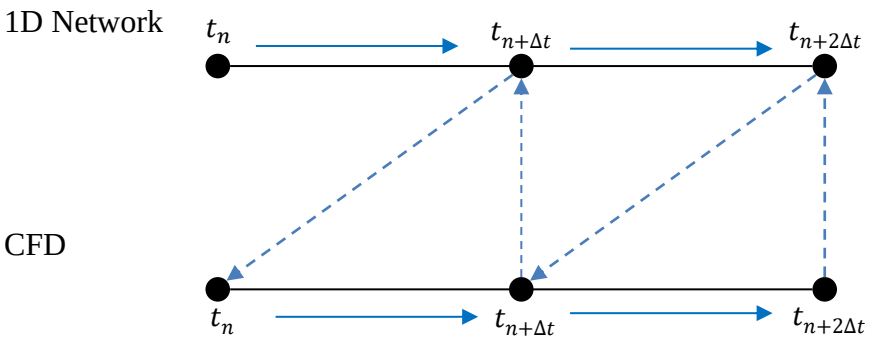

Figure 2.5: Gauss-Seidel transient coupling method.

2.3.3 **Relaxation Factors**

Relaxation factors were implemented to counter the residuals of the solution that have tendencies to become unstable or oscillate around the desired value. This primarily occurred for flow coupled variables which are strongly coupled implicit functions of each other. A relaxation factor ξ, between 0 and 1 is the factor of the newly obtained value to be used while $1 - \xi$ is the factor of the old value to keep. This dampened the oscillatory behaviour and resulted in better convergence. However, choosing a relaxation factor too close to zero could also slow convergence as the values update each iteration insignificantly. The right balance was, therefore, required.

Convergence factors were applied in two areas. The first was the heat transfer rate obtained from Fluent. For this, ξ_q,was set to 0.8, which was also used by Verstraete and Van den Braembussche (2009) in their conjugate heat transfer approach. The value of 0.8 for the thermal relaxation factor provided the right balance of damping. A different relaxation factor was used for the maldistribution flow coupling, in which ξ_p was set to 0.15. This value was set purposefully stiff as the backflow pressure and Reynolds number are strongly coupled. As a result, the backflow pressure could easily unbalance the mass flow within a particular group, and therefore, a very small allowance for change was implemented. The backflow pressure only affects the distribution of the flow within tubes, but the conservation of mass was still fulfilled even if the pressure lags in a transient simulation for rapid changes in the input conditions.

2.4 Zone Discretisation

In any heat exchanger, heat transfer characteristics differ substantially between zones. For instance, a baffled heat exchanger exhibits predominantly cross flow in certain zones and parallel flow in other. In a heat exchanger, many of these zones can usually be identified, and this methodology seeks to account for the uneven distribution of heat across tube bundles by defining sections in these zones. It would follow that a higher resolution of the defined sections would always provide better results but is laborious to implement. Therefore, a good understanding of the problem is essential so that redundant zones can be avoided. Two methods of discretising the fluid domains were developed. The associated terminology with the discretisation is firstly explained for better understanding. Three synonymous terms in general context, but have different meanings in this investigation, is used to describe the zones and are listed below in the following list in ascending hierarchal rank:

- A ***Section*** refers to the divided intervals that are used to transfer data between boundaries. There often exists several sections within a segment depending on the accuracy desired for the polynomial approximation. Values within sections are averaged and transferred from CFD to 1D network solver. Sections do not have to be uniform in size and can vary for resolution control.
- A ***Segment*** refers to the tubes that are expected to have a continuous function that is representative of the data transferred. Segments usually contain a few sections from which are used to fit a curve for mapping purposes. Segment assignment is based upon geometrical and flow characteristic discontinuities and behaves like piecewise functions. For instance, a straight tube, U-bend, sensible heat transfer, and condensing flow would each be represented by a different segment.
- A ***Flow Group*** refers to tubes that are lumped together that are assigned the same mass flow rate. A flow group can contain several segments, and there can also be several flow groups in a model.

2.4.1 Flow Group Discretisation

In Section 2.4, it is described how flow groups are defined depending on how the flow is distributed among tubes. The *Flow Group Discretisation* method is characterised by these flow groups and must be used when maldistribution is accounted for. The discretisation of the described zones was required to be able to capture the adverse effects of the maldistribution. To do so, flow groups are defined that do not overlap at any point along the tubes. Within the flow groups, the sections and segments can be defined freely wherever necessary to capture sufficient flow detail.

A simple example of the Flow Group Discretisation method is illustrated in Figure 2.6. It shows two flow groups, denoted with a G, where each one contains 5 sections located at zones of interest. It is shown how the sections can vary in size in zones of interest. Unless geometrical or flow discontinuities exist, every flow group requires only one segment. This method is not as effective to capture thermal detail due to the separation restriction and therefore another method was developed when maldistribution is negligible.

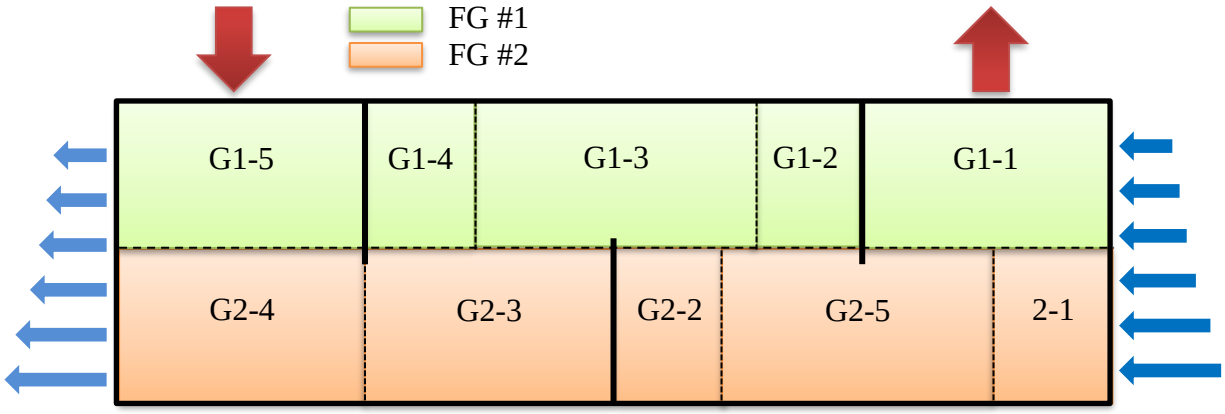

Figure 2.6: Flow group discretisation example.

2.4.2 Characteristics Discretisation

This method is referred to as the *Characteristics Discretisation* method as the location of defined sections depend only the characteristics of the flow within zones. Unlike the Flow Group Discretisation, flow groups overlap and sections and segments are defined freely. For instance, a domain can be discretised in cross-flow and window-type zones in a baffled STHX similarly to the study by Zaversky, Sánchez and Astrain (2014). This method is useful when precise control over the primary fluid temperatures are required, such as in disproportional heat transfer zones with high heat flux gradients. This method is especially useful for complex geometries and when additional heat transfer phenomena on the shell side need to be considered such as radiation.

The downside to this method is that a uniform mass flow must be assumed throughout all tubes as the scoping of the maldistribution to a particular group would be lost once groups overlap. Another slight downside is that every zone identified requires a segment of which each has a set of variables to transfer between solvers. If every segment still requires a polynomial representation of the auxiliary fluid, the amount of additional effort required to implement this method is noteworthy. However, using constant values for the transferring variables, which is suitable if segments are spaced reasonably close, would overcome this problem. In Figure 2.7 below, an example of this method is illustrated, which indicates segments appointed to expected cross-flow (X) and counterflow (C) zones, respectively. How the 1D network solver would be set up to model it is shown in Figure 2.7 b).

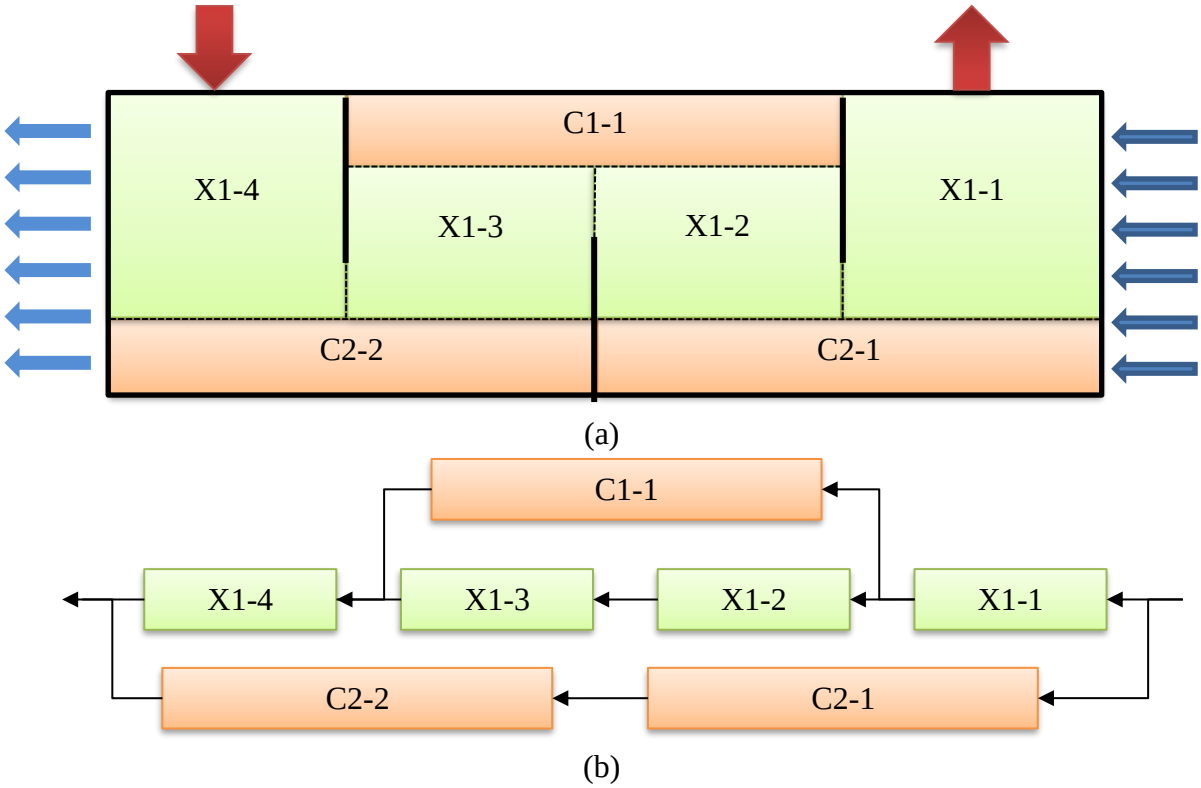

Figure 2.7: a) Heat transfer discretization counter and cross flow zone layout, b) 1D Network representation.

2.5 Mapping

The transfer variables that were discussed in the previous section must be mapped from the 1D network solver to CFD at the corresponding positions. As no third-party software was used, the network elements and CFD elements cannot be simply coupled in a node-by-node basis. This would also result in a greater computational expense. Rather, polynomial regression was used approximate the transferring variables' curves and then use the obtained coefficients for mapping purposes. The use of approximated polynomials is valid as no significant gradients in transfer polynomials are likely in segments due to the lumped sections. Also, it was found to be sufficient to use only second-order polynomials and even first order would suffice in many cases. The coefficients of the polynomials that are transferred between solvers were calculated using Excel's built-in functions and were in the form:

$$\phi(x) = ax^2 + bx + c \tag{2.1}$$

The dependent position values were expressed in terms of the global coordinates to ensure mapping from the network to the spatial domain was done from a common reference point. For instance, in the mapping of a straight pipe, the segment defined in the CFD solver must relate to the pipe component in the network solver. Therefore, the following expression must remain valid for each pipe component:

$$|X_0 - X_n| = L \tag{2.2}$$

where X_0 and X_n is the first and final coordinate respectively of the segment in CFD and L is the specified length of the 1D pipe component. The transfer variables from the CFD sections was mapped to the pipe nodes and vice versa. During the development, it was found that it was not possible to transfer the variables of all the 1D nodes due to software limitations. It was instead opted to create sections within the 1D network solver, and only a few values would be used. Again, the regions which required higher resolution can be defined accordingly. The positions of the CFD and 1D sections would typically not align due to the difference in discretisation between each. Therefore, each was treated separately with its position values for each section. The global coordinate midpoint of each section was used as the position coordinate and can either be calculated if sections were discretised uniformly or manually specified. The mapping procedure is summarised in Figure 2.8, which indicates example polynomial functions of the network and spatial domains, as well as the positions used to approximate these for a segment.

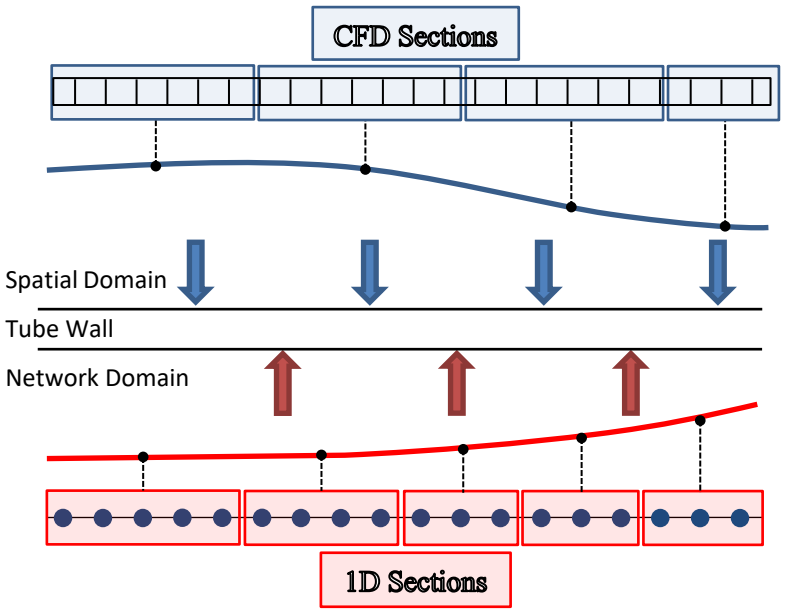

Figure 2.8: Mapping procedure example schematic of 1D and CFD zones.

The network approximating coefficients could then be transferred to the 1D pipe components using a heat distribution curve capability available in Flownex. The spatial approximating coefficients were transferred as scheme variables to Fluent, and by using a user defined function (UDF), the polynomial function can be fitted to the appropriate boundaries.

The mapping procedure for straight sections of tubes was a straightforward process, but a few additional adjustments were made for the U-tubes bend segment. The bend's section coordinates had to be transformed into a straight line to enable the use of the 1D solver's heat distribution curve. This was done by calculating the half-circle arc length, S_L, and is given by:

$$S_L = \pi \bar{R} \tag{2.3}$$

where $\bar{R}$ is the average radius of a flow group. The transfer variables along the arc length S_L were then mapped in a similar manner as described for straight pipes. After the 1D solver had completed its calculations, the 1D arc length was transferred back into the spatial domain. In Fluent, the UDF loops over all the faces of a boundary and returns their respective coordinates. These coordinates were used to determine the position of the arc using Equation 2.4 and were related to SL. The polynomials corresponding to the arc length could be mapped as straight lengths between software accordingly. For further reference, Appendix C contains the UDF, which includes the bend's mapping.

$$S_c = \left[\frac{\pi}{2} - \arctan\left(\frac{y}{x_0}\right)\right] R_W \tag{2.4}$$

The described mapping procedure diminishes the effects of lumping variables by applying a continuous distribution along the tube segments. This enables variability across segments to be captured which might have considerable effects, depending on the problem. The end result of the mapping procedure produces smooth transitions of transfer functions between segments and sections.

2.6 Solver Setup

This section describes the details of the setup of Flownex and Ansys Fluent. The most basic Flownex network for a straight segment is firstly described, followed by the CFD setup. Finally, the method in which data was transferred between the software is presented.

2.6.1 Flownex

The Flownex setup of a single segment is first described, this is the building block of the network model. Usually, several of these segments can be cascaded depending upon the problem. In Figure 2.9 below, this network model can be seen, and is referred to in all the explanations. The components are firstly discussed and thereafter the variables that are transferred by the data transfer links (DTL).

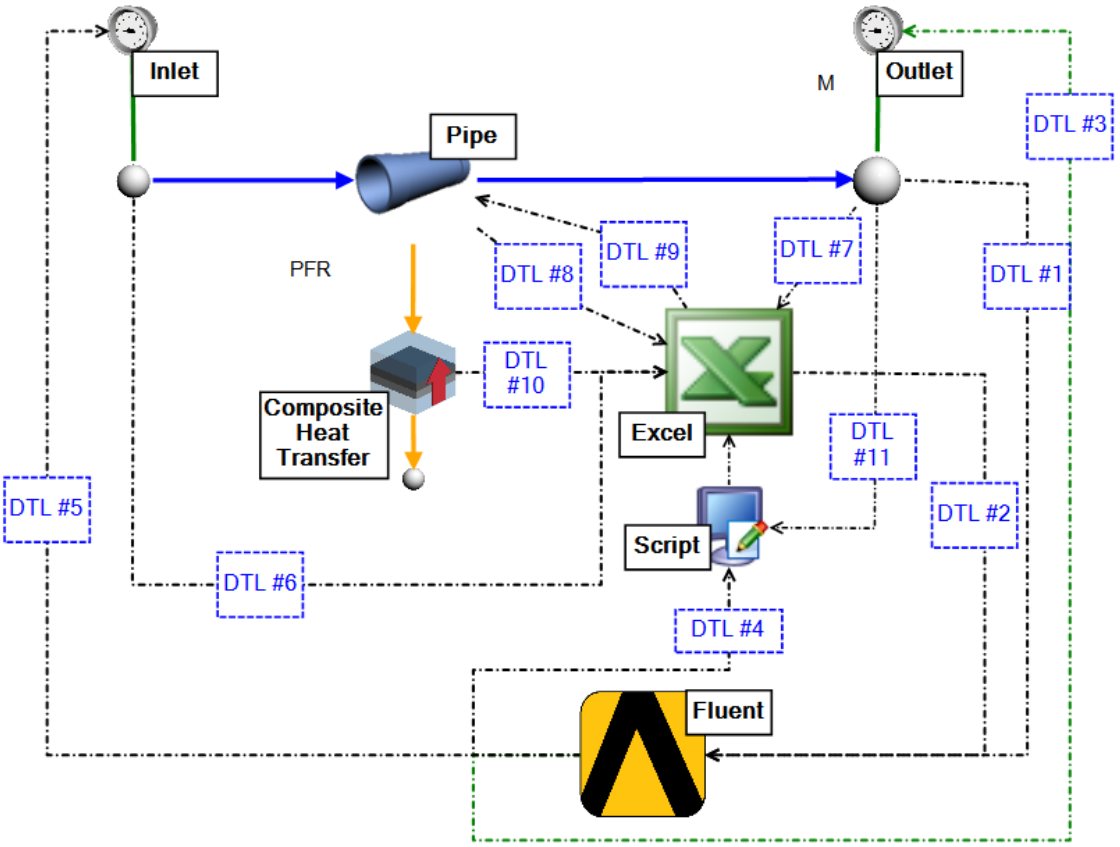

Figure 2.9: Flownex Segment Setup.

Pipe

Tubes are represented by the ‘pipe’ component in Flownex. Every segment is represented by a new pipe component. Every pipe component has geometrical inputs which include its length, diameter, surface roughness etc. It is convenient to multi-edit all the components that have identical parameters.

The pipe component can either represent all of the parallel tubes in its group or one of the tubes. There is no difference between these two methods in the results but only in the setup. For this project, the latter method was selected due to the simpler implementation. The data transfer to and from the pipe component includes the heat transfer rate polynomial coefficients calculated in an Excel workbook, as well as the mean fluid temperature to the same Excel workbook.

Script

Scripts are used to perform iterative calculations such as storing values, implementing relaxation factors and calculating custom values from numerical approximations. The scripts are convenient to use because a few of the solver inputs are already coded within and therefore fewer data transfer links are necessary to set up. The scripts use the programming language C and an example script is available in Appendix C.

Excel

An Excel workbook serves as the primary data storage and transfer tool. It is convenient to use as a summary of values can easily be observed for troubleshooting, and the use of the Excel's functions such as least squares approximations are essential for mapping purposes. An example of an Excel workbook can be seen in Appendix C. The Excel workbook receives the following inputs:

- Section heat transfer rate from Fluent
- Mean temperatures from Pipe nodes
- Heat transfer coefficients from Composite Heat Transfer component

The outputs from the excel workbook can be listed as:

- 1D polynomial coefficients of heat distribution to pipe component.
- CFD polynomial coefficient of convection coefficient and mean temperature to Fluent coefficient.

Fluent

The Fluent component is of the generic server type. This allows for the transfer of any variables using either scheme variables or parameters. This server type was preferred over the journal type of data exchange as it is better suited in terms of speed and reliability to transfer variables and set up. In the cases where there were multiple flow groups, a Fluent component was assigned to each flow group for organizational purposes. The Fluent component receives backpressures and polynomial coefficients, which then outputs the heat transfer rates obtained from the CFD sections.

Data Transfer Links

The DTL were used to transfer variables from one component to another during the simulation. It is required to explicitly specify that the transfer links should update during a transient simulation and before a steady state simulation so that information does not lag. Each DTL, as shown in Figure 2.9, are listed in Table 2.1 below:

Table 2.1: Flownex data transfer links.

DTL	Transferring Variables	From	To
#1	Outlet Temperature	Outlet Node	Fluent
#2	Convection polynomial coefficients	Excel	Fluent
	Mean temperature polynomial coefficients		
#3	Mass flow rate	Fluent	Outlet Boundary Condition
#4	Heat transfer rates of sections	Fluent	Script
#5	Inlet primary fluid temperature	Fluent	Inlet Boundary Condition
#6	Segment inlet temperature	Inlet Node	Excel
#7	Segment outlet temperature	Outlet Node	Excel
#8	Nodal temperature values	Pipe	Excel
#9	Heat distribution polynomial coefficients	Excel	Pipe
	Total heat transfer magnitude		
#10	Nodal convection values	Composite Heat Transfer	Excel
#11	Segment pressure loss	Outlet Node	Script

2.6.1 Fluent

The computational work was executed on the commercial software Ansys Fluent V19.4. Fluent is a fully three dimensional CFD tool based on the finite volume method and is currently one of the most well-known CFD packages. Steady and transient Reynolds averaged Navier-Stokes (RANS) equations of continuity, momentum, and energy are solved numerically to obtain results.

This section briefly describes the collective CFD setup for the simulated problems and briefly discusses the reasoning for specific choices. It includes the boundary conditions, solvers and turbulence models used. These CFD settings remained constant throughout all the simulations. The settings can considerably affect the results and need to be adjusted according to the problem type and flow phenomena specific to the problem. As there was no experimental data available, these settings might have possibly not been the ideal combination to represent the real flow problem. However, the decisions made in CFD models were based upon existing literature that modelled heat exchangers. It should be noted that regardless of the CFD settings, the 1D coupled and full CFD approach should compare well provided that the internal flow of the CFD is approximated

sufficiently. The reason being that the same shell-side flow is subjected to both methods. Nevertheless, a high-quality CFD analysis was conducted.

Geometry

All the geometries in this investigation were created using Ansys SpaceClaim. Implementing this methodology requires that no significant changes may be made to the standard CFD analysis geometry. The only alteration required was that surfaces had to be defined that corresponded with the locations of the discretised CFD sections. These surfaces can be created by splitting the tubes into separate neighbouring pipes or by splitting the surfaces which lie upon the tubes. Either way, a surface is explicitly defined during pre-processing or post-processing to extract averaged values from it. The sections are then named accordingly to the created surfaces that interface the network and spatial elements.

Mesh

After the geometry is modelled in SpaceClaim, it is required to be mesh for CFD. It was sought to mesh the model as coarse as possible while retaining values that were independent of the cell size. Therefore, a mesh independence study was performed for each simulated problem of which the results are available in Appendix A. Inflation layers at the boundary were required in order to ensure that the CHT and complex flows near the boundaries were captured sufficiently.

The mesh was created using the Ansys Workbench Mesher with the Ansys customisation toolkit (ACT) extension ‘Fluent Meshing’. To create the mesh, the appropriate boundary conditions were categorised into ‘Named Selections’. This is also an essential part of the methodology, as the Named Selections must correspond to the discretised sections so that the desired report variables may be transferred to and from those surfaces. In terms of improving modelling efficiency, each inner surface of every tube does not need to be manually selected. Macros exist that can select surfaces based on their size, type, and location within the cartesian coordinate system. This is useful if the geometry contains hundreds of tubes. The ACT Fluent Meshing extension automatically meshes the geometry and implements boundary layers in the fluid domain at all the fluid-solid boundaries, which are hexahedral cells. Nearly all remaining tetrahedral elements are then converted to polyhedral, which results in more efficient computing compared to the tetrahedral cells. A mesh independence study is essential for any model and is described in Appendix A.

CFD Methods

The pressure-based solver is an algorithm wherein the constraining of mass conservation of the velocity field is achieved by solving a pressure equation (Ansys, 2019). This solver is commonly used in CFD applications and was selected for this investigation as the Mach numbers of the flow in heat exchangers are relatively small. The Coupled Pseudo-Transient SIMPLE was used as the solution method, which is robust for achieving convergence in most cases.

The internal flow can range from a fully laminar case to a fully turbulent. The viscous sublayer could not be resolved due to the available computing power. It was, therefore, opted to use wall functions of which the mesh was required to produce y+ values between 5 and 300 for reasonable results (Ansys, 2019). The k-epsilon realizable model was selected based upon the features that it has, which is its superiority to capture the mean flow of complex structures compared to the standard formulation. The k-epsilon realizable model has been used in numerous studies that have modelled STHXs with results that generally correspond well with experiments. Scalable wall functions were used due to the variability in y+ values within the domain. However, when simulations were performed, it was observed that the vast majority of y+ values were between 22 – 150 for which the scalable wall function produces the same results as standard wall functions.

The convergence of the solution was dictated by the norm of the residuals and the outlet temperature of the primary and auxiliary fluid. The convergence criteria that were used is given in Table 2.2 below:

Table 2.2: CFD Convergence criteria.

Equation	Convergence Criteria
Continuity	1×10^{-4}
X-Velocity	1×10^{-4}
Y-Velocity	1×10^{-4}
Z-Velocity	1×10^{-4}
Energy	1×10^{-6}
Turbulence Kinetic Energy	1×10^{-4}
Turbulence Dissipation	1×10^{-4}
Outlet Temperatures	1×10^{-4}

All of the computations were performed on a desktop with the following hardware specifications: AMD Ryzen 7 2700X Eight-Core Processor rated at 3.7 GHz CPU, 32 GB 2400 MHz RAM, and NVIDIA GeForce GTX 1050 GPU. This desktop was sufficiently powerful to run all the simulations in a reasonable amount of time. The simulations were performed using parallel computing with 15 processes dedicated to solving. All the simulations were conducted on the described PC and the simulations that investigate the computational savings between methods were simulated with minimal background processes for consistent comparisons.

Boundary Conditions

The type of boundary conditions that were imposed on the problem consists of walls, inlets, outlets and symmetry. The coupled 1D and full CFD had the same boundary conditions in the spatial domain. The inlets were provided with a fully turbulent power-law velocity profile and were implemented using a UDF. The standard one-seventh power-low velocity profile

$$\frac{\bar{u}}{U_{max}} = \left(1 - \frac{r}{R}\right)^{1/n} \tag{2.5}$$

was used with an exponent $n = 7$, under the assumption that the flow was fully developed pipe flow at the inlet. The inlet turbulence conditions at the inlet could be described in terms of the turbulence intensity and the hydraulic diameter. The inlet turbulence intensity was calculated with the expression (Ansys, 2019).

$$I = 0.16 Re_{d_h}^{-1/8} \tag{2.6}$$

where Re_{d_h} is the Reynolds number based on the pipe hydraulic diameter. The outlets were specified as pressure outlets with zero-gauge pressure. The symmetry boundary condition was applied to the symmetry plane, which assumes a zero flux of all quantities across the boundary.

The walls were specified the non-slip condition with a roughness of 40 μm specified for the internal tube walls for the full CFD. The other surfaces were left smooth. For the thermal conditions of the wall, the outer walls were set as insulated boundaries as heat exchangers are typically insulated to increase efficiency. The interfaces between the solid and fluid media were specified as a coupled boundary condition which performs CHT as described in the previous section. For the interface between the 3D and 1D elements, a convection boundary condition was specified, which also enables a user to input the wall thickness and material of a tube to accounts for the tube's thermal resistance.

Media

The fluid media that were used was a selection of water-liquid, water-vapour and air. It is well-known that material properties are a function of several parameters, but in this investigation, the properties are only described in terms of temperature. The liquid-water properties given below are based upon the IAPWS IF-97 standard. The polynomials are in the following form in which the temperature is in Kelvin units:

$$\phi(T) = A_0 + A_1 T + A_2 T^2 + A_3 T^3 + A_4 T^4 \tag{2.7}$$

Table 2.3: Liquid water at 1 bar pressure.

Property	Unit	Polynomial Coefficients				
		A_0	A_1	A_2	A_3	A_4
ρ	kg/m^3	765.33	1.8142	-0.0035	-	-
C_p	kJ/kg·K	28.07	-0.2817	1.25×10^{-3}	-2.48×10^{-6}	1.857×10^{-9}
μ	Pa·s	9.67×10^{-2}	-8.207×10^{-4}	2.344×10^{-6}	-2.244×10^{-9}	-
k	W/m·K	-0.5752	6.6397×10^{-3}	-8.151×10^{-6}	-	-
β	1/K	-1.908×10^{-3}	7.318×10^{-6}	-	-	-

For the air, similar properties were defined in terms of the temperature. Although the purpose of this investigation is not to match experimental results, it was of interest to see whether the current default library is sufficient to obtain reasonable results. The air was modelled as an ideal gas with

density being calculated from the ideal gas law and the viscosity obtained from the Sutherland equation given as:

$$\mu = \frac{bT^{\frac{3}{2}}}{T + S} \tag{2.8}$$

where $S = 110.4K$ and $b = 1.458 \times 10^{-6}$. The other thermophysical properties of air at 1 bar in the form of temperature dependent polynomials are given in the table below:

Table 2.4: Air at 1 bar atmospheric pressure.

Property	Unit	Polynomial Coefficients			
		A_0	A_1	A_2	A_3
C_p	kJ/kg·K	0.9289	8.978×10^{-5}	3.246×10^{-7}	-2.625×10^{-10}
k	W/m·K	-3.933×10^{-4}	1.0184×10^{-4}	-4.857×10^{-8}	1.521×10^{-11}

For the water-vapour (steam), the density was modelled as an ideal gas which is reasonable for superheated steam at high pressures. The remaining thermal properties were described by polynomials of which the coefficients are given in the table below:

Table 2.5: Properties of water-vapour at 20 bar pressure.

Property	Unit	Polynomial Coefficients				
		A_0	A_1	A_2	A_3	A_4
C_p	kJ/kg·K	1563.08	1.6038	-2.933×10^{-4}	3.216×10^{-6}	-1.157×10^{-9}
k	W/m·K	-7.968×10^{-3}	6.881×10^{-5}	4.49×10^{-8}	-9.1×10^{-12}	6.173×10^{-16}
μ	Pa·s	-4.419×10^{-6}	4.688×10^{-8}	-5.389×10^{-12}	3.203×10^{-16}	-

2.6.2 **Flownex – Fluent link**

The Flownex network and the Fluent Model were set up separately, but to transfer data the software had to be linked. This section describes the software considerations relevant to coupling solvers. In a conventional full CFD approach, the simulation would obviously be controlled by Fluent, but in the coupled 1D method, Flownex controls the simulation. This includes the initialization, duration and time step sizes of the simulation.

As was previously mentioned in Section 2.6.1, the Fluent Generic component in Flownex was used to connect the software. The generic interface transferred the variables by means of updating input parameters or scheme variables using the Text User Interface (TUI) in Fluent. Initially, only input parameters were transferred, but it was found to take substantially more time to transfer data between software than scheme variables. The Flownex outputs would update at the start of a CFD simulation before any iterations were performed. The scheme variables were firstly initialized by using a scheme file which contained the TUI commands to define the scheme variables of all the mapping polynomial coefficients. The scheme variables were then incorporated and used within the

Fluent UDF. The Scheme file and UDF of the TEMA-FU type STHX is available in Appendix C for reference.

Another method exists which was used by Koekemoer, Du Toit and Kruger (2018) in which the journal link in Flownex was used. The Fluent journal link can be used to transfer data between Flownex and Fluent by means of a text file. This text file can be created in Ansys by recording the actions in which parameters are changed. Flownex then seeks these defined recorded command lines and alters the values to the output values. The journal file is read after each global iteration, and changes occur in the graphical user interface (GUI). This approach was also followed initially in this investigation. However, it was soon realized that it was significantly less computationally efficient and frustrating to set up.

The initialization of any model is performed as depicted in Figure 2.10 below. Flownex is started and the project is loaded, while the Fluent server is started with a batch file that also specifies the simulation settings. These settings include double precision accuracy and the amount of processes used. If there is a previously simulated case and data, it is loaded and blank iterations are performed to synchronise solvers. A steady state simulation is performed thereafter. Once completed, the Fluent case is set to a transient type from which a transient simulation commences.

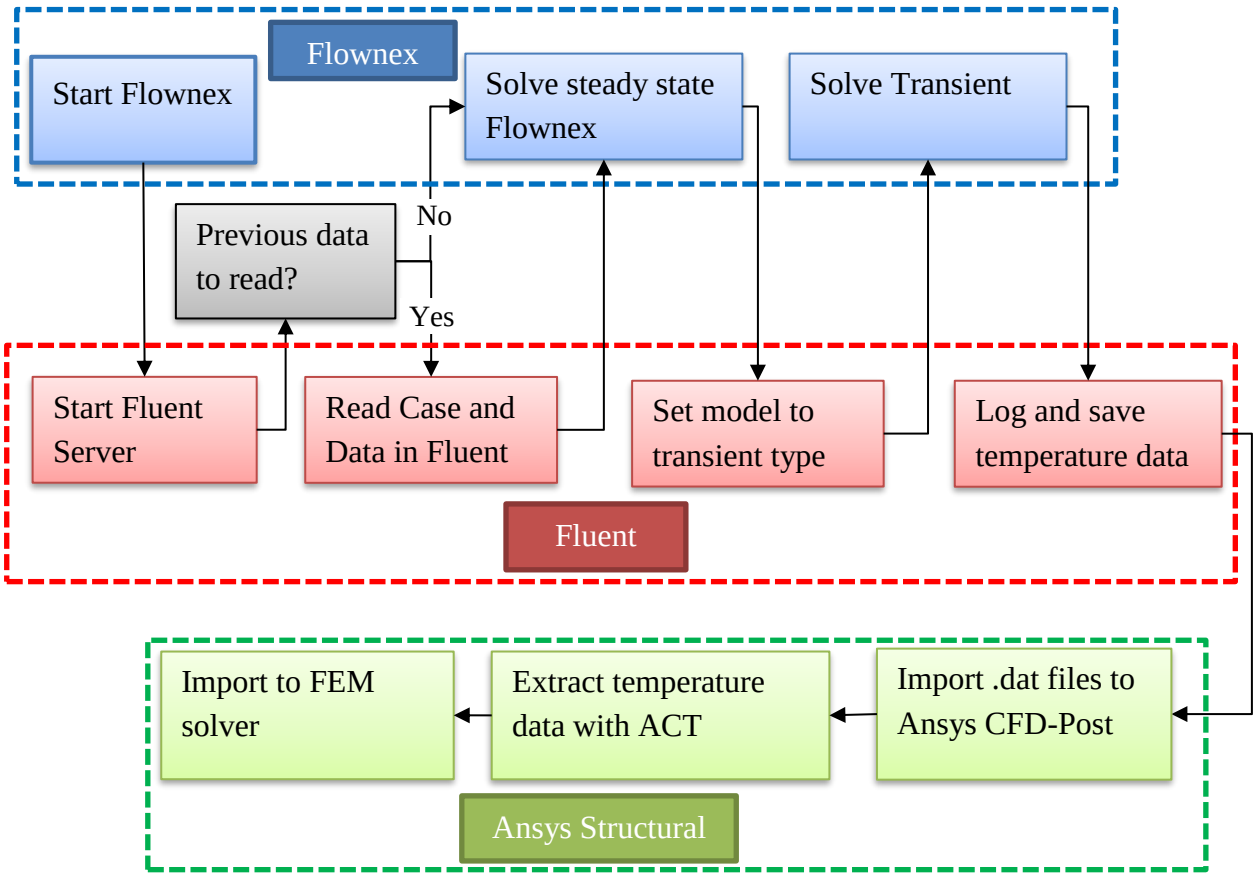

Figure 2.10: Software model initialization.

If a structural analysis due to the thermal loads must be performed, the time-dependent temperature data during the transient simulation is saved at specified intervals of timesteps. Although no structural analysis was performed in this investigation, the method of transferring data to a FEM code was still explored, and, arguably, the simplest is presented here. The saved temperature data can be exported to Ansys CFD-post in which an Ansys ACT called 'FSI Transient Load Mapping' is employed. The ACT extracts the temperature values for every node and timestep and creates data files compatible for a structural analysis. These data files can be imported to a structural analysis by using the 'External Data' component in Ansys. This tabulates the temperature values of each node for every timestep in the correct format.

2.7 Conclusion

This chapter presents the methodology that is applied for both parts of the investigation. It discusses the coupling process and algorithms that allows for 1D network and 3D CFD elements to be coupled. Considerations are made towards improving the convergence rate by implementing relaxation factors, global iteration trigger timings, and Gauss-Seidel numerical schemes. Two methods to discretise the 1D elements and their applications are described. The mapping procedure between software that uses polynomial regression to fit a curve to obtained section values is presented. The Fluent and Flownex setup are discussed as well as the procedure for performing a co-simulation. Finally, the method of transferring the thermal loads to a structural FEM solver for a one-way FSI is briefly described.

3. TEMA-FU type STHX

Section 1.4 introduced the TEMA-FU type heat exchanger and the methodology described in Chapter 2 was used to model this problem. However, this problem has unique setup considerations and approach characteristics are not described in the general methodology and are therefore presented in the following sections. Afterwards, the results of the various analyses are presented and discussed.

3.1 Problem Setup

This section describes the details of the design and setup considerations that are specific to this problem. This includes geometrical, numerical and software considerations. The decisions that were made between the various options presented in the methodology are also discussed.

3.1.1 Geometry

The geometry was designed to be compact to reduce mesh size so that re-runs could be easily performed when adjustments were made. This resulted in a relatively small heat exchanger whilst in industry FWHs are much larger and longer. To further reduce mesh size, the geometry was modelled symmetrically in the Y-Z plane so that the symmetry boundary condition could be applied. The geometry is symmetric in the X-Z plane as well, but the flow is not and a symmetry boundary condition, therefore, could not be applied. For reference purposes, a full section view of the final CAD geometry can be seen in Figure 3.1 below.

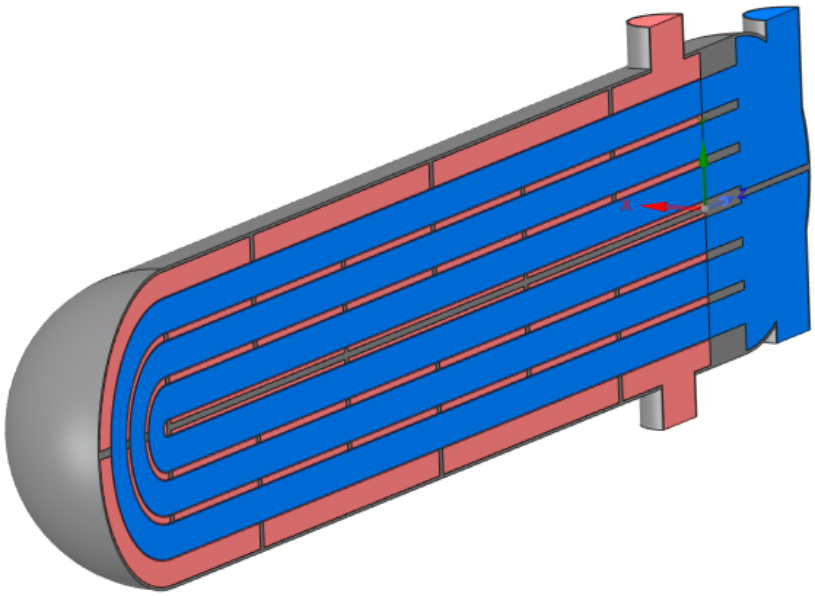

Figure 3.1: Geometry of FWH-FU.

The baffles were spaced evenly and at lengths that promoted transverse flow across the tubes. The commonly used range of baffle spacing is typically between 0.1L and 0.3L. The baffles were spaced 240mm from each other. The baffle cut was selected to be between 0.2D to 0.25D, which is commonly used in heat exchanger design (Than, Lin and Mon, 2008). There was no need for an optimal baffle sizing and spacing, but it allowed for a more realistic representation. The auxiliary fluid was subjected to a two-pass flow which meant a longitudinal baffle was modelled.

The channel side consisted of a feedwater inlet and outlet. The inlets were directed radially which is quite common in STHXs. A tubesheet was modelled that was 100 mm thick to analyse the temperature gradients along the tubesheet on the channel and shell side. This temperature gradient was essential to evaluate as it is the cause of the high thermal stress regions within an industrial tubesheet. A summary of the model dimensions is given in the table below.

Table 3.1: TEMA-FU Geometry sizes

Property	Symbol	Size (mm)
Outer Diameter	D	384
Shell Thickness	t_s	4
Tubesheet Thickness	t_t	100
Tube inner diameter	d_i	41
Tube thickness	t	1.5
Shell length	L	1500
Material	-	Stainless Steel

3.1.2 **Mesh**

The mesh of the problem was generated using Ansys Meshing as well as ICEM Meshing which is superior in creating structured meshes. An initial mesh was generated using an Ansys Fluent meshing ACT which could generate a sufficient mesh with minimal pre-processing effort required. The mesh was quite coarse, and the majority of elements were polyhedral elements while the inflation layers were hexahedral. This was by no means an ideal mesh but served the purpose of performing many simulations in a short time to develop the methodology. The general mesh can be seen in the following figure:

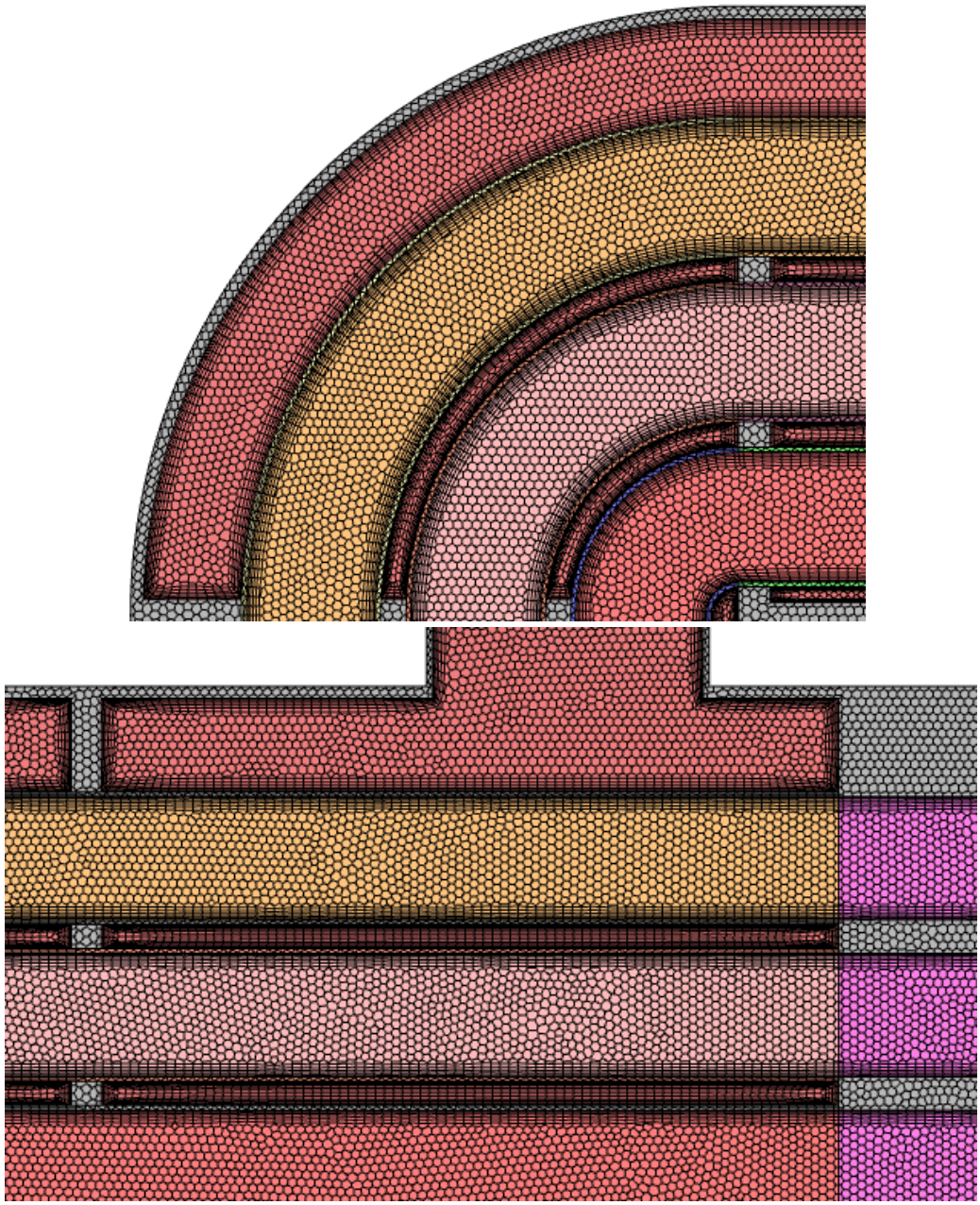

Figure 3.2: Initial mesh of TEMA F type heat exchanger.

The final mesh was created using ICEM meshing, which was also used to evaluate the previous elementary mesh. The results compared very well, however, the simulation time using the structured mesh reduced significantly as was expected. The structured mesh can be seen in the following figure and is apparent that the majority of elements are high-quality hexahedral elements.

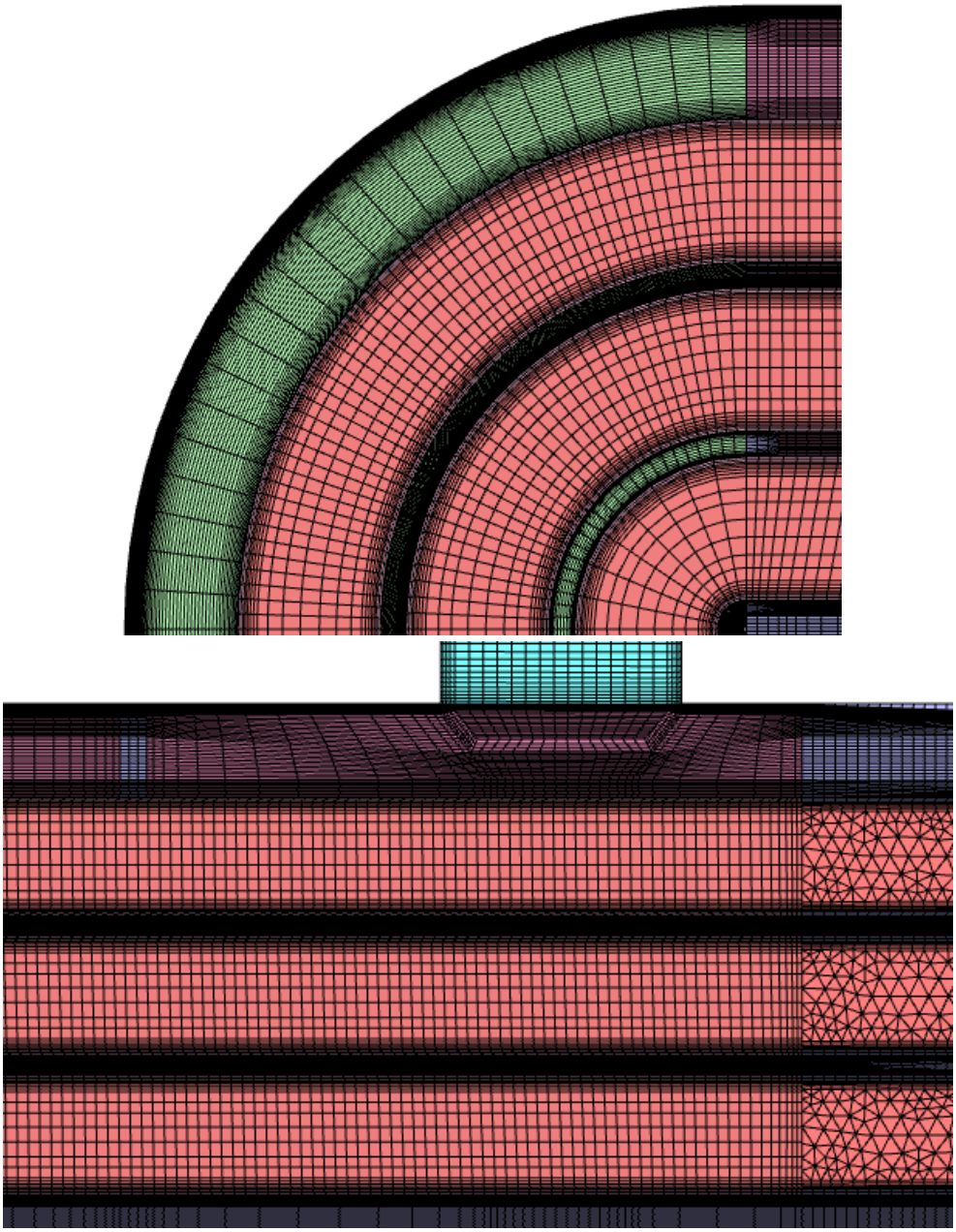

Figure 3.3: Final mesh of TEMA F type heat exchanger.

A mesh independence study was performed to ensure that the results were unaffected by the size of the mesh. This resulted in using a mesh that wasn't excessively fine nor one that was too coarse which could result in an inconsistent solution. The details of the mesh independence study can be found in Appendix A.

3.1.3 Network Solver

The Flownex model could be set up according to the discretisation of this problem. Two flow groups were assigned as the 'low', and 'high' mass flow groups after the results of the zero backpressure were obtained. Furthermore, the model existed out of three segments that were assigned, which represented the two geometrical straight sections and the bend in between. The straight segments each had 3 sections from which the heat transfer rate $\dot{Q}$ from Fluent could be obtained. The bend was assigned only 1 section due to its small area. The internal convection coefficients of all the tubes were calculated using the Gnielinski's correlation. For laminar flow, $Nu = 4{,}36$ and the downstream tube's Nusselt number was adjusted according to Abdelmessih's (1979) correlation to account for the induced secondary flow from the bend. For pipe pressure losses, the Colburn correlation was employed for all internal flow.

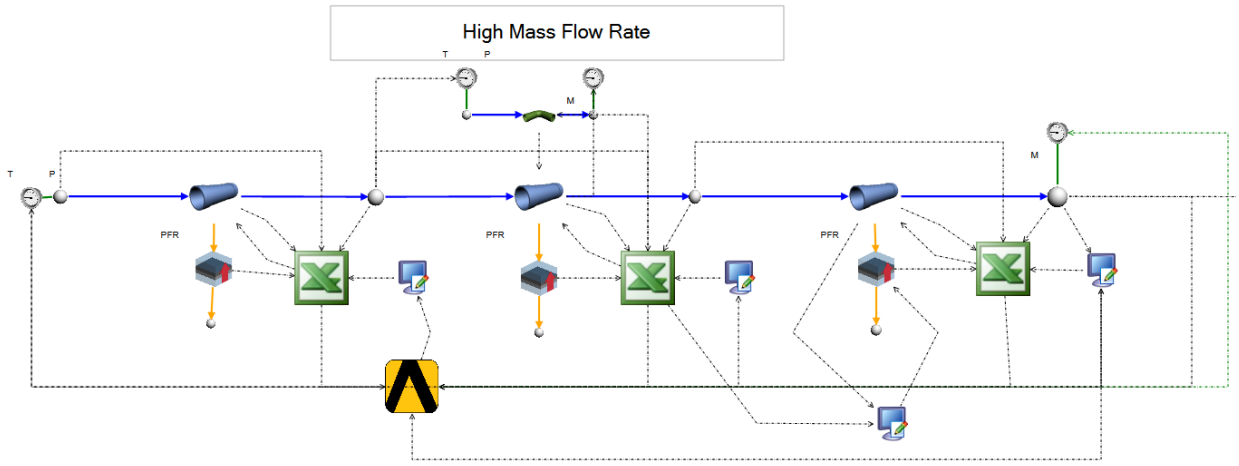

Figure 3.4: Flownex TEMA-FU type flow group network.

Each segment had its parameters and inputs that needed to be transferred to Flownex. The Flownex network of a flow group can be seen in Figure 3.4. The network did not take long to set up as the template segment model could be copied and pasted, and only the transfer links to the Fluent component had to be defined.

3.1.4 Design of Analyses

This section describes the various analyses conducted and their justification to be included in this study. The most important evaluation parameter was the temperature distribution on the tubesheet while the outlet temperatures also aided towards evaluating the overall performance of the cases.

Maldistribution

The first analysis was to evaluate the proposed 1D coupled flow maldistribution methods with CFD. These methods are described in Chapter 2. It was to be determined whether there was indeed significant flow maldistribution and if it could be modelled using a 1D-CFD coupled approach. This is important as flow maldistribution can have a substantial effect on the heat transfer. Three methods

to model maldistribution were identified and compared with a full CFD. These were in the form of boundary conditions and are listed as:

- *Zero backpressure* assumes that the outlet of the CFD domain has a backpressure $P_b = 0$.
- *Analytical* boundary uses the parallel pipe theory (PPT)
- *1D-CFD* boundary condition is the iterative method that adjusts the backpressure based upon the CFD results.

Average Reynolds numbers in the tubes between 12000 and 17000 were simulated. The flow maldistribution was evaluated based upon the percentage of maldistribution as well as the error between each method and the full CFD approach.

Reynolds number

In this simulation, steady state results were obtained by varying flow rates of the auxiliary and primary fluid. This sought to show the applicability of the proposed methodology in certain cases and where it can fall short. Simulations were performed with liquid water as the primary and auxiliary fluid to avoid compressibility in high flow rate cases. The Reynolds number of the primary fluid within the tubes ranged from laminar (Re < 2300) to turbulent (Re > 4600) flow with emphasis on the turbulent cases which are much more common in industry. The cases that were run was done with liquid water as primary and auxiliary fluid with temperatures of 5°C and 150°C respectively.

Four different primary fluid flow rate cases were simulated, and the outlet temperatures of the primary and auxiliary fluid were to be compared against the full CFD model. The temperatures along the tubesheet on both the channel and shell side were also compared so that it could be established whether the 1D-CFD approach is suitable for stress calculations.

Media

A discrete variation in the fluid media was simulated both for the primary and auxiliary fluid. Slight changes in the mesh were required in order to adhere to the y+ values. Three cases were simulated, which were a combination of either air-air, air-water or water-air as the primary-auxiliary fluid types. The reason for varying the media is again to determine the range of applicability and where shortcoming might arise. The temperatures and mass flow rates at the inlets are varied with the three cases to induce substantial temperature variation between the inlet and outlet of both fluids.

Transient

If the steady state simulations provided reasonable results, a transient simulation would be the next step to ensure the 1D pipe flow differential equations, with time dependencies included, match CFD capabilities. The types of transients that are present in heat exchangers are changes in the inlet temperature, flow rate and pressure. The fluid medium was for both the primary and auxiliary fluid selected to be liquid water. The capability of the methodology to capture transients was thoroughly tested by applying step changes to the input parameters and comparing the response with full CFD. Two cases were simulated, of which the first was a basic step in the primary fluid's temperature,

while the second was a combination of steps in temperature and flow rates of the primary and secondary fluid.

3.2 Results and Discussion

This section presents the results that were obtained from the simulations. The results are critically discussed in terms of the deviations between the CFD and the proposed methodology.

3.2.1 Maldistribution

Analysing the flow maldistribution required that flow groups be assigned. This was done by evaluating the velocity contours of a zero-backpressure case and assigning flow groups accordingly. The velocity contour of a zero-backpressure case can be seen in Figure 3.5 below from which two flow groups could be identified. It is evident from the figure that the bottom tubes have a higher degree of flow than the upper tubes. This is due to the impinging flow onto the channel separator, which has a direct path to the bottom tubes. The two newly defined flow groups are referred to as the '*high*' and '*low*' mass flow groups.

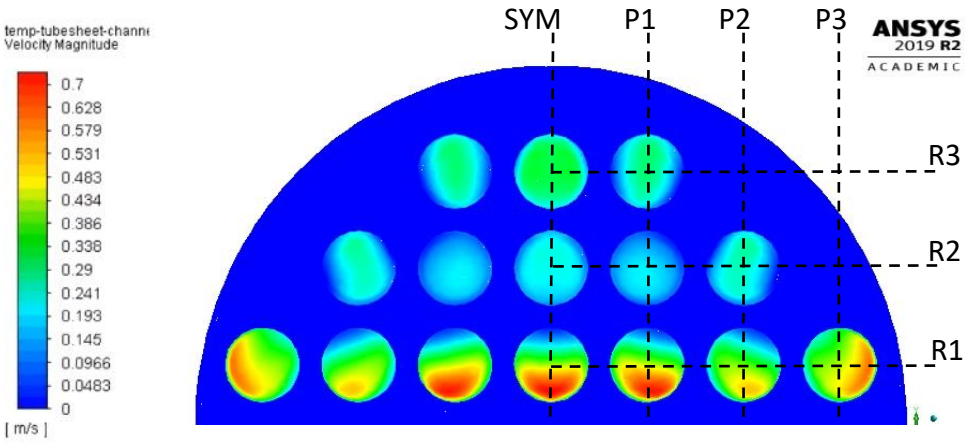

Figure 3.5: $P_b = 0$ velocity contour into tubes ($Re = 17000$).

As was discussed, two cases for different Reynolds numbers were simulated for each method. The results are presented in Table 3.2 below. It can be seen that the full CFD results indicate approximately 29% of flow maldistribution between the two assigned groups. This is quite significant and will adversely affect the heat transfer between the fluids and to the tubesheet. It was interesting to find how consistent the results between each of the methods differed with varying Reynolds numbers. The effect of the Reynolds number on the maldistribution for this problem and range could be regarded as negligible, and the flow distributes in the same proportion.

It is clear from Table 3.2 that the 1D-CFD approach corresponds best to the CFD and using a backflow pressure equal to zero the worst. The analytical solution underpredicts the maldistribution, which is expected as no biased flow into specific tubes could be accounted for in its formulation. Conversely, the zero-backflow pressure method overpredicts the maldistribution significantly,

which is also expected as higher inlet flow resistance is anticipated in higher mass flow groups which this method neglects.

Although the 1D-CFD coupled method obtained outstanding accuracy compared to the CFD, it was challenging for the solution to converge due to the stiff relaxation factors that were specified. Triggering a global iteration more frequently partially solved this problem and was noted to incorporate for subsequent simulations. The 1D-CFD approach also overpredicts the maldistribution slightly and could perhaps have been improved by adding the loss coefficients of the inlets and outlets.

Table 3.2: TEMA-FU type flow maldistribution results summary.

Case	Method	Group Velocity [m/s]			Error
		Low	High	Difference	
Re = 12000	CFD	0.230	0.296	28.7%	-
	$P_b = 0$	0.185	0.348	88.8%	18.7%
	1D-CFD	0.224	0.303	35.5%	2.6%
	Analytical	0.259	0.263	1.8%	11.7%
Re = 17000	CFD	0.325	0.421	29.5%	-
	$P_b = 0$	0.260	0.495	90.1%	18.7%
	1D-CFD	0.314	0.433	37.8%	3.1%
	Analytical	0.366	0.374	2.4%	11.8%

The graphical results of the flow within each of the tubes is shown in Figure 3.6 below. In Figure 3.6 a) the full CFD results of all the tubes are summarised with respect to the pitches defined in Figure 3.5. It can be observed that there is indeed a preference of flow into the tubes of Row 1. For better accuracy, it would have been beneficial to assign three flow groups along each row rather than two, as there is also a difference in flow rates between Row 3 and 2. Subplots b) - d) show the comparison of the coupled 1D-CFD and the zero backpressure methods to the CFD results. The results of Table 3.2 are confirmed.

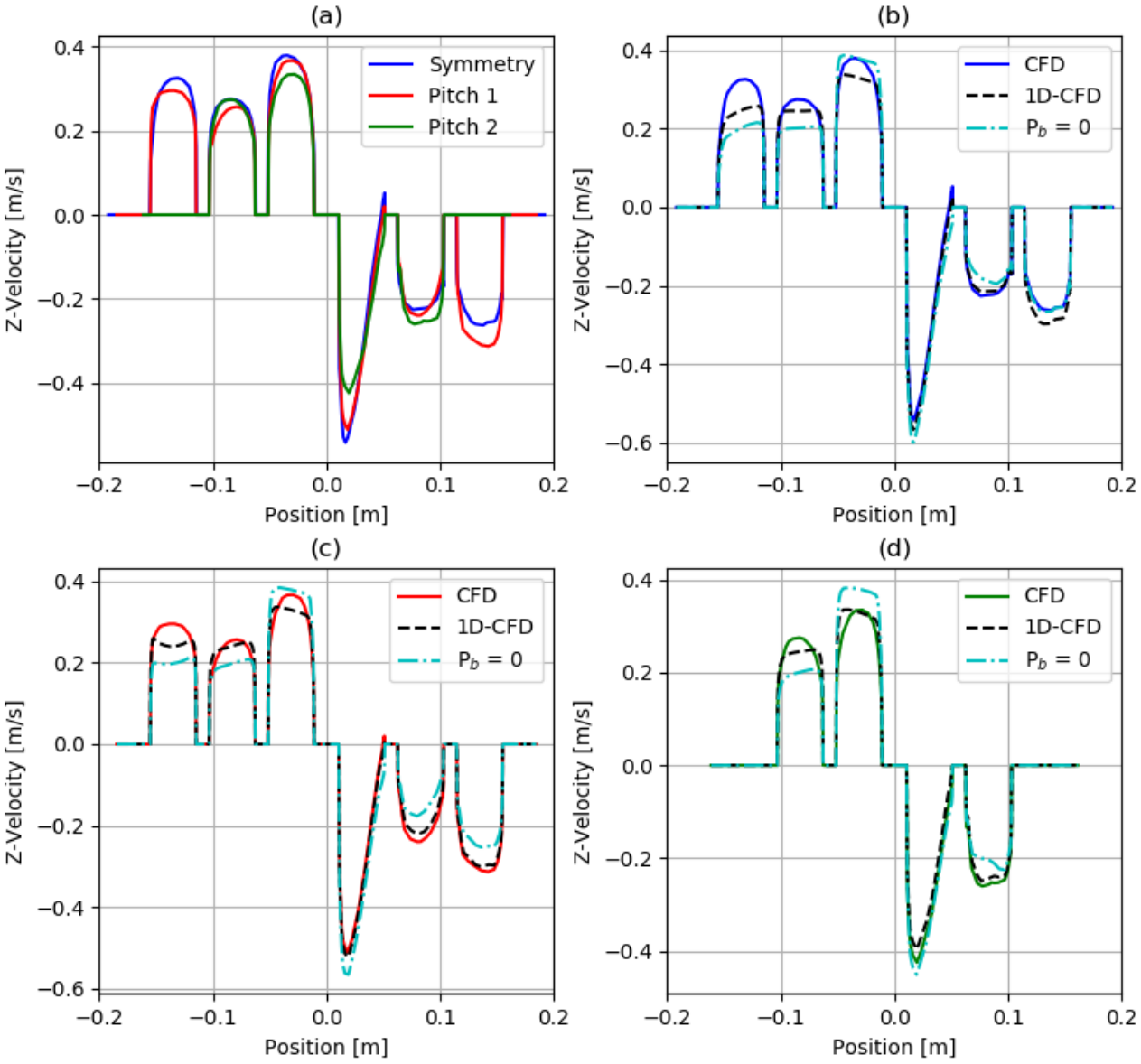

Figure 3.6: Tube velocities along tubesheet a) CFD results summary, b) Symmetry, c) Pitch 1, d) Pitch 2.

It should be noted that the flow in the negative region of the CFD was fully developed while the 1D approximations were not. Defining fully developed profiles to each tube proved to be challenging to implement as hundreds of tubes may exist in a group and allocating individual boundary conditions was not as straightforward as it seems. Consequentially, the radial heat transfer into the tubesheet from the tubes at the outlet section inaccurate. However, the solution to this problem was to overwrite the spatial domain heat transfer into the tubesheet by 1D fully developed tube correlations. This solution proved to be adequate in subsequent simulations.

In the later stages of simulating, a transient analysis was conducted in which a mass flow and temperature step to the primary fluid inlet condition was applied. After performing the simulations, the behaviour of the convergence between the different flow groups could be analysed, and the significance of the flow maldistribution was apparent. The primary outlet results are presented in Figure 3.7 below, in which the intuitive effects of flow maldistribution can be confirmed. In Figure

3.7 a), it was observed that the flow rate does not remain uniform immediately after the step, like the analytical solutions for incompressible flows would. It displays an overdamped response, similarly to spring theory, as the pressure coupling algorithm stabilises with time. This highlights the stiffness of the relaxation factors as well. Figure 3.7 b) indicates that the outlet temperature of the 'high' group is lower than the 'low' group at steady state conditions due to its higher heat capacity. However, the temperature of the 'high' flow group surpasses the 'low' group as the temperature step propagates at a higher velocity through the tubes and reaches the outlet earlier. In volatile transient conditions, this may have a substantial effect.

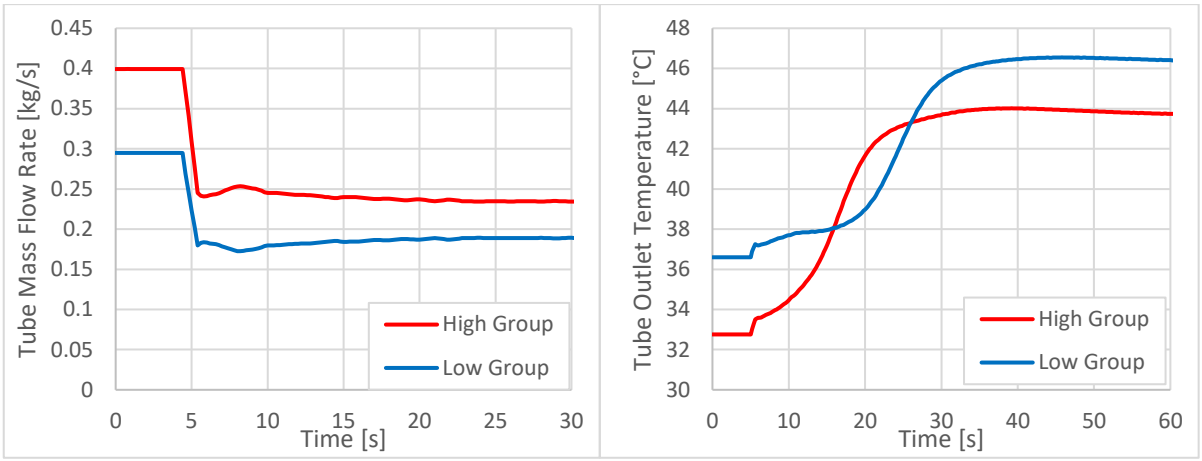

a) b)

Figure 3.7: Significance of 'high' and 'low' flow group in a transient simulation; a) Mass flow rate, b) Temperature.

The flow maldistribution was simulated, and results were obtained for four different methods for two flow cases. The proposed 1D-3D coupling method proved to be most reliable as compared to the CFD, but there were indeed areas where improvements could be made. These were discussed.

3.2.2 Reynolds Number

The outlet temperatures of the primary and auxiliary fluid were evaluated as well as the tube sheet temperature distribution along the symmetry plane. Contours of the velocity distribution are presented to validate the flow rate group assignment. The first set of simulations pertained to the variation of the primary fluid flow rate. The cases and outlet results are given in Table 3.3. The error between the 1D-3D coupled approach and full CFD was based upon the logarithmic mean temperature difference (LMTD) which is given by:

$$\Delta T_{lmtd} = \frac{\Delta T_1 - \Delta T_2}{\ln\left(\frac{\Delta T_1}{\Delta T_2}\right)} \tag{3.1}$$

where $\Delta T_1 = T_{h_i} - T_{c_i}$ and $\Delta T_2 = T_{h_e} - T_{c_e}$ and the subscripts h and c denote the hot and cold fluids respectively. Four different cases were simulated with varying Reynolds numbers. These results are presented in Table 3.3 below, which give the outlet temperatures of the primary and auxiliary fluids as well as the LMTD.

Table 3.3: Variation of primary fluid Reynolds number results for STHX.

Primary Fluid Inlet		CFD [°C]			1D-CFD [°C]			Error
Tube Re	Mass Flow Rate [kg/s]	$T_{e,p}$	$T_{e,a}$	LMTD	$T_{e,p}$	$T_{e,a}$	LMTD	
1800	0.77	57.21	136.69	111.11	63.76	133.08	106.66	-4.00%
7000	3.01	43.05	112.32	107.13	41.06	114.31	109.13	1.86%
12000	5.15	35.77	97.74	103.11	34.75	99.60	104.59	1.43%
17000	7.30	30.97	87.51	99.66	30.26	89.22	100.94	1.29%

As can be seen, the most significant discrepancy was the laminar flow case with an LMTD error of -4.0%, which indicates that the 1D-CFD approach resulted in more heat transferred between fluids than the CFD did. This indicated that the implemented downstream correlation over approximated the induced turbulence of the bend. Further revisions to the laminar model and correlations could be beneficial, but this study is more concerned with the turbulent flow. However, the three turbulent flow cases' results matched very well with a very slight improvement in accuracy as the Reynolds number increased. All three turbulent cases indicated that the 1D-CFD approach estimated slightly less heat transfer compared to the full CFD. The speculated reason is that the induced turbulence resulting from the bend was not accounted for turbulent flows. This reason was supported by the consistent increase in accuracy as the Reynolds number increases and the secondary flow from the bends became less significant.

The temperature variation of the symmetry plane can be seen in Figure 3.8 below for the Re = 12000 CFD case. It is evident that the top and bottom regions of the tubesheet have significant temperature gradients. This is confirmed in Figure 3.9, which displays the temperature contours of the shell and channel-side, respectively.

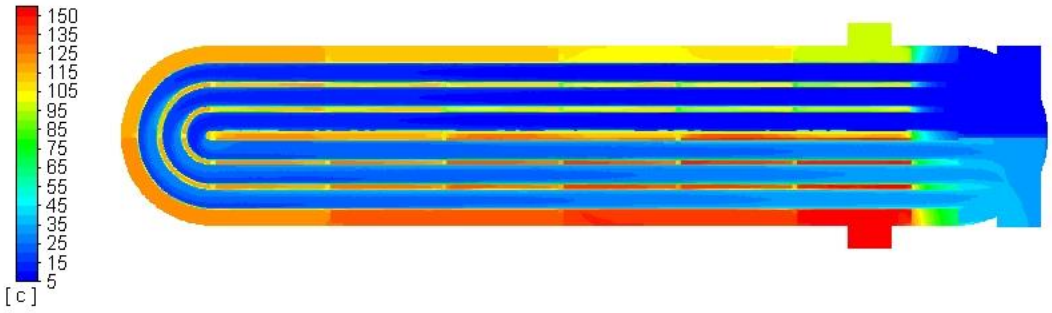

Figure 3.8: Re = 12000 CFD Symmetry temperature contour.

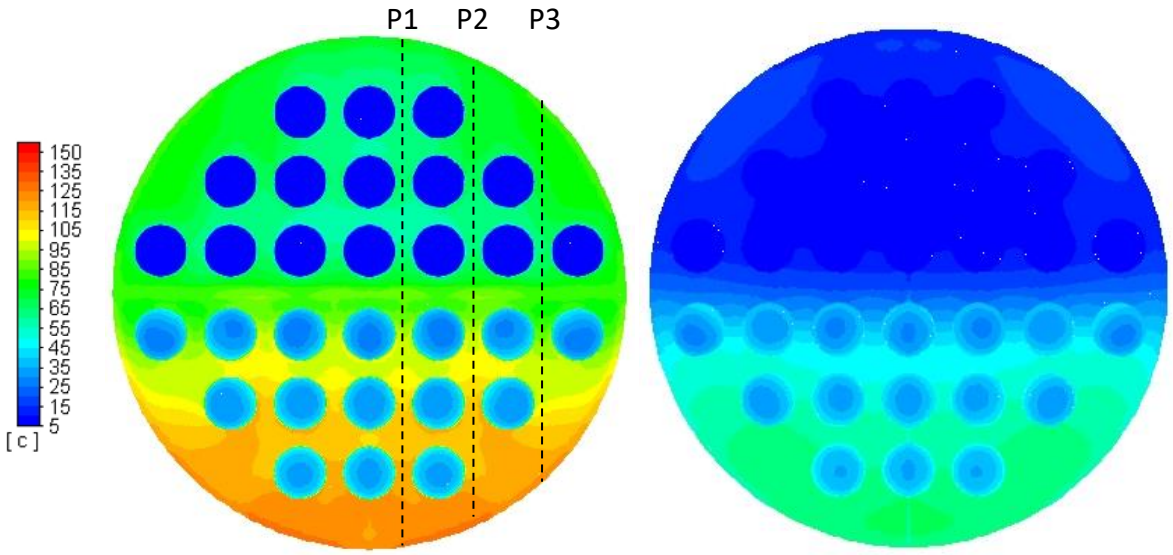

a) b)

Figure 3.9: a) Shell-side CFD contour; b) Channel-side CFD Contour.

In Figure 3.9 above, the temperature contour plot of the shell and channel-side emphasizes the significance of the temperature gradients. The dashed lines indicate the pitch lines for which temperature values were extracted and plotted so that the coupled 1D and full CFD approaches could be compared quantitively. Figure 3.10 graphically represents the distribution where a negative x-value corresponds to the bottom of the tubesheet, where the hot auxiliary fluid enters and primary fluid outlet and vice versa for a positive x-value. Figure 3.10 (a) depicts the temperature variation between the different pitches of the full CFD results. Figure 3.10 (b), (c), and (d) indicate each of the pitch comparisons between the methods. A good agreement between the results can be observed, especially in the positive y-value region. Notable discrepancies exist in the negative y region with temperatures of both the steam and channel side slightly lower for the 1D-CFD method compared to the CFD. The most considerable difference is approximately 5 °C which is unexpected because the outlet temperatures differed with less than 1 °C. Nonetheless, the results are reasonable for the reduction in computational time which is discussed in the following section.

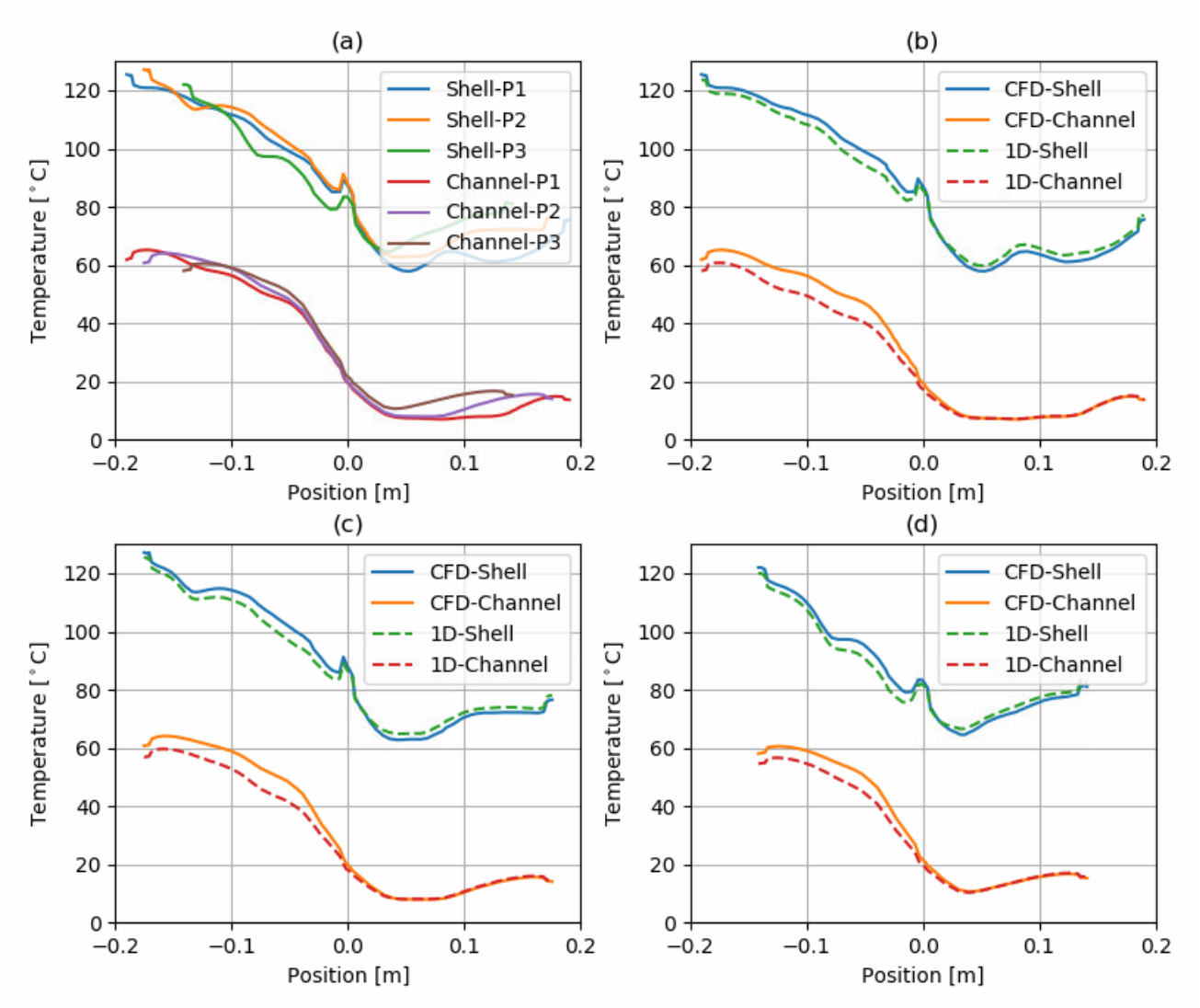

Figure 3.10: a) CFD Summary of pitch temperatures; b) Comparison pitch 1; b) Comparison pitch 2; b) Comparison pitch 3.

Convergence and Computation

From the results, the reduction in computational time was compared between the 1D-CFD and full CFD approach. The computational time and amount of iterations for both methods are provided in Table 3.4 below. It is evident that the reduction in computational time is consistently about 44% for all cases. However, this value is highly dependent upon the problem and could vary substantially based on the problem and extent of 1D elements used. It was observed that the 44% reduction was closely related to the reduction in mesh size between the two methods. The 1D-CFD mesh and full CFD consisted of approximately 2.3 million and 3.7 million elements, respectively. This was approximately a 38% reduction in mesh size.

Table 3.4: Computational time results.

Re	Full CFD			1D-CFD			Time Reduction
	Time/Iter [s]	Iterations	Total Time [h]	Time/Iter [s]	Iterations	Total Time [h]	
1800	18.07	545	2.75	9.49	533	1.55	43.8%
7000	18.64	560	2.91	9.92	535	1.62	44.4%
12000	18.05	603	3.04	10.43	539	1.72	43.5%
17000	18.19	608	3.09	10.35	538	1.70	44.9%

The 1D-CFD method certainly has a computational advantage in both the time/iteration as well as the total number of iterations required. The reduction in time/iteration was due to the reduction in mesh size. The 1D-CFD method used less iteration due to the Pseudo Transient solution algorithm that was employed. The primary fluid in the 1D-CFD method does not propogate through the tubes in the Pseudo scheme in CFD as it was modelled with 1D-elements and, therefore, the pseudo solution time decreases, and the outlet temperature respond faster. The difference in the number of iterations was considerable but not substantial. This is highlighted in Figure 3.11 below which is an example of the outlet temperatures as the solution converges. It is clear that the primary and auxiliary fluid reaching a converged state in fewer iterations compared to the CFD method. Figure 3.11 also highlights the global iteration triggers in the form of stepping primary fluid temperatures. The auxiliary fluid is not sensitive the steps due to the Pseudo transient solving algorithm. It can be deduced that the choice of solving algorithm certainly affects the convergence.

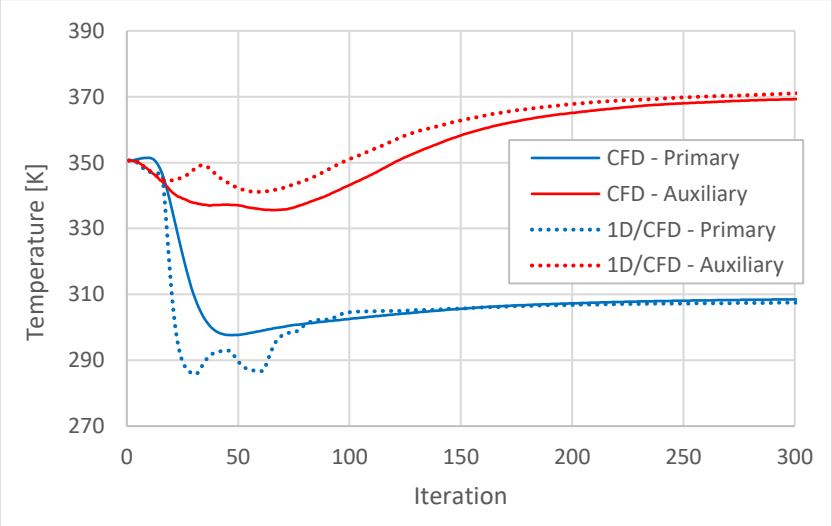

Figure 3.11: Outlet temperatures vs. number of iterations for both methods.

3.2.3 Media Variation

In the previous cases, liquid water was selected as both the primary and auxiliary fluids. The results in this section investigates the effects of media selection between air and liquid-water. This further evaluates the proposed methodology's range of applicability. The cases were designed such that it tested a variety of temperature distributions in the primary and auxiliary fluid. This resulted in unique temperature distributions on the tubesheet, and the full extent of the methodology application was therefore verified. The input parameters of the three simulated cases, in a primary-auxiliary fluid format, are presented in the following table:

Table 3.5: TEMA-FU type media variation case summary.

Case	Primary Fluid Inlet		Auxiliary Fluid Inlet	
	Temperature [°C]	Mass Flow Rate [kg/s]	Temperature [°C]	Mass Flow Rate [kg/s]
Water-Air	5	3.01	800	0.20
Air-Air	5	0.10	800	0.10
Air-Water	5	0.10	150	2.00

The cases were set up and simulated as described, from which a summary of the macroscopic heat exchanger results can be found in Table 3.6 below. The results indicate reasonable accuracy with the LMTD errors between the coupled 1D-3D and full CFD approach at a maximum of 3%. Again, the LMTD of the coupled approach resulted in an underestimation of heat transfer which is not conservative from a design perspective.

Table 3.6: Media variation macroscopic results.

Case	CFD [°C]			1D-CFD [°C]			Error
	$T_{e,p}$	$T_{e,a}$	LMTD	$T_{e,p}$	$T_{e,a}$	LMTD	
Water-Air	17.02	50.04	258.42	16.98	51.75	261.24	1.09%
Air-Air	395.73	409.29	404.28	383.96	421.82	416.43	3.00%
Air-Water	117.98	148.64	74.36	117.60	148.70	74.72	0.48%

The contour plots of the CFD symmetry plane temperature for the three cases can be seen in the Figure 3.12 below. It is evident that all the results indicated very different thermal characteristics in which the water-air and air-water cases almost have the opposite result. As expected, in these two cases the water remains at a relatively constant temperature while the air changes drastically due to its lower heat capacity. It was shown that the significant temperature gradients could be captured by the 1D approach using the polynomial mapping procedure as described in Section 2.5.

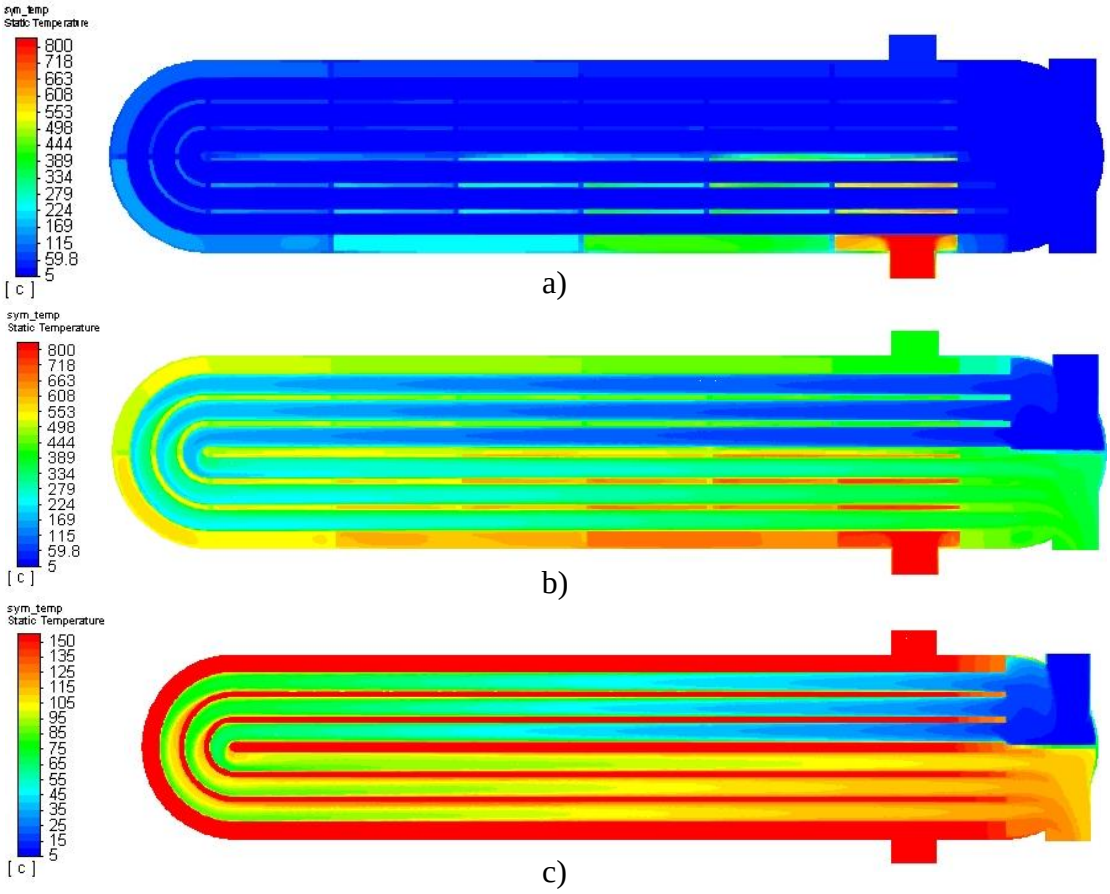

Figure 3.12: Media variation symmetry temperature; a) Water-Air, b) Air-Air, c) Air-Water.

As before, a more quantitative measure of results is presented by graphing the tubesheet temperature at position P1 for all three media variations and is provided in Figure 3.13. It can be seen that the 1D-CFD method's temperature distributions align tremendously well with the full CFD for both the shell and channel side. The temperatures in the positive x-coordinates matched exceptionally well due to the negligible change in temperature of the feedwater from its inlet. Downstream, the feedwater undergoes temperature variations and sequential errors are induced. This indicates that the flow of the primary fluid predominantly affects the temperature distribution on the tubesheet as the auxiliary fluid has not undergone significant change at its inlet. The effects of the media on the temperature distribution is apparent by comparing the three different cases. In a realistic feedwater heater, the water-air case is most likely the best representation as hot air and superheated steam are comparable with regards to the thermal properties. The negative x-positions in Figure 3.13 a) would be the area of concern for thermal fatigue which corresponds to the steam inlet.

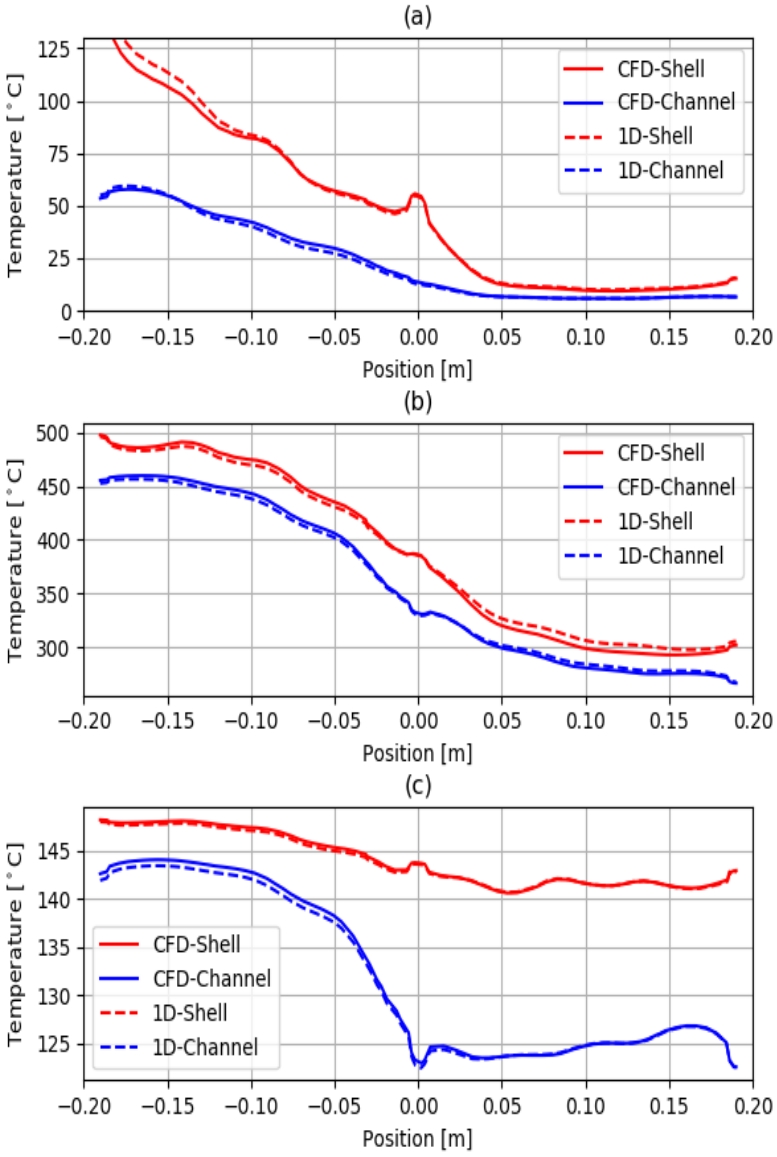

Figure 3.13: Media variation tubesheet temperature distribution along P1; a) Water-Air, b) Air-Air, c) Air-Water.

3.2.4 Transient Behaviour

Two different simulations were performed, of which one was purely a step in the temperature of the inlet primary fluid, while the latter stepped the temperatures and flow rates of both fluids. The primary fluid for the specified flow rates was propagating relatively slowly through the tubes and required in all cases an average of more than 50 seconds for a particle to enter and exit the heat exchanger. All the transient simulations were initialized from the steady state case. The results for the first case was only a step input of 30 °C was chosen to easily observe the effects of a step. The step occurred at $t = 0$. The normalized outlet temperature, as given in Equation 3.2, of the 1D-CFD method and full CFD is presented in Figure 3.14.

$$\theta = \frac{T - T_{min}}{T_{max} - T_{min}} \tag{3.2}$$

During the development of the proposed method, the results obtained from the transient simulations did not correspond well with the full CFD model. The apparent reason was that the 1D network components required a significant number of nodes to describe the transient condition accurately. Therefore, the number of nodes, n, was increased from 5 to 44, and the results improved considerably as depicted in Figure 3.14.

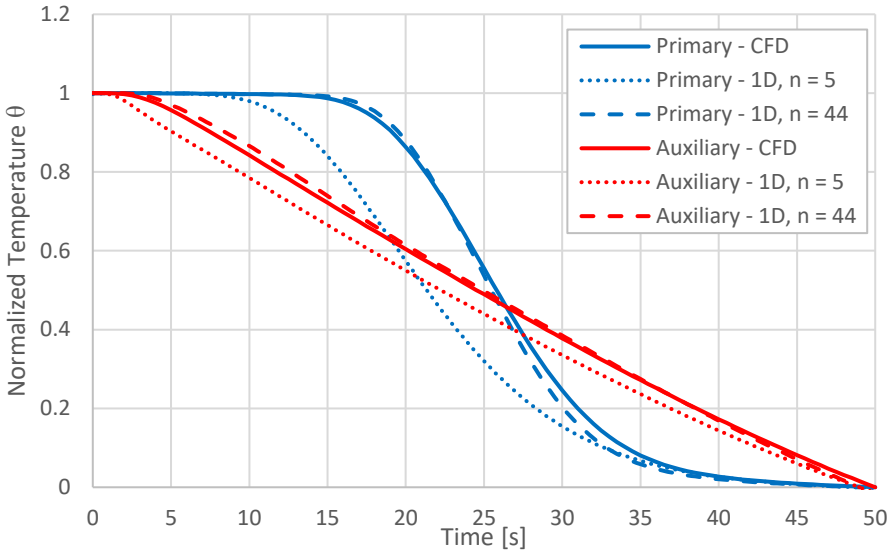

Figure 3.14: Transient outlet temperature for a single applied step.

For the second case of transient simulations, the temperature and mass flow inputs were stepped for both the primary and auxiliary fluid. These steps occurred at different times of the simulation in order to see the effect of each. The table below is a summary of the steps and the times at which they occur.

Table 3.7: Transient step inputs for Case 2

Time Condition	Auxiliary fluid		Primary fluid	
	Temperature [°C]	Mass flow rate [kg/s]	Temperature [°C]	Mass flow rate [kg/s]
Initial	150	1.5	5	2.58
Final	130	2	15	1.58
Occurring Time [s]	10	15	0	5

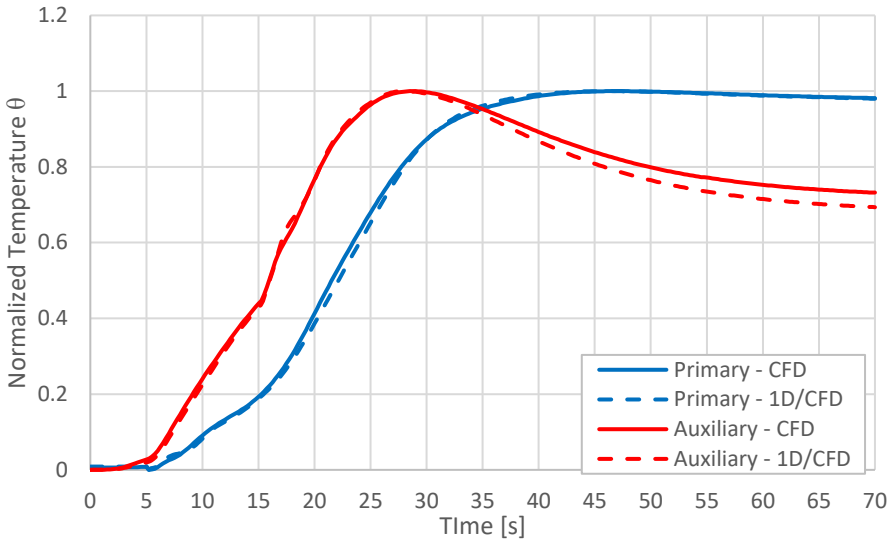

Figure 3.15: Normalized transient results for multiple step inputs.

From Figure 3.15 it can be seen that the results match very well. It is evident that stepping the mass flow has an immediate effect on the outlet temperatures of both fluids. This is due to the convection coefficients that are immediately adjusted with a change in mass flow rates. Conversely, the temperature steps lag substantially as the fluid propagates from inlet to outlet in either the tubes or shell. The results agree very well with each other especially, the primary fluid's transient behaviour. The auxiliary fluid resulted in a small offset near the final steady state conditions which was attributed to the inherent error of the method.

3.3 Conclusion

In this chapter we tested the proposed methodology to a problem that is representative of a realistic feedwater heater. The primary fluid's Reynolds number was varied in which the turbulent cases obtained LMTDs that were within 2% accurate compared to the full CFD case. The laminar flow was not as accurate with errors of approximately 4% compared to the CFD. The reason being that the downstream heat transfer correlation by Abdelmessih (1979) overestimated the heat transfer and, if required, the composition of correlations for the laminar case could be revisited in future studies.

Three cases with differences in the primary and auxiliary media were simulated. The methodology proved capable of capturing considerable temperature gradients because of the polynomial mapping procedure that was applied. Furthermore, the temperature distributions differed significantly between cases, yet, the results remained agreeable for each, which highlights the applicability range of the methodology. Lastly, the transient capabilities of the methodology were tested. Two different cases were simulated that differ in complexity. The first case was merely a single step input in the primary fluid's temperature, while the second comprise of step inputs for the mass flow rates and temperatures of the primary and auxiliary fluids. The obtained results agree very well with the full CFD for both cases.

4. FWH-5A

In this chapter, the thermal modelling of an industry feedwater, which is referred to as FWH-5A, was conducted. This chapter presents the methodology, setup, and results. In the previous chapter, the TEMA-FU type heat exchanger was used to develop and validate the model, but it was still not an entirely accurate representation of a FWH. In this section we attempt to model a feedwater heater accurately to provide an example of how to apply the proposed methodology. Reliable experimental data could not be obtained, and the results are therefore validated only for the steady state case using the manufacturing design parameters.

One problem during the time of this study was that simulating the steam flow in all of the zones with CFD would still have been impractical due to the computational expense and model complexity. Without any experimental data, the results would also be unreliable. Consequently, it was opted to use an approach that incorporated 1D network elements and empirical correlations to approximate the condensing zone while CFD was used in only a small portion of the DSZ. The suitability of this approach was supported by the fact that the DSZ only consists of single-phase superheated steam, and the highest temperature gradients in the tubesheet were expected near the bled steam inlet. The key portion of FWH-5A is illustrated with labels of the specific components in Figure 4.1 below for reference:

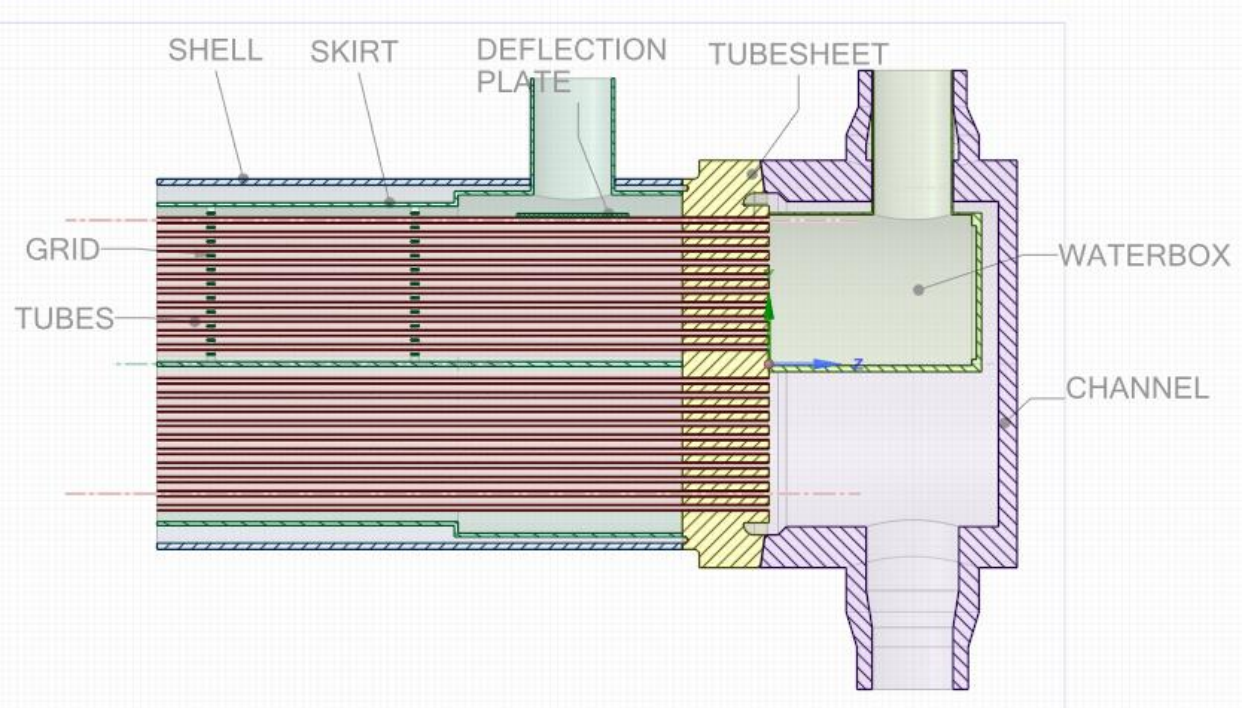

Figure 4.1: Labelled illustration of FWH-5A.

4.1 Problem Setup

Similar to the TEMA-FU type problem, aspects of the setup had to be considered were not discussed in the general methodology described in Chapter 2. The most notable difference in the problem setup was devising a thermal analysis approach for the vast size of the feedwater heater and coupling to the 1D-CFD zones. The methodology to do so is discussed systematically in this section.

4.1.1 Thermal Analysis Approach

This section presents the approach that was used to calculate the various thermal parameters. This problem was conducted very similarly to the TEMA project except that the entire shell side could not be modelled using CFD, due to computational limitations. Therefore, the shell-side zone was reduced substantially to make it computationally viable. The inputs to the CFD zone would be obtained using various flow correlations, and only the DSZ was modelled using spatial elements with CFD. This was due to two reasons: The first is that the most significant thermal stress regions within the tubesheet are located near the steam inlet. The second is that the two-phase areas are notoriously complex to simulate using CFD. The available information was the steady state design conditions provided by the feedwater heater's manufacturer and the thermodynamic process diagram in which FWH-5A is located. The available parameters calculated by FWH-5A's supplier are summarised in the table below:

Table 4.1: Design conditions for FWH-5A obtained from Arnot Power Station.

Type	Parameter	Location	Magnitude	Unit
FW	Temperature	FWH Inlet	170.5	°C
	Temperature	FWH Outlet	212.3	°C
	Temperature	DSZ Inlet	208.6	°C
	Temperature	DSZ Outlet	212.4	°C
	Mass flow rate	-	177.95	kg/s
	Pressure	FWH Inlet	192	bar
Steam	Temperature	FWH Inlet	420	°C
	Temperature	DSZ Outlet	312	°C
	Mass flow rate	-	12.455	kg/s
	Pressure	FWH Inlet	19.91	bar
General	Heat transfer	Total	33.152	MW
	Heat transfer	DSZ	3.004	MW
	Heat transfer	Condensing Zone	30.148	MW

As was stated, the model was significantly reduced, and various solvers and methods were used in a multiscale manner. The main objective was to obtain the temperature distribution on the tubesheet. Therefore, the flow adjacent to the tubesheet required a high level of detail and was modelled using the proposed 1D/CFD coupled approach. Further away for the tubesheet, macroscopic empirical correlations sufficed to obtain the respective input conditions for the CFD. The goal of these correlations was to minimise the amount of CFD spatial elements for computational efficiency. However, the main drawback using this method compromises the true transient capabilities. The

reason is that the utilized heat transfer correlations are only valid for steady state conditions. However, power plant cycling is considered as a relatively slow transient, and thus the induced errors from the neglected time dependency of the correlations are reduced. The various solvers and boundary conditions are graphically summarised in Figure 4.2 below. It should be noted that FWH-5A's orientation is in practice vertical and is only shown horizontally in the figures for general consistency of presentation.

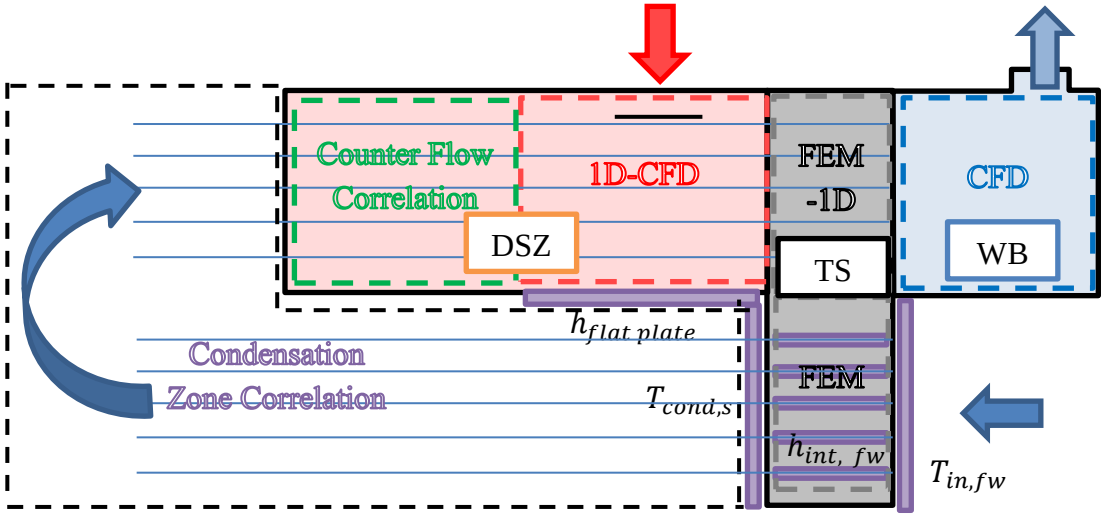

Figure 4.2: Graphic representation of thermal modelling strategy for FWH-5A.

As can be seen in Figure 4.2, only a small portion of the steam flow in the DSH was modelled with CFD. The region was just large enough for the flow to resemble characteristics associated with flow correlations. The first correlation that was confidently identified downstream (steam perspective) of the CFD was a counter flow correlation specifically tailored to heat exchangers that use eggcrate grids. This correlation was used to complete the modelling of the DSH, after which the condensing zone followed. The condensing zone was modelled using a correlation that has been used in the past by the involved utility. These correlations are described more in detail in the proceeding sections. The waterbox of the feedwater was also modelled using CFD as the channel side of the tubesheet would benefit from accurate heat transfer. The internal flow within all the U-tubes was modelled as 1D network elements in Flownex.

Boundary conditions were imposed in the lower regions of the FWH where extensive detail was not required. The longitudinal baffle was prescribed as a convection boundary condition using flat plate flow correlations at saturated temperature. The bottom of the tubesheet (as illustrated in Figure 4.2) was prescribed as a temperature boundary condition with internal pipe flow correlations obtained from Gnielinski's correlation described in Section 1.2. The temperature on the steam side was set to the saturated steam temperature, as condensate would collect in this region. The channel side temperature boundary condition was set to the inlet temperature of the FW.

The shell-side CFD zone was discretised as three segments that separated three different flow groups. Each segment was assigned three sections from which the heat transfer rates from the CFD was transferred to Flownex. The defined sections nearest to the tubesheet were relatively small in comparison with the other sections, for more accuracy. The theory and implementation of the used flow correlations are conveyed in the following sections.

Condensation Zone

In the condensing zone, the steam has transferred the bulk of its sensible heat, and condensate forms on the tubes as further heat is transferred to the feedwater. Several factors influence the heat transfer of which the vertical or horizontal orientation of the feedwater heater is most substantial. To find a correlation in the literature that is specifically suited for the current feedwater heater proved futile. Therefore, the condensation zone's correlation was provided by the utility which has been used in FWH-5A's thermal design. The correlation is given by

$$h_{cond} = 1.668\left(\frac{\rho_c(\rho_c - \rho_v)\cdot k_c^3 \cdot l_v}{15\mu \cdot d_o \cdot \Delta T}\right)^{0.25} \tag{4.1}$$

where l is the latent heat of phase change at steam pressure and the subscripts c and v refer to the properties of saturated water and steam respectively. The ΔT term is the temperature difference between the saturation temperature of the steam, T_c, and the exterior lining T_s. At this point, T_s and h_{cond} was unknown and another equation was necessary to solve. A simple energy balance of the overall tube heat transfer sufficed for that purpose. The heat transfer from the feedwater must equal the heat transferred through the tube wall and to the steam. This was expressed in terms of thermal resistances shown for each respective mode of heat transfer below:

$$R_{conv,int} = \frac{1}{(2\pi r_i)h_i} \tag{4.2}$$

$$R_{cond} = \frac{\ln(r_o/r_i)}{2\pi k} \tag{4.3}$$

$$R_{conv,ext} = \frac{1}{(2\pi r_o)h_{cond}} \tag{4.4}$$

Using the thermal resistances, an implicit relationship was formed for which a residual was defined and numerically approximated to zero using the simple bisection method. The residual function is given by Equation 4.5. As a result, h_{cond} can be estimated and used to approximate the condensing zone's heat transfer.

$$Res = \frac{T_{\infty,fw} - T_s}{R_{conv,int} + R_{cond}} - \frac{T_s - T_{cond}}{R_{conv,ext}} \tag{4.5}$$

As design conditions were provided for the temperature of the feedwater entering the DSZ, h_{cond} can also be found using these. The obtained h_{cond} from the correlation was found to correspond quite well with the design condition's convection coefficient. However, the correlation's h_{cond} was adjusted to match the design condition's h_{cond} to account for the unique design of this specific feedwater heater. This allowed for h_{cond} to be changed accordingly when transients in the input conditions were modelled.

Counter flow

Within the DSZ, a large portion of the steam flow exhibits parallel flow characteristics. Fortunately, a heat transfer correlation exists, which was able to predict the heat transfer within this region. The correlation that was found to be most suitable was the correlation developed by Shiina, Nakamura and Matsumura (1998) for heat exchangers that contain eggcrate support plates. They found that the heat transfer with eggcrate supports was nearly twice as large as standard parallel flow correlations would have predicted. They presented a simple correlation which was used for this problem and given by:

$$Nu_s = 0.14 Re_s^{0.7} \, \mathrm{Pr}_s^{0.4} \tag{4.6}$$

For the counter flow section, the flow characteristics are dominated by the maximum velocity which occurs between the tubes. Therefore, special geometrical considerations were required, and the Reynolds number was defined on the basis thereof as:

$$Re_s = \frac{\rho_s d_e V_s}{\mu_s} \tag{4.7}$$

where d_e is the equivalent diameter and V_s is the maximum velocity. Determining the maximum velocity requires the arrangement of the staggered tube bank to be considered. The geometrical parameters of the tube arrangement are illustrated in Figure 4.3.

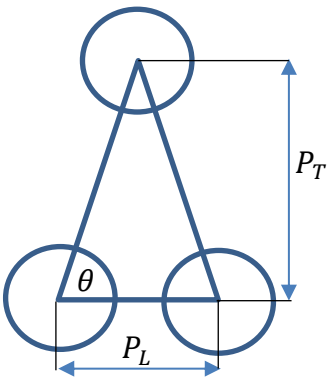

Figure 4.3: Staggered tube bank section arrangement.

To determine the equivalent diameter the following set of equations were used and described in terms of the flow area, A, and the wetted perimeter L:

$$d_e = \frac{4A}{L} \tag{4.8}$$

$$A = \frac{1}{2} P_L \, P_T - 2 \cdot \frac{1}{8} \theta d_t^2 \; - \frac{1}{8} (\pi - \theta) d_t^2 \tag{4.9}$$

$$L = \theta d_t + \frac{d_t(\pi - \theta)}{2} \tag{4.10}$$

Finally, to obtain the velocity used to calculate the Reynolds number, the following analytical equations were used as derived from the staggered arrangement and shell geometrical inputs.

$$V_s = \frac{\dot{m}_s}{\rho A_s} \tag{4.11}$$

$$A_s = A_o - n_t A_t \tag{4.12}$$

$$A_s = \frac{\pi}{4} D_o^2 - \frac{n_t \pi}{4} d_t^2 \tag{4.13}$$

where $\dot{m}_s$ and A_s is the shell mass flow rate and flow area, respectively. It was noted that the average velocity between the tubes can also be obtained from the CFD in the defined zones, which was considered to provide more realistic results than using a uniform flow assumption. This was another benefit of using a 1D-CFD coupled approach. It was found from the results that the velocity between flow groups differed slightly, but certainly considerably from approximately 5 m/s to 7 m/s. The Reynolds number in Equation 4.7 could then be solved and subsequently also the Nusselt number.

4.1.2 **1D Network Setup**

The 1D network solver was employed for evaluating all of the tube's internal flow parameters. This consisted of the heat transfer and pressure drop in each respective zone. It would be too voluminous to discuss the function of each component and the data transfer links, but an effort was made to provide a brief overview of each zone. Figure 4.4 shows the Flownex network of the different zones and thermal method applied to each is indicated.

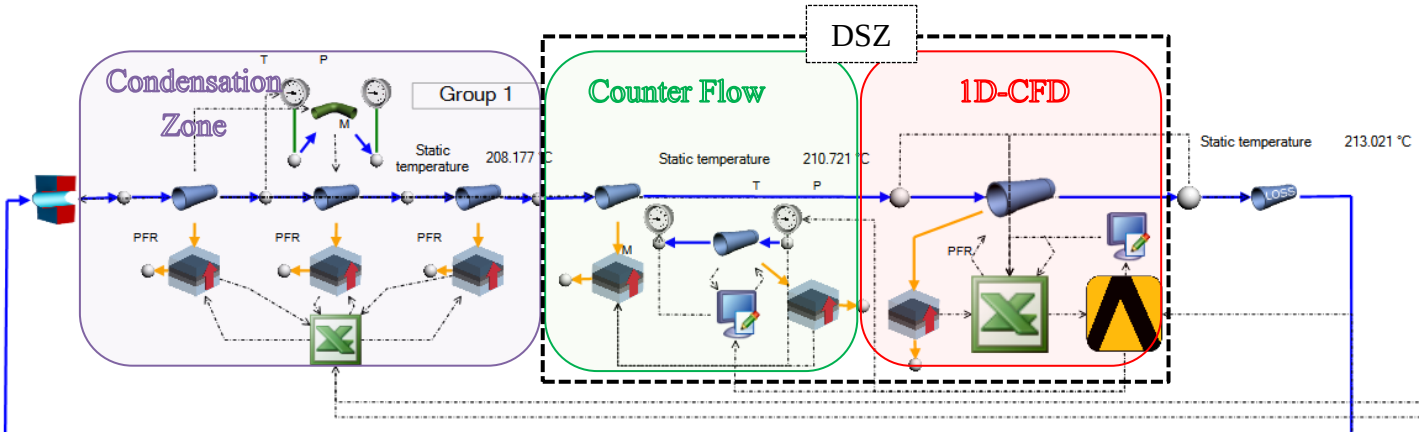

Figure 4.4: Flownex network of a FWH-5A flow group.

In the condensing zone, three pipe components represent the two straight sections and the bend of the U-tubes from the inlet up until the DSZ. The composite heat transfer components are identical with the Excel component summarising the total heat transfer for comparison purposes. The Script component calculates the thermal properties of the steam that was used to obtain h_{cond}, which was assumed constant throughout the condensing zone. The counter flow regions and 1D-CFD regions were located in the DSZ. The counter flow region consisted of one Pipe component connected to the main pipe network with a Composite Heat Transfer component attached. A secondary network was created alongside which calculated the parameters for the parallel flow correlations and transferred the obtained convection coefficient to the main network's Composite heat transfer component.

4.1.1 CFD Setup

The FWH-5A model used the same setup as was discussed in Section 2.6, and therefore this section only conveys the unique geometrical and mesh considerations for FWH-5A. The feedwater heater was modelled using technical drawings provided by the utility. Simplifications to geometrical features that did not significantly affect the flow of the fluid were made. The details of the geometry cannot be disclosed as it is the intellectual property of the utility. The final CAD model can be seen in the figure below, which again emphasizes the significant spatial element reduction, compared to a full model. The tube bundle consisted of 560 tubes which were supported by eggcrate grids.

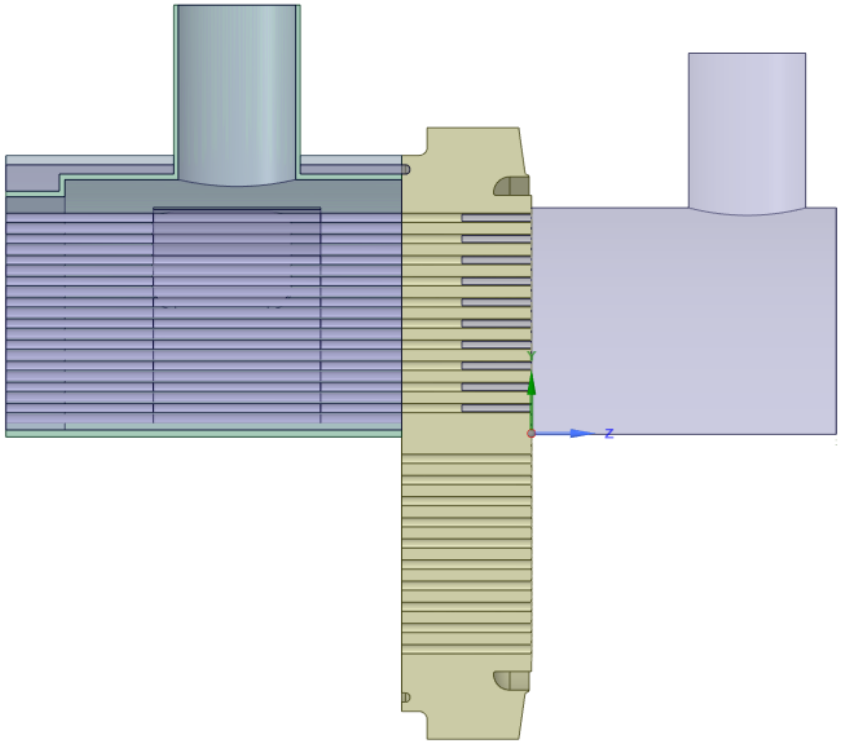

Figure 4.5: Reduced CFD geometry of FWH-5A.

An unstructured mesh was used for this problem as the geometry was not consistent enough to create a structured mesh without excessive effort. Similarly, to the TEMA-FU type problem, the unstructured mesh was generated using the Fluent Meshing ACT. The size of the elements in the solid domain was set relatively large because high levels of mesh refinement were not required to solve simple conduction. The cells near the walls were refined to capture the boundary layers of the flow accurately. A total of just over 12 million cells were used, of which approximately 91% were fluid elements and the remaining solid. The overall mesh can be viewed in Figure 4.6, in which the blank spaces are domains that are approximated using 1D network elements.

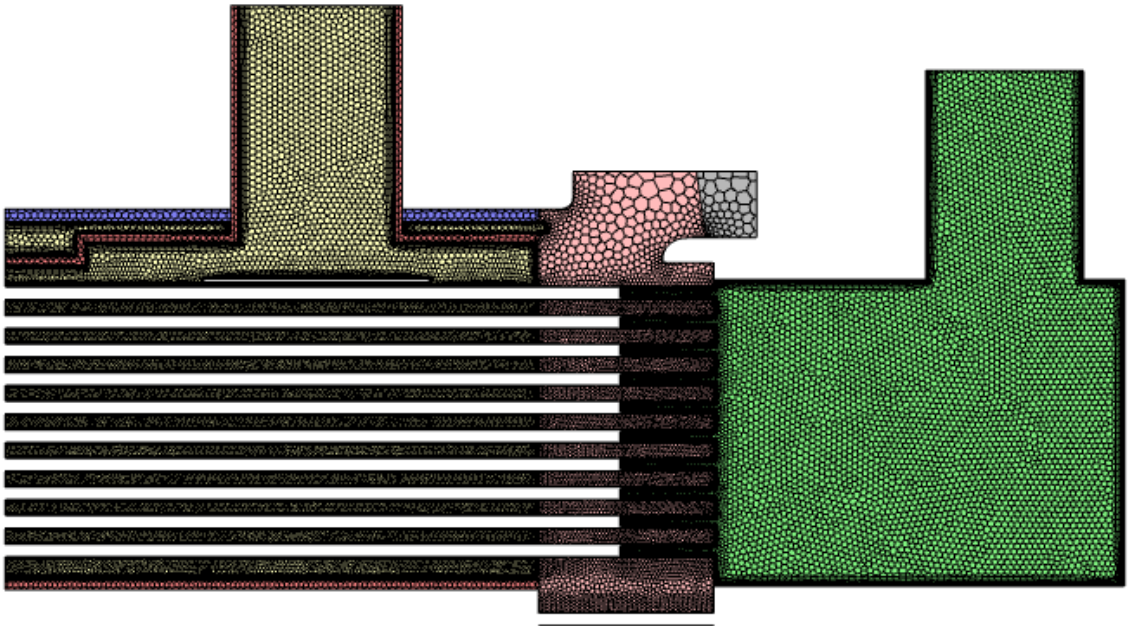

Figure 4.6: Overall FWH-5A CFD mesh.

The mesh on the channel-side was refined only near the tubesheet wall to capture the convection heat transfer between the tubesheet and outlet feedwater. Relatively large elements were used in the tubesheet, especially in the lower tubesheet region, as simple conduction was only solved. Therefore, the rest of the channel was meshed rather coarsely. The mesh near the outer tube surface was of highest priority which is evident in Figure 4.7 (a) and (b) that show the longitudinal and cross-sectional mesh, respectively. Improvement to the aspect ratio of the cells in future studies is recommended.

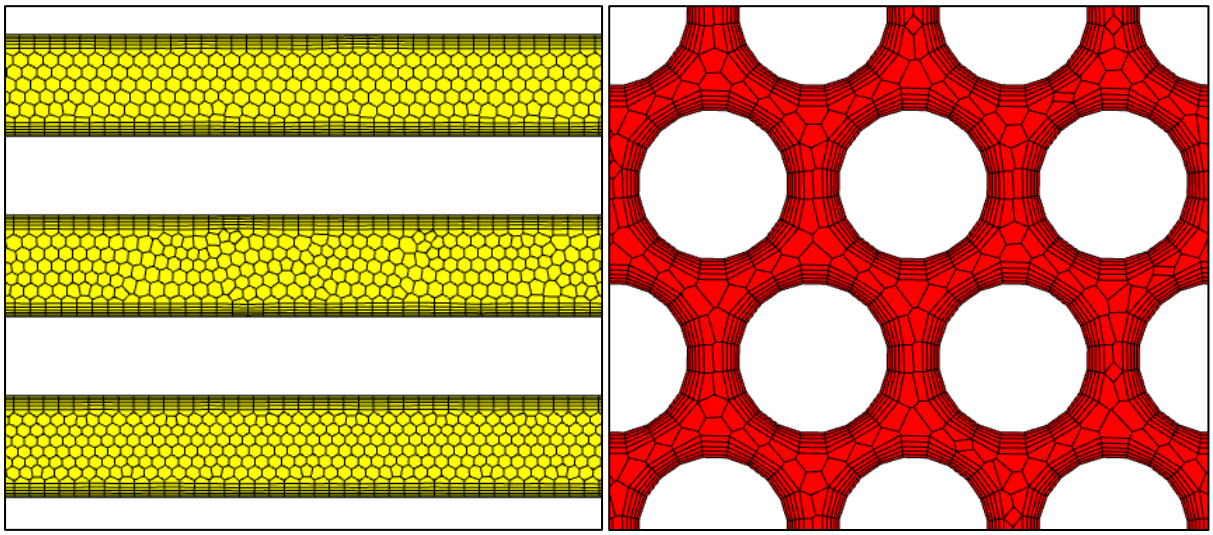

a) b)

Figure 4.7: Mesh of between FWH-5A tubes, a) side-view, b) section-view.

4.2 Results

The setup was completed, and results were extracted to analyse and validate the methodology. These include the results obtained from the flow maldistribution analysis as well as a steady state and transient run. The results were not validated against experimental data as there was none available at the time nor with full CFD as it would be computationally impractical. Nonetheless, the TEMA-FU type problem proved that the developed coupled approach is reliable compared to full CFD and the results obtained for FWH-5A serve as a first-order indication of the thermal gradients on the tubesheet.

4.2.1 Flow Maldistribution

A flow maldistribution analysis was conducted to determine the significance thereof in FWH-5A. The PPT and coupled 1D-CFD methods explained and evaluated in Sections 1.5 and 3.2.1 were used to for this analysis. The utilization of the PPT method consisted of assigning three flow groups corresponding to different radii and modelling it within Flownex. For the coupled 1D-CFD method, the first step was to conduct a first-order CFD simulation with zero backpressure prescribed at the outlet boundary conditions to determine the flow bias. These velocities at the tubesheet outlet are presented in Figure 4.8 below, which indicate slight velocity discrepancies between regions. A total of four flow groups were defined for the 1D-CFD method by evaluating the velocity contour as labelled in Figure 4.8.

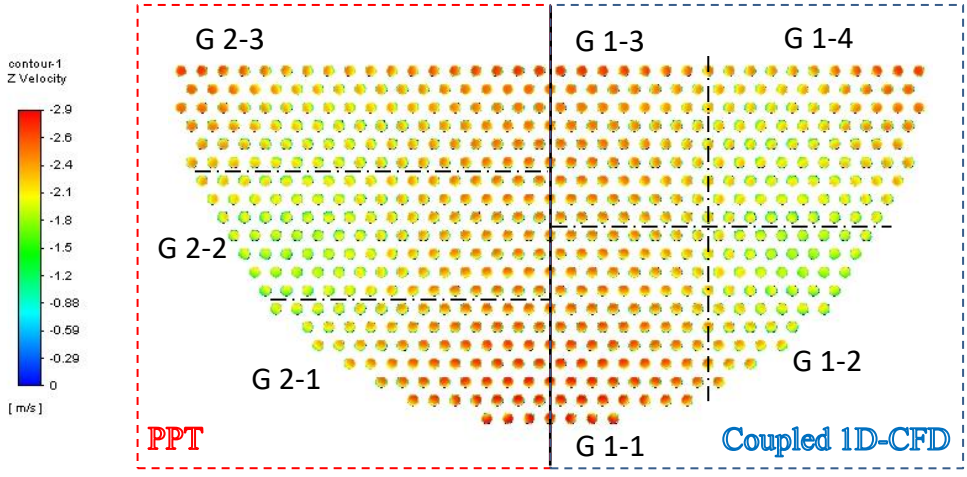

Figure 4.8: Zero backpressure outlet velocity contour and zone discretisation.

The PPT and coupled 1D-CFD methods were then modelled separately in Flownex which calculated the primary pressure losses from tube friction as well as secondary losses of the bend, inlet and outlet. For the PPT method, the total pressure losses in each tube was set equal to one another and flow rates were obtained iteratively. The 1D-CFD approach applied total pressure losses obtained from the 1D solver of each respective group as backpressures in CFD. The respective solvers

exchanged the discussed flow parameters until the solution converged. The average velocities that were obtained in each group are given in Table 4.2 below in which the extent of maldistribution can be seen was approximately between, -2% and 3% which was considered small. The percentage maldistribution was based off the average calculated velocity obtained using the total mass flow rate in a simple continuity calculation.

Table 4.2: Flow maldistribution results of defined groups.

Solver	Flow Groups	Tube Velocity	Percentage Maldistribution
1D/CFD Coupled	G 1-1	2.053	-1.80%
	G 1-2	2.047	-2.10%
	G 1-3	2.128	1.79%
	G 1-4	2.119	1.35%
1D Theory	G 2-1	2.022	-3.26%
	G 2-2	2.083	-0.34%
	G 2-3	2.139	2.35%

It is interesting to note was that the PPT method approximated a larger degree of maldistribution than the coupled 1D-CFD method. This was unexpected as the TEMA-FU type problem indicated the PPT method to be conservative. Nonetheless, the results obtained for both methods are sufficiently close to one another and were aligned with the expected outcome which was that the smaller U-bend radii tubes experience higher flow rates than larger radii ones.

It was concluded that significant maldistribution was not present and therefore a valid assumption would be that the flow distribution in the tubes are uniform. However, the PPT method uses negligible computational resources and as the model was already setup, the small maldistribution in the heat analysis could just as well be considered in the thermal analysis.

4.2.2 Steady State

A steady state case was simulated to validate the accuracy of the model against given design parameters. All the inlet design steady state conditions were known as the feedwater heater's supplier provides this information in the datasheet. The outlet temperatures obtained at different zones were compared to the design conditions, which are presented in the table below.

Table 4.3: Steady state FWH-5A results.

Location	Results [°C]		
	Design	Methodology	Difference
DSZ Inlet	208.60	208.50	0.10
FWH Outlet	212.40	213.06	-0.66

It was found that the greatest discrepancy occurs within the DSZ but still amounts to only 0.6 °C which would have negligible effects on the thermal stresses. This minor discrepancy was expected as the CFD approach is more detailed than the first order thermal analysis used by manufacturers. Based on the corresponding thermal results, the model was validated to some extent. However, further validation with experimental results in future studies is recommended.

The demonstration of the methodology continues by presenting the thermal distribution along FWH-5A, given in Figure 4.9 below. The high thermal gradients within the tubesheet are visible, especially at the shell and shroud's connection to the tubesheet. This was expected and also corresponds to numerous reports of weld failure at these connections. It was found that the pressure drop within the tube bundle is substantial, and the steam flow rate is highest in the outer skirt. This results in the portion of flow that travels through the tube bundle to cool down rapidly, and the inner tubesheet temperature is dominated by the feedwater temperature. The benefits of this methodology are highlighted by noting that a constant surface temperature does not exist along the tubesheet, which many researchers impose for stress analysis as described in Section 1.3.1.

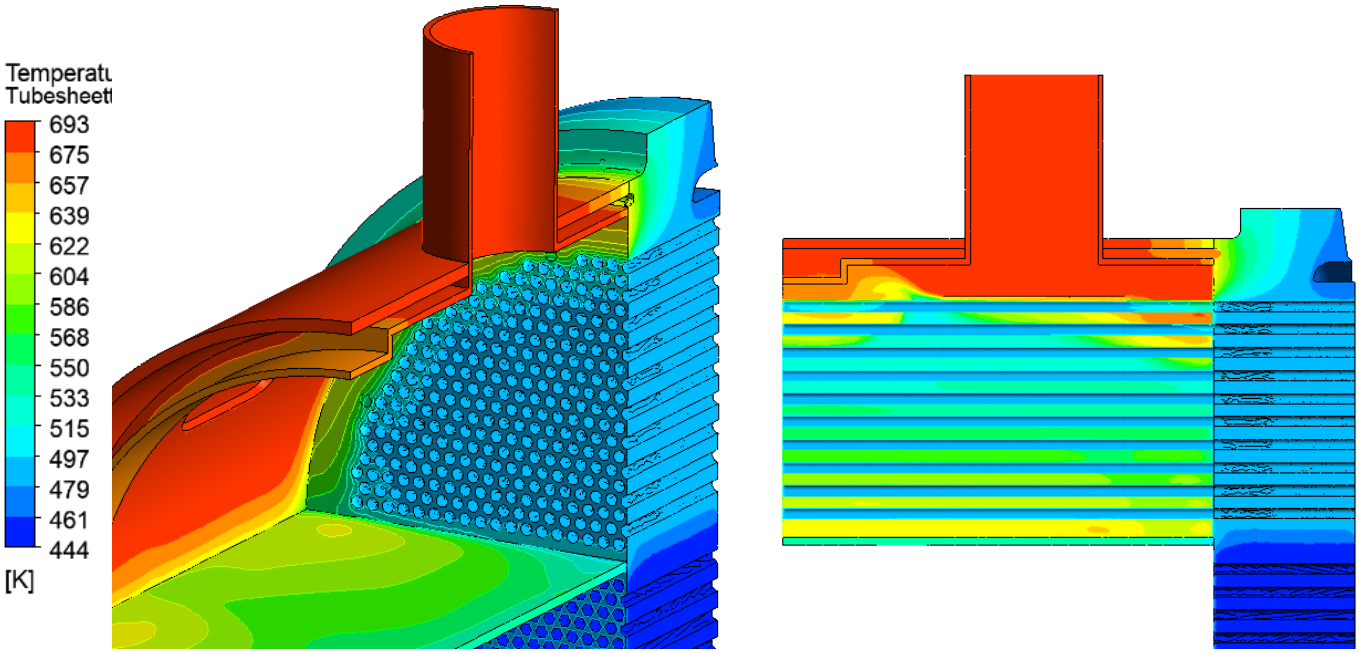

a) b)

Figure 4.9: Temperature distribution of steady state, a) Trimetric view, b) Symmetry view.

The steady state case provides results that are consisted with the design values. The obtained temperature distribution provides insight into the flow characteristics and the severity of the thermal gradients. In future investigations, it would be useful to direct more steam flow towards the tubesheet to evaluate a worst-case scenario, which is proportional to a higher convection coefficient.

4.2.3 **Transient**

A transient simulation was performed to analyse the thermal gradients imposed by the transients. These thermal gradients are a result of uneven load variations in the steam and feedwater inputs and thermal inertia of the solids. This transient cyclic behaviour of thermal stresses ultimately leads to fatigue failure. The transient cases that were performed were set up according to a real power plant's start-up conditions. A typical load change in the reference power plant is about 40MW, which undergoes a change of approximately 12 MW/min during start-up. This meant that a power shift of 40 MW is performed in 3 minutes and 20 seconds. The power change and the feedwater mass flow rate were assumed to be directly proportional at 1.2 MW/kg/s. From the steady state design conditions, the initial conditions were determined by using the crude assumptions that the load changes are linear and that the parameters are proportional to each other. These assumptions are suitable for the demonstration of the methodology, whilst real plant data would be ideal. The final conditions of the steam and feedwater inputs have been conveyed in Table 4.1 but extrapolated initial conditions is presented in Table 4.4below.

Table 4.4: Initial input conditions.

Fluid	Property	Value	Unit
Feedwater	Mass Flow	161.28	kg/s
	Temperature	166	°C
Steam	Mass Flow	11.29	kg/s
	Pressure	18.05	bar

The results that are of interest are the temperatures of the channel-side and shell-side. This is plotted in Figure 4.10 below, which shows the change in the average surface temperatures of each side. Only the change in temperature is depicted and was found by subtracting each value by approximately 209 °C and 278 °C for the channel and tube-side respectively. It is obvious that the linearly imposed transients result in a linear temperature output, but a growing offset between the average temperatures exists as the new conditions are approached. This offset between the results increases the thermal gradient perhaps, but it is not of a cyclic nature which accelerates fatigue. Therefore, the region of most concern for this load case is the initial 20 seconds of the simulation due to the variable offset between temperatures. Furthermore, the transient temperature difference was deemed small enough that the concern for fatigue failure would be negligible.

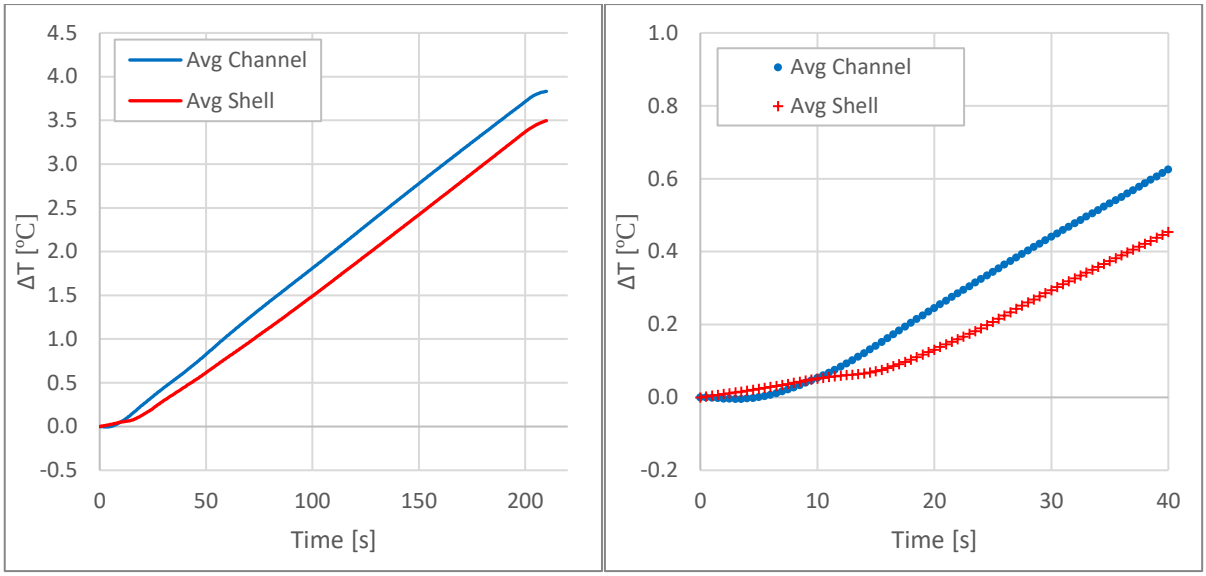

a) b)

Figure 4.10: Linear transient input results of average surface temperature vs. time; a) full time, b) zoomed.

It was sought to better compare the transient temperature differences in which the purely linear transient case failed. An elementary analysis was designed to accomplish this by perturbing the input parameters with sinusoids of different frequencies. These sinusoids represent to an extent the start-up noise that is present within a real start-up. Each of the varying inputs was assigned a unique sinusoidal perturbation of which the amplitude was a fraction of the total change. The sinusoid coefficients are given in

Table 4.5 in the form:

$$\delta(t) = A\sin\big((2\pi f)t\big) \tag{4.14}$$

Table 4.5: Sinusoidal perturbation coefficients.

Fluid	Parameter	A	f [Hz]
Feedwater	Mass Flow [kg/s]	0.06	0.10
	Temperature [°C]	0.19	0.10
Steam	Mass Flow [kg/s]	3.33	0.05
	Pressure [bar]	1.35	0.03

A simulation of 200 seconds was performed, and the results are given in Figure 4.11. These coefficients are more notable with the obtained results which are again the average surface temperatures of the shell and channel-side. In this perturbed loading case, the cyclic temperature differences within the tubesheet are easily more distinguishable than the linear case. This implies that cyclic stresses are occurring considerably more with transients that have variable slopes. This is the case for averaged temperatures, and it may be expected that locally these adverse effects are even more considerable.

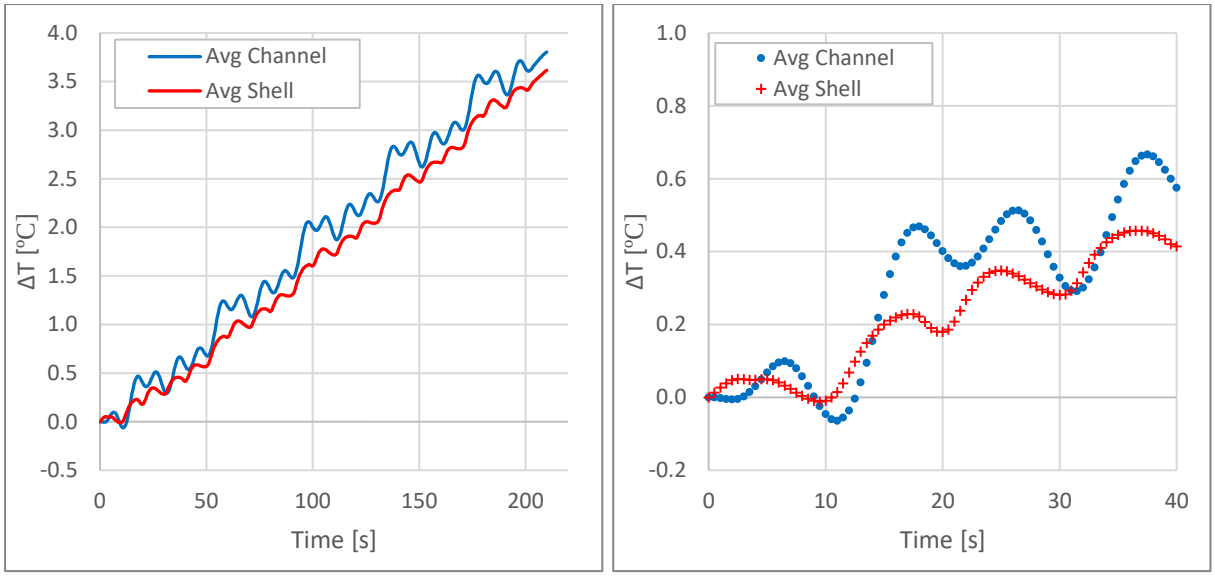

a) b)

Figure 4.11: Sinusoidally perturbed transient shell and channel-side temperatures.

A Fast Fourier Transform (FFT) was performed in order to evaluate the effects of each perturbation and is shown in Figure 4.12. It was found that both the channel and shell-side average temperatures respond to each of the perturbations. However, the shell-side temperatures are less affected. This is due to the significantly more heat transfer area that the feedwater has on the tubesheet compared to the steam. The differences in amplitudes portray the cyclic stresses that would evolve from a similar signal. This transient analysis can be improved and extended significantly, due to lack of actual experimental data, and as this only serves as a demonstration, it was deemed sufficient.

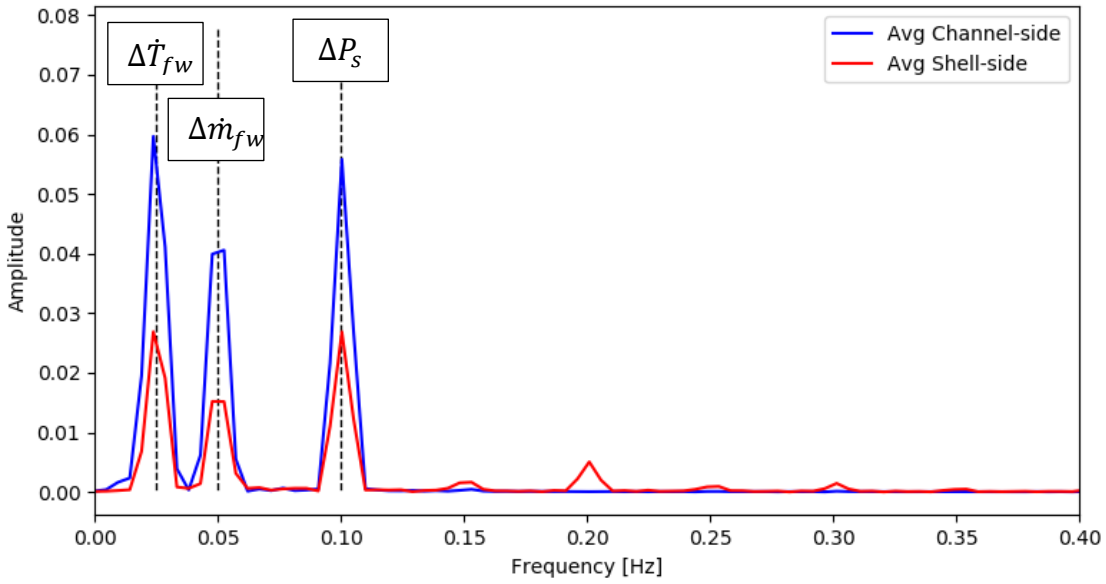

Figure 4.12: FFT of perturbed transient FWH-5A response.

4.3 Conclusion

The methodology has been applied to the industrial feedwater heater FWH-5A. The results provide insights into the real thermal gradients that are present in a tubesheet. The model compares well with the supplier's design thermal data, but further validation with experimental data is highly recommended in future studies. The steady state temperature distribution indicated significant temperature gradients near the shell to tubesheet connection. Numerous failure reports of the weld in this region have been filed. The effects of a transient simulation were analysed, and it could be concluded that fluctuating thermal differences do exist between the shell and channel-side, which consequently induces cyclic stresses. These accelerate fatigue and must be mitigated if the tubesheet type feedwater heater is to replace the header type in high-pressure applications.

5. Conclusion and Recommendations

This study developed a methodology that is capable of reducing the computational time of a full CFD to obtain the temperature distribution along a tubesheet of a feedwater heater. This temperature distribution can aid in the determination of the thermal fatigue that occurs in the tubesheet. If the thermal fatigue can be alleviated, the tubesheet-type feedwater heater offers significant cost savings compared to the header type.

This dissertation introduced the reader to the problem and theory at hand. Literature was surveyed, which consisted of work done in the field of tubesheet structural analyses, solver coupling, and flow maldistribution. The scope of the work was also outlined in Chapter 1, thoroughly. The general methodology was presented in Chapter 2, which included the coupling and mapping procedure, convergence considerations, and solver setup. Additionally, the method of transferring transient cell temperatures to a FEM analysis for a one-way FSI was described to complete the objectives outlined.

The testing and development of the methodology were conducted on a TEMA-FU type heat exchanger which is representative of a tubesheet-type feedwater heater in Chapter 3. A variation in the primary fluid's Reynolds number resulted in the turbulent cases of the 1D-CFD method to have errors within 2% compared to the full CFD case. The laminar flow was not as accurate with errors of approximately 4% compared to the CFD. The deduced reason was that the downstream heat transfer correlation by Abdelmessih (1979) over approximated the heat transfer and, if required, the composition of correlations for the laminar case could be revisited in future studies. Cases were simulated with different media, and the tubesheet temperature distributions agreed very well with the full CFD. The transient capabilities of the methodology were lastly tested, and it was found that the transients could be captured sufficiently in every regard. However, care must be exercised when considerable fluctuations in the flow are modelled as the solution's stability may be compromised. The proposed methodology was successfully developed and numerically validated over a wide range of conditions at this stage.

In Chapter 4 the developed methodology was applied to an existing feedwater heater. The heat transfer in the condensing zone and a portion of the DSH was modelled using appropriate correlations. The inlet steam flow section nearest to the tubesheet was modelled with the proposed 1D-CFD coupled method. A detailed temperature distribution in the critical areas of the tubesheet was obtained, which is essential for stress analyses. The demonstration problem was validated only by comparing one steady state case with the FWH-5A's provided vendor values. For demonstration purposes, this sufficed, but further validation is required if the method is to be applied to analyse thermal fatigue. Additionally, transient load cases, based on a local utility's operation, were simulate which confirmed the variable differential temperatures on either side of the tubesheet. Transients in the inputs highlighted the thermal phase lag in temperatures on either side of the

tubesheet. These temperature misalignments confirm the cyclic stresses within the tubesheet, which finally fails due to thermal fatigue.

It can be concluded that the developed methodology successfully achieved the objective to reduce the computational time of a full CFD. The proposed methodology would certainly prove useful for applications other than feedwater heaters. The methodology was validated by comparing the temperature distribution of the tubesheets along various positions with a full CFD and the results agreed very well. This indicates that the proposed methodology can adequately obtain a transient detailed temperature distribution of a tubesheet to be used for thermal fatigue calculations. New designs of the tubesheet-type feedwater heater can be practically evaluated with the proposed methodology, which can ultimately lead to the tubesheet-type to be just as well suited for high pressure applications as the header-type.

5.1 Recommendations

This study represents an early step towards analysing the stresses in a tubesheet with one-way FSI. There is therefore still much of work to be completed before the shift from header-type feedwater heaters to tubesheet-type can be made. The first step would be to perform another iteration of improvements on the proposed 1D-CFD coupled methodology. The effects of other aspects, such as the employed numerical schemes, turbulence models, tube fouling, and radiation effects, should be investigated. Finally, the methodology must be validated with experimental data to ensure full validation.

Several recommendations with regards to the application of the methodology to an industry feedwater heater were identified. The most important one was that the demonstration problem is validated with experimental results. Discrepancies should be expected between the model and experimental results, but shortcomings can then be identified and improvements consequently. The 1D network of FWH-5A can also be extended to include upstream and downstream components for more accurate input conditions and representation of a power plant. Secondary recommendations for the proposed methodology are listed below:

- Review laminar primary flow method.
- Determine the effects of using velocity profiles for each tube.
- Improve flow coupling numerical scheme for better stability.
- Review CFD mesh and setup for FWH-5A.

References

Abdelmessih, Amanie, N. (1987) *Laminar Flow Heat Transfer Downstream from U-bends*. Oklahoma State University.

Abraham, J. P., Sparrow, E. M. and Tong, J. C. K. (2009) 'Heat transfer in all pipe flow regimes: laminar, transitional/intermittent, and turbulent', *International Journal of Heat and Mass Transfer*. Elsevier Ltd, 52(3–4), pp. 557–563. doi: 10.1016/j.ijheatmasstransfer.2008.07.009.

Allie, M. and Fuls, W. (2016) *Thermal Modelling of Feedwater Heaters*. University of Cape Town.

Ansys (2019) *Ansys Fluent Theory Guide*.

Arias, D. A. (2006) 'Advances on the Coupling Between a Commercial CFD Package and a Component-based Simulation Program', *SimBuild 2006*, (April), pp. 231–237.

Band, D., Benten, T. and Stahlhut, J. (2007) 'Heat Exchange Technology: Supercritical power plants offer new lease of life for header-type heaters', *Power Engineering International*, January. Available at: https://www.powerengineeringint.com/2007/07/01/heat-exchange-technology-supercritical-power-plants-offer-new-lease-of-life-for-header-type-heaters/.

Bejan, A. and Kraus, A. D. (2003) *Heat transfer handbook*. John Wiley & Sons.

Botha, M. and Hindley, M. P. (2015) 'One-way Fluid Structure Interaction modelling methodology for boiler tube fatigue failure', *Engineering Failure Analysis*. Elsevier Ltd, 48, pp. 1–10. doi: 10.1016/j.engfailanal.2014.10.012.

Cengel, Y. and Ghajar, A. (2015) *Heat and Mass Transfer*. Fifth. McGraw-Hill.

Checcucci, M., Sazzini, F., Marconcini, M., Arnone, A., Coneri, M., De Franco, L. and Toselli, M. (2011) 'Assessment of a Neural-Network-Based Optimization Tool: A LowSpecific-Speed Impeller Application', *International Journal of Rotating Machinery*, 2011. doi: 10.1155/2011/817547.

Dorfman, A. and Renner, Z. (2009) 'Conjugate Problems in Convective Heat Transfer: Review', *Mathematical Problems in Engineering*, 2009(January), pp. 1–27. doi: 10.1155/2009/927350.

Fang, T., Spoor, P. S. and Ghiaasiaan, S. M. (2017) 'A computational approach for coupled 1D and 2D/3D CFD modelling of pulse Tube cryocoolers', *IOP Conference Series: Materials Science and Engineering*, 278(1). doi: 10.1088/1757-899X/278/1/012172.

Filimonov, S. A. et al (2017) 'Hybrid Methods for Simulating Hydrodynamics and Heat Transfer in multiscale (1D-3D) Models', *Journal of Physics*, 899(052004).

le Grange, W. (2018) *Component development for a high fidelity transient simulation of a coal-fired power plant using Flownex SE*. University of Cape Town.

Guo, L. and Jianping, Z. (2011) 'Design by Finite Element Analysis on Tubesheet of Heat Exchanger with a Central Hole', in *American Society of Mechanical Engineers, Pressure Vessels and Piping Division (Publication) PVP*, pp. 755–760. doi: 10.1115/PVP2011-57867.

Hanna, K., Bornoff, R., Murray, J., Kolak, D., Gruetzmacher, M. and Jenkins, M. (2017) '1D-3D CFD and 3D-1D CFD: Simulation Based Characterization', *Metnor Graphics Corporation*.

El Hefni, B. and Bouskela, D. (2018) *Modeleing and Simulation of Thermal Power Plants with ThermoSysPro*. Chatou: Springer.

Jiuyi, L., Caifu, Q. and Huifang, L. (2018) 'Thermal Stress Analysis on the Thick Tubesheet with Square Layout of Tubes', *International Journal on Interactive Design and Manufacturing*. Springer-Verlag France, 12(1), pp. 243–251. doi: 10.1007/s12008-016-0363-y.

Johnson, D. A., Rose, W. C., Edwards, J. W., Naik, U. P. and Beris, A. N. (2011) 'Application of 1D blood flow models of the human arterial network to differential pressure predictions', *Journal of Biomechanics*, 44(5), pp. 869–876. doi: https://doi.org/10.1016/j.jbiomech.2010.12.003.

Kim, M. Il, Lee, Y., Kim, B. W., Lee, D. H. and Song, W. S. (2009) 'CFD modeling of shell-and-tube heat exchanger header for uniform distribution among tubes', *Korean Journal of Chemical Engineering*, 26(2), pp. 359–363. doi: 10.1007/s11814-009-0060-7.

Kitto, J. B. and Robertson, J. M. (1989) 'Effects of Maldistribution of Flow on Heat Transfer Equipment Performance', *Heat Transfer Engineering*. Taylor & Francis, 10(1), pp. 18–25. doi: 10.1080/01457638908939688.

Koekemoer, O., Du Toit, C. and Kruger, J. (2018) *Investigation into the coupled 1D and 3D numerical modeling of an air-cooled heat exchanger configuration OC Koekemoer*. North-West University.

Kruger, J. H., Le Grange, L. A. and Greyvenstein, G. R. (2009) 'Integrated systems cfd modelling applied to diffusion-bonded compact heat exchangers', *2008 Proceedings of the 4th International Topical Meeting on High Temperature Reactor Technology, HTR 2008*, 1, pp. 49–56. doi: 10.1115/htr2008-58143.

Kruger, J. and Du Toit, C. (2006) 'The Simulation of a Thermal-Fluid System Using an Integrated Systems CFD Approach', (December), pp. 1–7.

Lalot, S., Florent, P., Lang, S. K. and Bergles, A. E. (1999) 'Flow maldistribution in heat exchangers', *Applied Thermal Engineering*, 19(8), pp. 847–863. doi: 10.1016/S1359-4311(98)00090-8.

Li, H., Qian, C. and Yu, X. (2011) 'Thermal Stress Analysis of a Tubesheet with a Welding Clad', pp. 302–307. doi: 10.4028/www.scientific.net/AMR.201-203.302.

Liu, M. S., Dong, Q. W., Wang, D. B. and Ling, X. (1999) 'Numerical simulation of thermal stress in tube-sheet of heat transfer equipment', *International Journal of Pressure Vessels and Piping*, 76(10), pp. 671–675. doi: 10.1016/S0308-0161(99)00037-X.

Ljubijankic, M., Nytsch-Geusen, C., Janicke, A. and Schmidt, M. (2011) 'Advanced Analysis of Coupled 1D/3D Simulation models by the use of a Solar System', in. Sydney: Conference of International Building Performance Simulation Association, pp. 14–16.

Malatip, A., Wansophark, N. and Dechaumphai, P. (2006) 'Combined Streamline Upwind Petrov Galerkin Method and Segregated Finite Element Algorithm for Conjugate Heat Transfer Problems', *Journal Of Mechanical Science and Technology*, 20, pp. 1741–1752.

Mao, J., Tang, D., Bao, S., Luo, L. and Gao, Z. (2016) 'High temperature strength and multiaxial fatigue life assessment of a tubesheet structure', *Engineering Failure Analysis*. Elsevier B.V., 68, pp. 10–21. doi: 10.1016/j.engfailanal.2016.05.030.

McAdams, W. H. (1942) *Heat Transmission*. 1st edn. New York Mcgraw-Hill Book Company.

Meinke, S., Gottelt, F., Müller, M., Hassel, E., Simulation, X. R. G. and Schlossstr, H. (2011) 'Modeling of Coal-Fired Power Units with ThermoPower Focussing on Start-Up Process Scope of Investigations and Ther- modynamical Model', pp. 353–364.

Mohammadi, K. and Malayeri, M. R. (2013) 'Parametric study of gross flow maldistribution in a single-pass shell and tube heat exchanger in turbulent regime', *International Journal of Heat and Fluid Flow*. Elsevier Inc., 44, pp. 14–27. doi: 10.1016/j.ijheatfluidflow.2013.02.010.

Papukchiev, A., Lerchl, G., Waata, C. and Frank, T. (2009) 'Extension of the simulation capabilities of the 1D system code ATHLET by coupling with the 3D CFD software package ANSYS CFX', *Proceedings of The 13th International Topical Meeting on Nuclear Reactor Thermal Hydraulics (NURETH-13)*, pp. 1–13. Available at: http://www.drthfrank.de/publications/2009/Papukchiev_et_al_NURETH-13_2009.pdf%5Cnpapers3://publication/uuid/7BF30CBF-EC79-4844-B103-5ADD08EE7BC9.

Patil, R. and Anand, S. (2017) 'Thermo-structural fatigue analysis of shell and tube type heat exchanger', *International Journal of Pressure Vessels and Piping*. Elsevier Ltd, 155, pp. 35–42. doi: 10.1016/j.ijpvp.2017.03.004.

Rousseau, P. G. and Gwebu, E. Z. (2018) 'Modelling of a Superheater Heat Exchanger with Complex Flow Arrangement Including Flow and Temperature Maldistribution', *Heat Transfer Engineering ISSN:* Taylor & Francis, 7632. doi: 10.1080/01457632.2018.1446816.

Said, S. A. M., Ben-Mansour, R., Habib, M. A. and Siddiqui, M. U. (2015) 'Reducing the flow mal-distribution in a heat exchanger', *Computers and Fluids*. Elsevier Ltd, 107, pp. 1–10. doi: 10.1016/j.compfluid.2014.09.012.

Sherwin, Formaggia, Peiro and Franke (2003) ‘Computational modelling of 1D blood flow with variable mechanical properties and its application to the simulation of wave propagation in the human aterial system’.

Shiina, K., Nakamura, S. and Matsumura, S. (1998) ‘Shell side heat transfer characteristics to water flowing parallel with an Eggcrate Support Plate’, *Nihon Kikai Gakkai Ronbunshu, B Hen/Transactions of the Japan Society of Mechanical Engineers, Part B*, 64(620), pp. 1187–1195. doi: 10.1299/kikaib.64.1187.

Terranova, T. and Gibbard, I. (2006) *Power Plant Feedwater Heaters*. Cheltenham: Power Plant Engineering.

Than, S. T. M., Lin, K. A. and Mon, M. S. (2008) ‘Heat Exchanger Design’, *World Academy of Science*, 22.

Verstraete, T. and Van den Braembussche, R. A. (2009) ‘A Novel Method for the Computation of Conjugate Heat Transfer with Coupled Solvers’, in. Antalya: INt. Symp. on Heat Transfer in Gas Turbine Systems. doi: 10.1615/ICHMT.2009.HeatTransfGasTurbSyst.570.

White, F. M. (2011) *Fluid Mechanics*. Seventh. McGraw Hill.

Yari, A., Hosseinzadeh, S., Golneshan, A. A. and Ghasemiasl, R. (2015) ‘Numerical Simulation for Thermal Design of a Gas Water Heater with Turbulent Combined Convection’, in. Seoul: ASME. Available at: https://asmedigitalcollection.asme.org/FEDSM/proceedings-abstract/AJKFluids2015/57212/V001T03A007/227946.

Youssef, M. (1993) ‘Header Type Feedwater Heaters As Retrofits for Cycling Units’, in *Power-Gen Europe*, pp. 25–27.

Zaversky, F., Sánchez, M. and Astrain, D. (2014) ‘Object-oriented modeling for the transient response simulation of multi-pass shell-and-tube heat exchangers as applied in active indirect thermal energy storage systems for concentrated solar power’, *Energy*. Elsevier Ltd, 65, pp. 647–664. doi: 10.1016/j.energy.2013.11.070.

Appendix A: GCI Calculations

Given a series of meshes, r defines the grid refinement ratio and in this investigation, there were two. The performance parameter f, which in TEMA-FU and FWH-5A case is the outlet temperatures, indicates the accuracy of the solution. The order of convergence, p, is given by:

$$p = \ln\left(\frac{f_3 - f_2}{f_2 - f_1}\right)$$

When 3 solutions are available GCI_{23} and GCI_{12} is calculated in a dimensionless form in order to be compared. GCI_{23} and GCI_{12} is given by the following:

$$GCI_{12} = \frac{F_S\left|\frac{f_2 - f_1}{f_2}\right|}{r^p} \quad \text{and} \quad GCI_{12} = \frac{F_S\left|\frac{f_2 - f_1}{f_2}\right|}{r^p}$$

If the values lie within the asymptotic range of convergence, then

$$GCI_{23} \approx r^p GCI_{12}$$

The results for the FWH-5A is given below:

Table A.1: TEMA-FU Mesh independence results

Mesh	Cells	Primary T_{out}	Auxiliary T_{out}
Coarse	2238185	326.93597	372.46008
Medium	3732002	327.47409	371.82407
Fine	6541863	327.88986	371.15948

Parameter		Results	
Refinement Ratio	r =	1.32	
Order of Convergence	p =	0.94	-0.16
Safety Factor	Fs =	1.25	1.25
Grid Convergence Index	GCI_{12} =	0.01	-0.05
	GCI_{23} =	0.01	-0.05
Asymptotic Range	-	100%	99.8%
Exact f	$f_{h=0}$ =	329.30	386.61

Table A.2: TEMA-FU Mesh independence results

Mesh	Cells	Primary T_{out}	Auxiliary T_{out}
Coarse	4235645	314.245	503.224
Medium	9872564	313.248	476.126
Fine	17315970	313.0215	465.453

Parameter		Results	
Refinement Ratio	r =	1.57	
Order of Convergence	p =	3.28	2.06
Safety Factor	Fs =	1.25	1.25
Grid Convergence Index	GCI_{12} =	0.01%	1.9%
	GCI_{23} =	0.02%	1.4%
Exact *f*	$f_{h=0}$ =	312.95	458.52

It is evident that the results for both problems proved to be independent of the mesh and the medium meshes were selected as the obtained results were computationally more efficient.

Appendix B: Additional Studied Effects

This appendix conveys the effects of the flow maldistribution methodology. The first interesting effect can be noted in the residuals as for a case as presented in Figure B. 1. When the zero backpressure is initialized, Flownex does not contribute and the residuals decline smoothly. Once flow groups have been assigned, Flownex is incorporated and data is transferred between the solvers. This is shown by the evenly spaced agitations in the residuals. Even with the residual agitations, the residuals ultimately converge to zero. With regards to the coupling strategy, if a global iteration was issued only when the CFD converged fully, the amount of iterations required for full convergence would be immense. Figure B. 1 demonstrates the effectiveness of rather specifying a fixed amount of iterations.

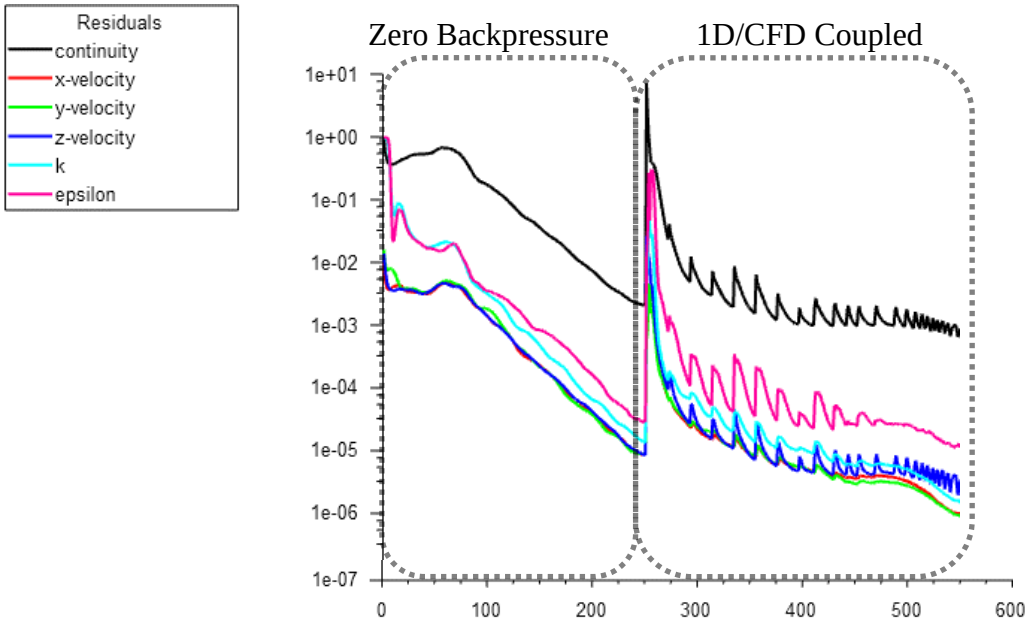

Figure B. 1: Residuals of a flow maldistribution group

The process of convergence can also be analysed when only considering the thermal link between solvers, without any flow dependency. This is the case for the FWH-5A after it was established that maldistribution is negligible. Figure B.2 below depicts the residuals and outlet temperatures of a converging solution for FWH-5A. As there are no flow dependencies, the continuity and momentum residuals are relatively unaffected by global iterations. However, the energy equation experiences a spike in its residual for each global iteration. As the solution converges, the extent of these spikes decreases. It is also evident in Figure B.2 b) that the FW outlet temperature converges to the steady state value relatively quickly. The steam outlet temperature converges at a slower rate compared to the FW's.

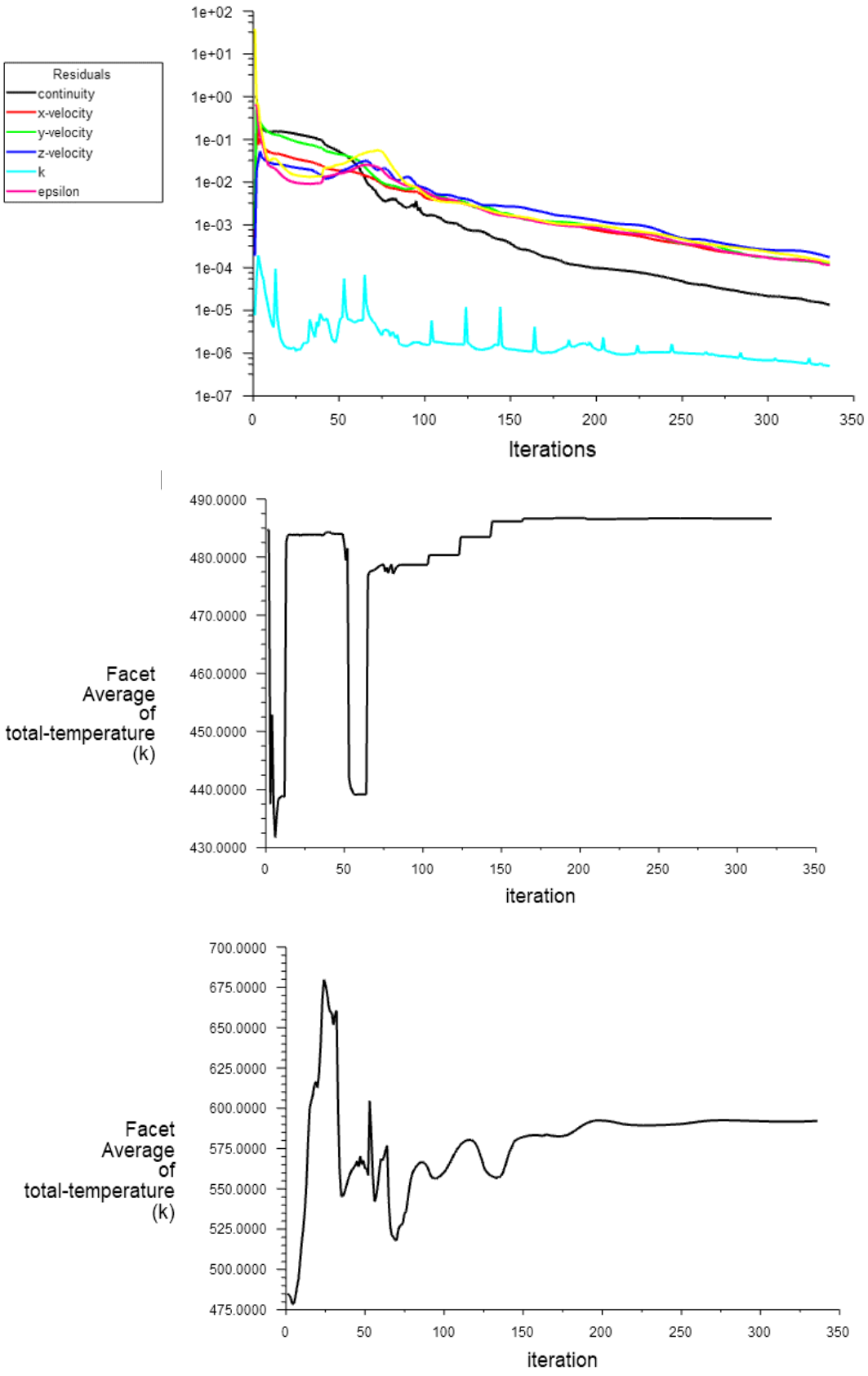

Figure B. 2: Thermal convergence of FWH-5A steady state, a) residuals, b) FW outlet temperature, c) steam outlet temperature

In the FWH-5A case, the flow maldistribution was deemed negligible. However, the existing flow groups was still used to discretise the heat transfer zones. The effect of the disproportional heat distribution due to the flow deflection plate can be clearly seen in Figure B.3. The 'Top' flow which is nearest to the deflection plate experiences low velocity vortices directly under the deflection plate and therefore has very low heat transfer in that region. Just downstream of the deflection plate the top flow group receives the highest magnitude of heat transfer as it is makes first contact with the incoming steam.

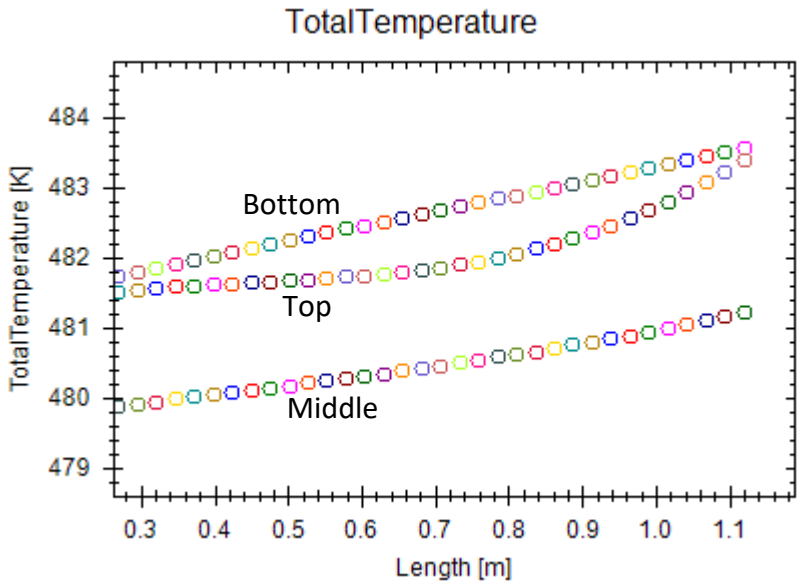

Figure B.3: Heat distribution in CFD domain of FWH-5A

Appendix C: Scripts

Scheme File (TEMA-FU)

```
(if (not (rp-var-object 'a_h_1))
    (rp-var-define 'a_h_1 0 'real #f))
(if (not (rp-var-object 'b_h_1))
    (rp-var-define 'b_h_1 0 'real #f))
(if (not (rp-var-object 'c_h_1))
    (rp-var-define 'c_h_1 0 'real #f))

(if (not (rp-var-object 'a_tinf_1))
    (rp-var-define 'a_tinf_1 0 'real #f))
(if (not (rp-var-object 'b_tinf_1))
    (rp-var-define 'b_tinf_1 0 'real #f))
(if (not (rp-var-object 'c_tinf_1))
    (rp-var-define 'c_tinf_1 480 'real #f))


(if (not (rp-var-object 'a_h_2))
    (rp-var-define 'a_h_2 0 'real #f))
(if (not (rp-var-object 'b_h_2))
    (rp-var-define 'b_h_2 0 'real #f))
(if (not (rp-var-object 'c_h_2))
    (rp-var-define 'c_h_2 0 'real #f))

(if (not (rp-var-object 'a_tinf_2))
    (rp-var-define 'a_tinf_2 0 'real #f))
(if (not (rp-var-object 'b_tinf_2))
    (rp-var-define 'b_tinf_2 0 'real #f))
(if (not (rp-var-object 'c_tinf_2))
    (rp-var-define 'c_tinf_2 480 'real #f))


(if (not (rp-var-object 'a_h_3))
    (rp-var-define 'a_h_3 0 'real #f))
(if (not (rp-var-object 'b_h_3))
    (rp-var-define 'b_h_3 0 'real #f))
(if (not (rp-var-object 'c_h_3))
    (rp-var-define 'c_h_3 0 'real #f))

(if (not (rp-var-object 'a_tinf_3))
    (rp-var-define 'a_tinf_3 0 'real #f))
(if (not (rp-var-object 'b_tinf_3))
    (rp-var-define 'b_tinf_3 0 'real #f))
(if (not (rp-var-object 'c_tinf_3))
    (rp-var-define 'c_tinf_3 480 'real #f))
```

UDF (TEMA-FU)

```
#include "udf.h"

//////////////////////////////////////
///// mdot 1 //////
//////////////////////////////////////
DEFINE_PROFILE(h_1,t,i)
{
    face_t f;
    real x[ND_ND];
```

```
10.
11.     real Ch_1,Bh_1,Ah_1;
12.     Ah_1 = RP_Get_Real("a_h_1");
13.     Bh_1 = RP_Get_Real("b_h_1");
14.     Ch_1 = RP_Get_Real("c_h_1");
15.
16.     begin_f_loop(f,t)
17.     {
18.         F_CENTROID(x,f,t);
19.         F_PROFILE(f,t,i)= Ah_1*pow(x[2],2) + Bh_1*x[2] + Ch_1;
20.     }
21.     end_f_loop(f,t)
22. }
23.
24. DEFINE_PROFILE(Tinf_1,t,i)
25. {
26.     face_t f;
27.     real x[ND_ND];
28.
29.     real CTinf1,BTinf1,ATinf1;
30.     ATinf1 = RP_Get_Real("a_tinf_1");
31.     BTinf1 = RP_Get_Real("b_tinf_1");
32.     CTinf1 = RP_Get_Real("c_tinf_1");
33.
34.     begin_f_loop(f,t)
35.     {
36.         F_CENTROID(x,f,t);
37.         F_PROFILE(f,t,i)= ATinf1*pow(x[2],2) + BTinf1*x[2] + CTinf1;
38.     }
39.     end_f_loop(f,t)
40. }
41.
42.
43.
44. ////////////////////////////////////////
45. ///// mdot 2 //////
46. ////////////////////////////////////////
47. DEFINE_PROFILE(h_2,t,i)
48. {
49.     face_t f;
50.     real x[ND_ND];
51.
52.     real Ch_2,Bh_2,Ah_2;
53.     Ah_2 = RP_Get_Real("a_h_2");
54.     Bh_2 = RP_Get_Real("b_h_2");
55.     Ch_2 = RP_Get_Real("c_h_2");
56.
57.     begin_f_loop(f,t)
58.     {
59.         F_CENTROID(x,f,t);
60.         F_PROFILE(f,t,i)= Ah_2*pow(x[2],2) + Bh_2*x[2] + Ch_2;
61.     }
62.     end_f_loop(f,t)
63. }
64.
65. DEFINE_PROFILE(Tinf_2,t,i)
66. {
67.     face_t f;
68.     real x[ND_ND];
69.
70.     real CTinf2,BTinf2,ATinf2;
71.     ATinf2 = RP_Get_Real("a_tinf_2");
72.     BTinf2 = RP_Get_Real("b_tinf_2");
73.     CTinf2 = RP_Get_Real("c_tinf_2");
74.
75.     begin_f_loop(f,t)
```

```
    {
        F_CENTROID(x,f,t);
        F_PROFILE(f,t,i)= ATinf2*pow(x[2],2) + BTinf2*x[2] + CTinf2;
    }
    end_f_loop(f,t)
}


//////////////////////////////////////
///// mdot 2 //////
//////////////////////////////////////
DEFINE_PROFILE(h_3,t,i)
{
    face_t f;
    real x[ND_ND];

    real Ch_3,Bh_3,Ah_3;
    Ah_3 = RP_Get_Real("a_h_3");
    Bh_3 = RP_Get_Real("b_h_3");
    Ch_3 = RP_Get_Real("c_h_3");

    begin_f_loop(f,t)
    {
        F_CENTROID(x,f,t);
            F_PROFILE(f,t,i)= Ah_3*pow(x[2],2) + Bh_3*x[2] + Ch_3;
        }
        end_f_loop(f,t)
    }

    DEFINE_PROFILE(Tinf_3,t,i)
    {
        face_t f;
        real x[ND_ND];

        real CTinf3,BTinf3,ATinf3;
        ATinf3 = RP_Get_Real("a_tinf_3");
        BTinf3 = RP_Get_Real("b_tinf_3");
        CTinf3 = RP_Get_Real("c_tinf_3");

        begin_f_loop(f,t)
        {
            F_CENTROID(x,f,t);
            F_PROFILE(f,t,i)= ATinf3*pow(x[2],2) + BTinf3*x[2] + CTinf3;
        }
        end_f_loop(f,t)
    }
```

Flownex Network Script

```
Q1_pre.Value  = Q1;
Q1.Value = Rlx_fac*Q1_pre+Q1_new*(1-Rlx_fac);


Q2_pre.Value  = Q2;
Q2.Value = Rlx_fac*Q2_pre+Q2_new*(1-Rlx_fac);


Q3_pre.Value  = Q3;
Q3.Value = Rlx_fac*Q3_pre+Q3_new*(1-Rlx_fac);


Rlx_P_i.Value = Rlx_P;
if ( Time > 0 ) {
    Rlx_P.Value = Rlx_P + (1-Rlx_P)/2;
}

P_g_new.Value = P_ref - P_e_new;
P_e_pre.Value  = P_e;
if (P_g_new.Value >= (1+(1-Rlx_P))*P_e_pre & P_e_pre !=0 ) {
    P_g_new.Value = (1+(1-Rlx_P))*P_e_pre;
    }
if (P_g_new.Value < Rlx_P*P_e_pre & P_e_pre !=0) {
    P_g_new.Value = Rlx_P*P_e_pre;
    }
P_e.Value = Rlx_P*P_e_pre+P_g_new*(1-Rlx_P);

Rlx_P.Value = Rlx_P_i;
```